Stefan Pagger, BSc

Radial Gate Excitation on a Gravity Dam due to Seismic Loading

MASTERARBEIT

zur Erlangung des akademischen Grades

Diplom-Ingenieur

Masterstudium Bauingenieurwissenschaften - Geotechnik und Wasserbau

eingereicht an der

Technischen Universität Graz

Betreuerin

Univ.-Prof. Dipl.-Ing. Dr.techn. Gerald Zenz

Institut für Wasserbau und Wasserwirtschaft

Zweitbetreuer
Dipl.-Ing. Markus Goldgruber

Graz, Juni 2015

EIDESSTATTLICHE ERKLÄRUNG

AFFIDAVIT

Ich erkläre an Eides statt, dass ich die vorliegende Arbeit selbstständig verfasst, andere als die angegebenen Quellen/Hilfsmittel nicht benutzt, und die den benutzten Quellen wörtlich und inhaltlich entnommenen Stellen als solche kenntlich gemacht habe. Das in TUGRAZonline hochgeladene Textdokument ist mit der vorliegenden Masterarbeit identisch.

I declare that I have authored this thesis independently, that I have not used other than the declared sources/resources, and that I have explicitly indicated all material which has been quoted either literally or by content from the sources used. The text document uploaded to TUGRAZonline is identical to the present master‘s thesis.

Datum / Date

Unterschrift / Signature

ABSTRACT

Dams are built and operated for water retention for different purposes. The water needs to be regulated at intake structures, bottom outlets, spillways with fixed crest or spillways with closure devices. Radial gates are common hydraulic closure devices for spillways. These radial gates consist of a curved skin plate for water retention and framework arms to transfer the occurring loads to the piers. Concrete gravity dams as well hydraulic steel parts as radial gates are stressed during their lifetime not only by static forces but also by dynamic forces. Beside floating ice and debris an earthquake event can be a dynamic loading on gravity dams and their facilities.

The first part of this work contains the summary of the dynamic and hydromechanical essentials. Furthermore the construction details of hydraulic gates and dams are considered. The modelling techniques of the specific loading due to earthquakes for closure devices at the top of spillways and for gravity dams and the different dynamic calculation methods are explained.

In the second part a dam-reservoir-foundation system with an installed radial gate is examined. At first the static stresses on the system due to dead weight and hydrostatic pressure are simulated. After the eigenfrequency analysis the earthquake accelerations excite the system. Different calculation methods, different reservoir modelling techniques and different masses and stiffnesses of the radial gates are used and compared. The seismic loading leads to an acceleration amplification factor of about 10 in the abutment of the gate and a threefold increase of the bearing forces.

KURZFASSUNG

Staumauern werden für den Rückhalt von Wasser für unterschiedlichste Nutzungszwecke errichtet und betrieben. Dabei muss das Wasser im Einlaufbereich des Triebwasserweges und Grundablasses und im Bereich von fixen oder beweglichen Hochwasserentlastungsanlagen reguliert werden. Bewegliche Hochwasserentlastungsanlagen können als Segmentwehre ausgeführt werden. Diese Segmentwehre bestehen aus einem Kreissegment zum Zwecke des Wasserrückhaltes und aus Fachwerksarmen, welche die auftretenden Kräfte in die Trennpfeiler der Staumauer ableiten. Sowohl die Betonmauer als auch die Stahlbauteile eines Wasserkraftwerkes, zu denen Segmentwehre zählen, werden nicht nur statisch sondern auch dynamisch beansprucht. Neben Eis und Schwemmgut können auch Erdbeben eine dynamische Beanspruchung von Staumauern darstellen.

Den ersten Teil der Arbeit stellt die Ausarbeitung der dynamischen und hydromechanischen Grundlagen dar. Des Weiteren wird auf den Aufbau und die Lagerung der Gewichtsmauer und der Verschlussorgane genauer eingegangen. Die Modellierungsmöglichkeiten der zusätzlich auftretenden Belastung auf die Staumauer und die Verschlussorgane zufolge eines Erdbebens des Stausees und die unterschiedlichen dynamischen Berechnungsmethoden werden erläutert.

Im zweiten Teil wird ein Gewichtsmauer-Stausee-Untergrund System mit installiertem Drucksegment numerisch untersucht. Zuerst wird die statische Beanspruchung des Systems zufolge Eigengewicht und statischem Wasserdruck simuliert. Nach der Eigenschwingungsanalyse werden Erbebenbeschleunigungen zur dynamischen Beanspruchung des Systems angesetzt. Dabei werden unterschiedliche numerische Berechnungsmethoden, unterschiedliche Stauseemodellierungen und unterschiedliche Massen und Steifigkeiten des Segments miteinander verglichen. Durch die dynamische Belastung ergab sich eine Erhöhung der Beschleunigungen im Lagerpunkt des Segments um das Zehnfache sowie eine Zunahme der Kräfte im Lagerpunkt um das Dreifache.

DANKSAGUNG

Eine Masterarbeit und die darauffolgende Masterprüfung stellen den Abschluss intensiver, lehrreicher aber auch anstrengender Studienjahre dar. In dieser Zeit, die sowohl aus Höhen als auch aus Tiefen bestand begleiteten mich zahlreiche Personen, bei denen ich mich bedanken möchte.

Ein großer Dank gebührt dem Betreuer meiner Masterarbeit Dipl.-Ing. Markus Goldgruber. Seine fachliche Kompetenz und seine Begeisterung hatten stets einen positiven Einfluss auf die Qualität dieser Arbeit und sind Motivation, mich intensiver mit der Thematik zu beschäftigen. Auch die kollegiale und unkomplizierte Zusammenarbeit wird mir sehr positiv in Erinnerung bleiben.

Bedanken möchte ich mich auch bei Univ.-Prof. Dipl.-Ing. Dr.techn. Gerald Zenz für die kompetenten Reflexionen und Inputs im Zuge meiner Masterarbeit.

In den letzten Jahren an der Technischen Universität Graz wurden einige neue Freundschaften geknüpft und sowohl schwierige Prüfungen als auch außeruniversitäre Aktivitäten erfolgreich absolviert. Diese Freundschaften bereicherten meinen Alltag und dafür möchte ich meinen Dank aussprechen.

Des Weiteren möchte ich mich bei Dipl.-Ing Walter Daninger und seinem Team von Daninger & Partner bedanken. Nette Arbeitskollegen und ein sehr gutes Arbeitsklima ermöglichten mir vier schöne und lehrreiche Arbeitsjahre neben dem Studium

Mein größter Dank gilt meiner Familie, insbesondere meinen Eltern Maria und Rudolf, die stets ein Rückhalt für mich waren und mich während meiner Ausbildung sowohl finanziell als auch mental unterstützten. Ich weiß sehr zu schätzen, Eltern zu haben, die bei jeglichen Entscheidungen, mir mit Rat und Tat zur Seite stehen und mir ein Gefühl der Sicherheit geben.

CONTENTS

LIST OF FIGURES

LIST OF TABLES

LIST OF SYMBOLS

General symbols

G	[N]	dead load
M	[Nm]	moment
A	[m²]	area
S	[m²]	static moment
W	[m³]	moment of inertia
I	[m^4]	area moment of inertia
γ	[N/m³]	density
a	[m/s²]	acceleration
g	[m/s²]	acceleration due to gravity
K_0	[N/m³]	earth pressure coefficient
φ	[°]	fricition angle

Symbols of the dynamic principals

f	[Hz]	frequency
ω	[Hz]	angular frequency
T	[s]	time
u_0	[m]	amplitude
φ_0	[°]	oscillation angle
m	[t]	mass
u	[m]	displacement
$\dot{u}$	[m/s]	velocity
$\ddot{u}$	[m/s²]	acceleration
c	[Ns/m]	damping coefficient
k	[Ns²/m]	stiffness coefficient
F_D	[N]	damping force
F_S	[N]	spring force
$f(t)$	[N]	exciting force
A,B,C	[-]	constant terms in a differential equation
ξ	[-]	damping factor
$[M]$	[-]	mass matrix

$[K]$	[-]	stiffness matrix
$[C]$	[-]	damping matrix
$\{U\},\{\dot{U}\},\{\ddot{U}\}$	[-]	motion vectors
$\{P(t)\}$	[-]	load vector
ψ	[-]	eigenmode
α	[-]	Rayleigh damping coefficient
β	[-]	Rayleigh damping coefficient
N	[-]	total value of a random displacement value
N_i	[-]	ratio of the eigenmode i on the displacement value
ϱ_{ij}	[-]	Factor of interpendency

Symbols of the hydromechanical essentials

τ	[N]	shearing force
η	[Pas]	viscosity
p	[Pa]	pressure
W	[Pa]	resulting water pressure
∇	[-]	function gradient

1 Introduction

Hydro power plants are designed and build to increase humans' living standards. Since the ancient time people try to store water to use it for satisfaction of elementary needs.

Beside the main benefit of hydro power plants to use it for electricity generation such facilities often have multipurpose-profit. Especially storage plants can be used for retention of drinking and service water for the agriculture, for generation of recreation rooms, for saving the ship traffic, for regulation of the groundwater level, for generating new jobs and are beneficiary of employees.

During the design of a hydro power plant different fields have to be considered precisely. This is necessary to guarantee the safety and the use of the facilities. In addition to a good hydraulic construction of the plant, to avoid claims and to guarantee a long lifetime also the civil design is of prime importance. Static and dynamic analyses are counted among civil design works.

Both the internal structural safety and the external structural safety have to be guaranteed. The internal safety contains especially concrete construction details like the reinforcement layout and the dimensioning of the structure. The external structural safety includes the consideration of the dam-foundation-reservoir system in static and dynamic fields. For consideration of the dynamic loads on a structure, numerical simulations are useful instruments. For these numerical simulations numerous open-source and commercial software packages exist.

At the Institute of Hydraulic Engineering and Water Resources Management of the Graz University of Technology one field of research is the numerical simulation of the fluid structure interaction on hydraulic retention structures. Based on the master's project "Seismic acceleration amplification over the height of a gravity dam" by Pagger (2014) in the course of this master thesis a numerical model of a gravity dam-reservoir-foundation system is developed and the static and dynamic forces on the structure due to an earthquake event are implemented.

The basis of the geometry of the model is the storage hydro power plant Birecik in South-East-Anatolia on the river Euphrates in Turkey. It was projected as BOT-model (Build-Operate-Transfer) and came into operation in 2000. In 2016 the ownership of the hydro power plant will be transferred to the Turkish government.

At first the static loading cases are computed to get the static behavior of the structure. Over the eigenmodes of the system the dynamic loads can be accurate and lead to oscillations of the structure. An artificial acceleration time history for an earthquake with a duration of 20 seconds is used for the stimulation of the system. Thereby accelerations in horizontal and vertical direction are acting.

For the numerical simulation the direct time integration method and the modal analysis method are used and the differences in the results are figured out. Also varying geometries and material parameters are applied and compared. The consideration of the dynamic pressure of the reservoir water is done with different approaches.

A detailed consideration of the installed radial gate on the spillway and the dynamic response on the abutment is in the focus of the simulation.

The numerical simulation of the gravity dam-reservoir-foundation system is performed by the commercial finite-element-analysis software Abaqus/CAE 6.13.

2 Targets and challenges of this work

Radial gates are designed and constructed by steel hydraulics construction engineers. Thereby the knowledge about the dynamic stresses due to an earthquake acting on the steel structure are often only estimated in an approximative way. The common procedure is the use of design spectra for the earthquake simulation. Therefrom artificial time histories are calculated and multiplied by a conservative factor to get the loadings for the design of the closure device.

To get more detailed information about the loading of the steel structure a numerical simulation of the whole system is needed.

In the framework of this work the first point is an introduction into the thematic basics. Thereby especially the dynamic essentials about oscillating systems and the hydrodynamic approaches are declared. After the general part the model is created with the software Abaqus/CAE. Especially the dynamic response of the abutment of the radial gate is examined. As definitive results the acceleration amplification in the abutment for the different model configurations should be illustrated and response spectra for the different variants should be created.

The following points are reasons for the different models:

- **Different models due to the hydrodynamic pressure consideration:**
  For the dynamic seismic step of the numerical simulation the model is performed for the empty reservoir and the full reservoir. The full reservoir is assumed with Westergaard's added mass technique and with acoustic elements.

- **Different models due to different calculation methods:**
  The different loading cases are computed with the direct time integration method or with the modal analysis with time history method. Different calculation methods lead to a variation of results.

- **Different models due to different stiffnesses of the gate:**
  The gate is discretized as rigid part with an infinite stiffness and as deformable part with common steel properties. The influence of the stiffness of the steel structure on the resulting accelerations and forces is examined.

3 Thematic basics

3.1 Dams

Dams are constructed as rock- or earth-fill dams as well as concrete dams. Dependent on the geology and the geotechnical properties of the foundation different types are built.

3.1.1 Concrete dams

Compared to rock- and earth-fill dams, concrete dams have to be based on a sustainable rock foundation. Nowadays unreinforced concrete is used for building such dams. Only in areas where tensile forces occur (e.g. bottom outlet, piers, etc.) the concrete has to be reinforced. During construction concrete blocks are manufactured and joined together to get the hydration heat under control.

The advantages of concrete dams according Strobl & Zunic (2006) are the unproblematic overflow of the dam in case of a flood event, the design of the intake in the dam structure and resultant the lower construction costs due to the easy installation of all facilities in the dam area.

Concrete dams can be divided into:

- Gravity dams
- Arch dams
- Buttress dams.

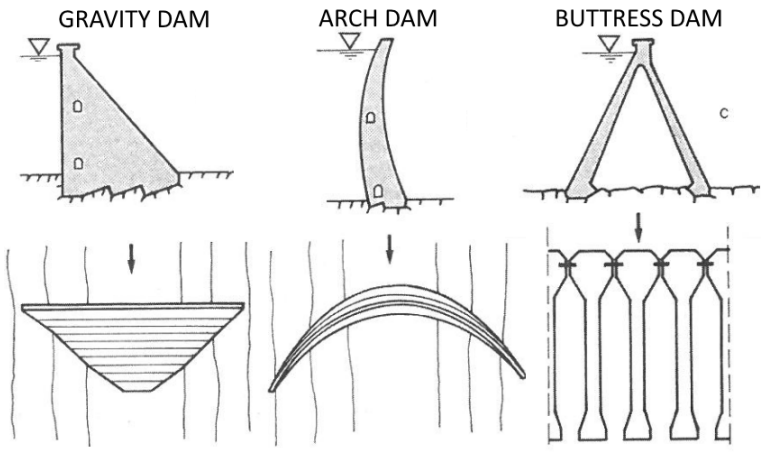

Figure 3-1: Types of concrete dams (Strobl & Zunic, 2006)

Also mixtures of these concrete dam types are designed. Due to the topic of this thesis only the gravity dam will be introduced.

3.1.1.1 Gravity dam

Gravity dams are built in wide U-shaped valleys on a sustainable rock abutment. Bandi, et al. (2006) limit the construction height of a gravity dam with 100 meters. Higher gravity dams are uncommon because an immense amount of concrete would be necessary due to the long contact path. The cross section of a gravity dam is a simple triangle geometry with truncated vertices.

The waterface is nearly vertical in contrast to the downstream face with a common ratio of inclination between 1:0.65 and 1:0.8. Concrete blocks with a width between 12 and 20 meters and a length between 30 and 40 meters are used for construction. (Bandi, et al., 2006)

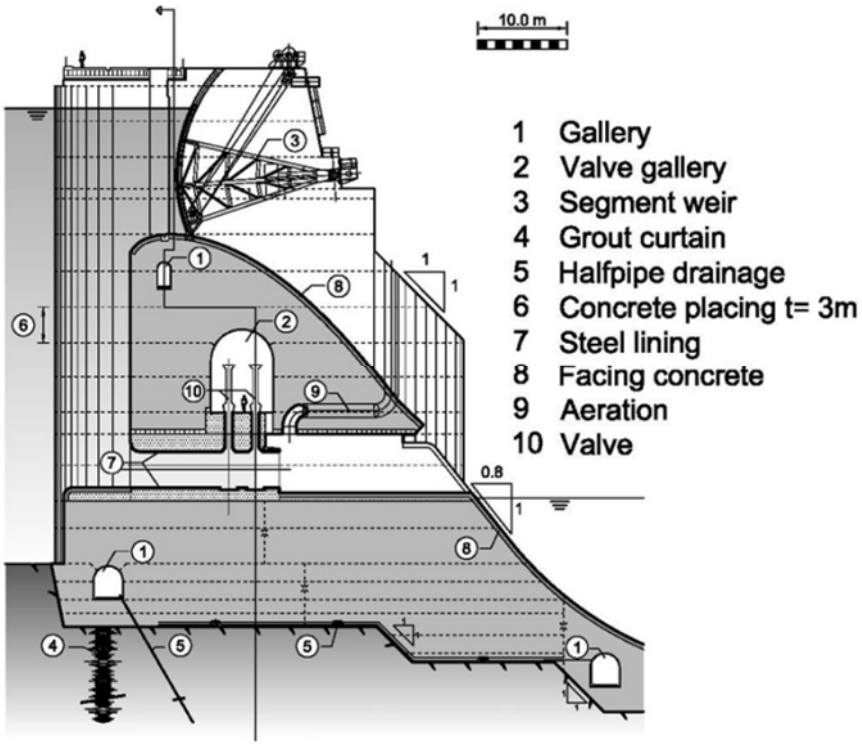

Figure 3-2: Example of a common design of a gravity dam: cross section through the spillway (Institut für Wasserbau und Wasserwirtschaft, 2012)

The layout of a gravity dam can be straight, curved or buckled.

On the contrary to arch dams gravity dams aren't in need of intact valley flanks. They only have to be founded on a sustainable base to transfer the occurred horizontal and vertical loads over the contact path into the abutment. Thereby only the mass of the structure acts against the working load.

On top of the spillway of a gravity dam different closure devices can be installed. These devices help to regulate the water level of the reservoir. These closure devices are declared in 3.2. The hydrostatic pressure which acts on a radial gate can be calculated as explained in 5.2.

The static basics of the gravity dam are declared in 5.3.

3.2 Gates

Hydraulic closure devices on dams can be installed as intake of penstocks or on spillways to regulate the flow. These spillways can be designed as fixed weirs with curved crests, as movable weirs with hydraulic gates for regulation or as combined versions.

The main applications of hydraulic gates according to Erbisti (2004) are:

- Flood protection
- Regulation of the water level to use the reservoir for secondary purposes or for guarantying a constant water level
- Flow regulation in case of intake devices
- Cleaning of reservoirs if floating debris or ice vitiate the use
- Cutting off the water in case of maintenance
- Protection in case of an flood event and protection of equipment as emergency gates

Erbisti (2004) defines several ways to separate hydraulic gates into categories.

Hydraulic gates can be divided due to their operational purpose. Thereby they can be used as service gates, as emergency gates and as maintenance gates.

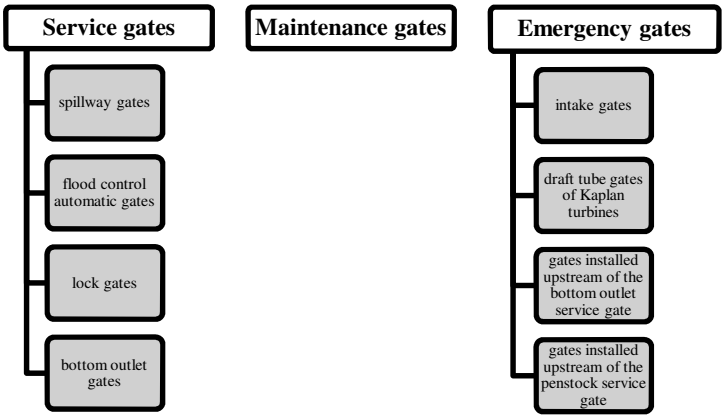

Figure 3-3: Classification of gates due to their purpose

Another way to classify hydraulic gates is the division according to their movement. In this case gates are distinguished into translational gates, rotation gates and translo-rotation gates.

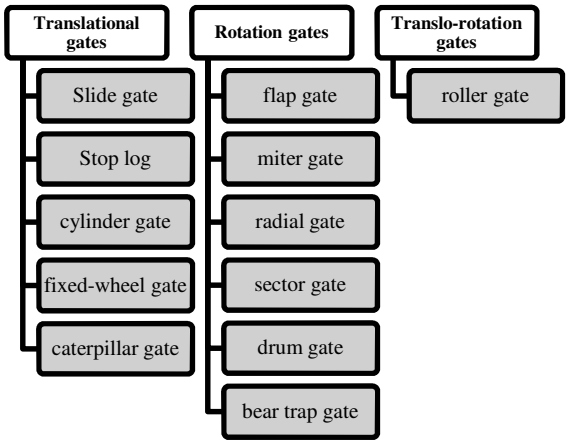

Figure 3-4: Classification of gates due to their movement

In addition gates can be classified due to the water passage. The discharge can be happen over the leaf, under the leaf or over and under the leaf.

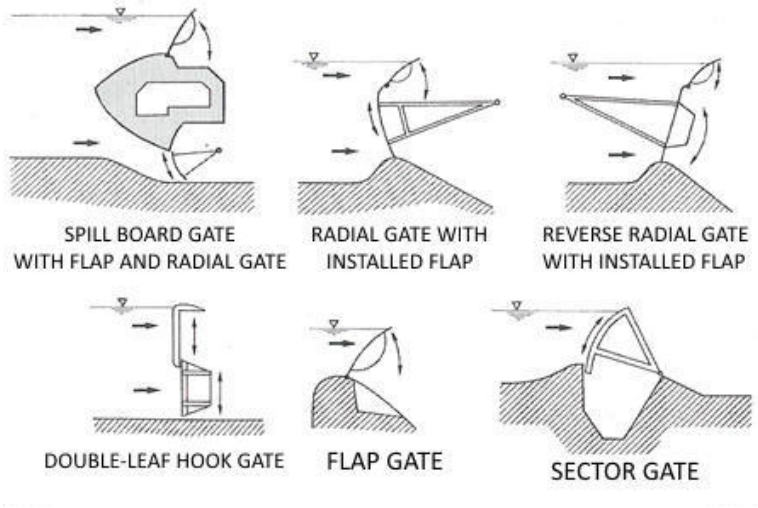

Figure 3-5: Different types of rotation gates (Strobl & Zunic, 2006)

Concerning to the topic of this thesis the radial gate will be illustrated in detail.

3.3 Radial gates

The in 3.3 mentioned essentials of radial gates are based on Erbisti (2004) and Strobl & Zunic (2006).

In storage hydro power plants there are mostly radial gates installed as closure device of a spillway. In combination with a fitted flap on the top it represents a good compromise of safety and easy handling. For lifting a radial gate only small forces are needed compared to translational gates. Furthermore these gates don't need guide rails so the piers can be designed slimmer. Due to the bearing in only two points the dimensions, especially the width is limited to 25 meters.

Because of the given advantages radial gates are ideally suited for high head storage power plants.

Radial gates can be designed and built as normal radial gates and as reverse radial gates. In case of normal radial gates the radial arms are compressed and the concrete in the pier is stressed by pressure forces. The good material characteristics of steel in case of tensile loading and the good material properties of concrete under pressure cannot be used. Due to the pressure forces on the steel components bigger cross sections of the steel beams because of buckling risk are necessary and the concrete has to be reinforced in the bearing area.

The material behavior of steel and concrete can considerably better used at reverse radial gates. Due to the upstream bearing of the gate the radial arms are stressed by tensile forces. The disadvantages of the reverse radial gate are the required bigger lifting forces and the bad accessibility for maintenance.

Figure 3-6: Radial gate with fitted flap of the run-off-river plant Rothleiten at the river Mur

The constituents of a radial gate are:

- the curved skin
- the radial framework arms
- the fixed bearings in the piers
- and the hydraulic hoists for operation.

The skin plate consists of horizontal and vertical beams and stiffeners and steel plates with thicknesses between 6.5 and 40 millimeters. On the two vertical main girders the radial framework arms are connected to the skin. These compressed arms transfer the loads to the bearings. The beams are fastened by welding seams or bolts. Common layouts for the vertical and horizontal orientation of the radial arms are shown in Figure 3-7.

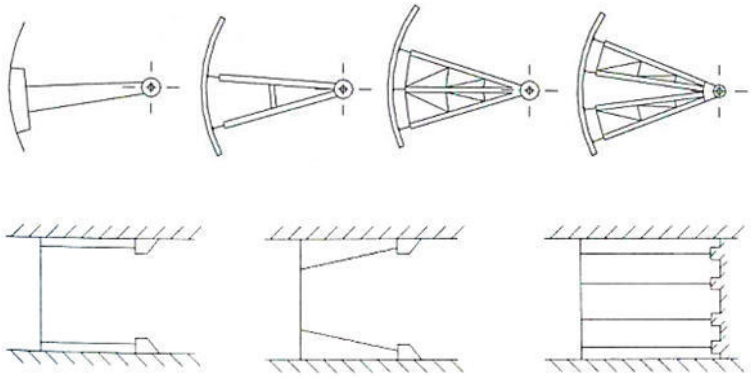

Figure 3-7: Common layouts of the radial arms of a radial gate (Erbisti, 2004)

The radial gate usually rotates about a horizontal axis, thereby the direction of the resulting force of the static water pressure should go through the pivot. Due to this geometrical condition no tendency to open or close the gate should appear.

Normal gates have to be lifted for discharge, though small openings result in large flows. With a fitted flap on top of the gate the discharge can happen over the leaf and it can be regulated exactly. Also the water level of the reservoir can be kept constant and debris and ice can be led away with this variation.

3.3.1 Geometry of radial gates

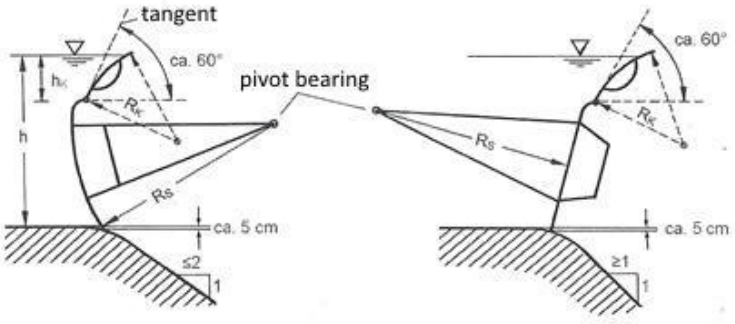

Figure 3-8: Geometry definitions of radial gates (Strobl & Zunic, 2006)

The radius R_s of a radial gate defines Strobl & Zunic (2006) as approximately 1.3 times the height h of the gate. The radius of the flap should be about 1.7 to 2.8 times the height h_k of the flap. The mass of a radial gate can be assumed by 3 to 5 kN/m² times the surface area of the skin plate.

Erbisti (2004) estimates the mass of a radial gate over the width B, the head on the sill H and the gate height h with the following formula:

$$G = 0.64(B^2 hH)^{0.682} \tag{3.1}$$

3.3.2 Variants of bearings and anchorages of radial gates

The classic version of a gate trunnion was mainly used until the 1960's. It consists of a trunnion hub, which is connected with the radial gates' framework arms by bolts or welding. The hub rotates around the pin, which is supported on both sides by the trunnion brackets. The trunnion pin is locked against rotation by a key plate.

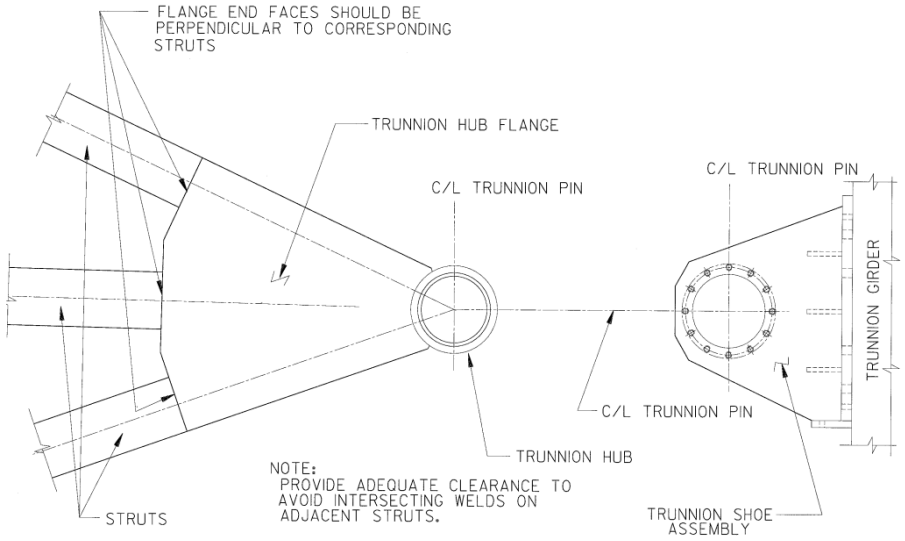

Figure 3-9: The classic version of a gate trunnion (US Army Corps of Engineers, 2000)

Due to the problems of pin misalignments, thermal elongation and elastic deformation of the pin the spherical plain bearing was innovated at the end of the 1960's. This spherical bearing contains an inner and an outer ring with spherical sliding surfaces.

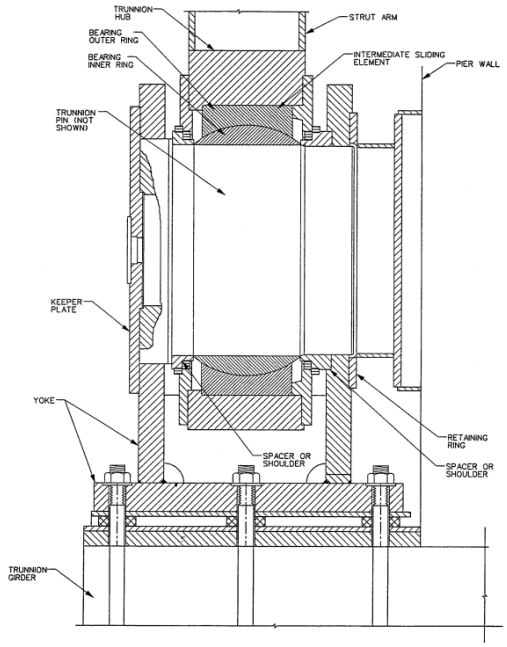

Figure 3-10: Spherical plain bearing for radial gates (US Army Corps of Engineers, 2000)

The static water pressure and the dead load of the gate can be transferred over the trunnion yokes (a) through the trunnion anchorage to the pier. Two systems for anchorage of trunnions are common:

- Structural anchorage over two longitudinal members
- Prestressed anchorage over post-tensioned round bars.

The structural anchorage consists of two longitudinal members (b) connected by a transverse anchor girder (c) on the upstream end. The direction of the longitudinal beams should be the direction of the resulting force of the acting loads.

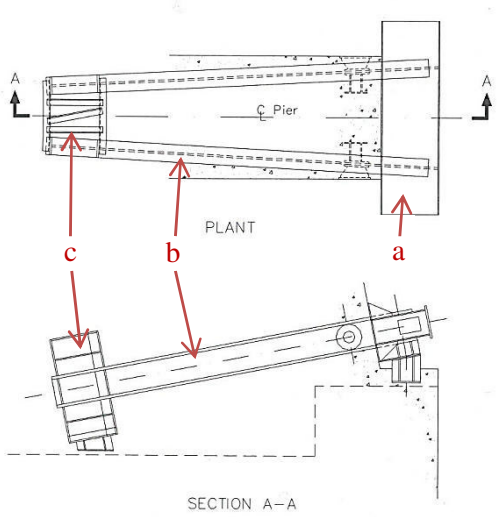

Figure 3-11: Structural anchorage of radial gates (Erbisti, 2004)

In case of larger radial gates the prestressed anchorage has turned out as the better system. The post-tensioned round tendons fix the trunnion yoke to the pier. Only the ends of the round bars are connected with the concrete. The residual tendon length is isolated from the pier by tubes. The tendons are also oriented longitudinally in direction of the resulting pressure force.

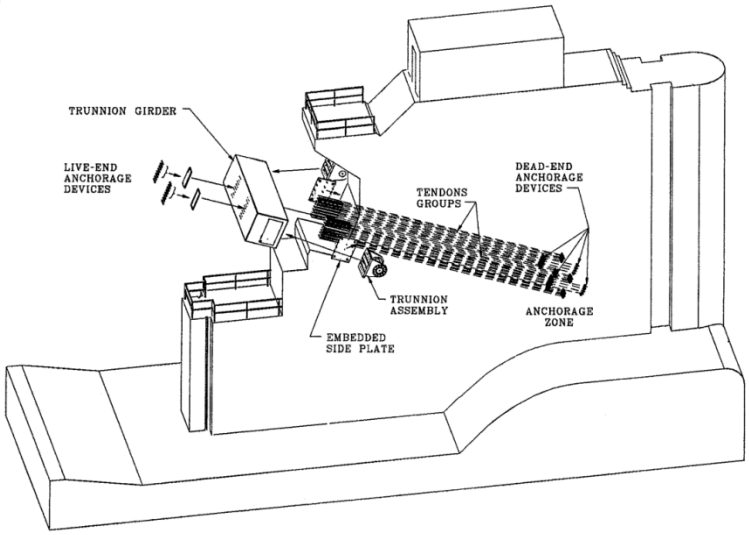

Figure 3-12: Prestressed anchorage of radial gates (US Army Corps of Engineers, 2000)

4 Dynamic Principals

4.1 Oscillations

Oscillations are temporal variations of a state variable. This state variable can be, e.g. the position, the force, the temperature or the electric voltage of a body. In connection with oscillations terms like period, frequency or angular eigenfrequency are used. The basics of oscillations are based on Freymann (2011).

The period is defined as the time T in which the movement proceeds until it repeats again.

The frequency can be calculated by stringing together of multiple periods. Hence the frequency is the oscillation per time:

$$f = \frac{1}{T} \tag{4.1}$$

Resultant from angle relations the angular eigenfrequency is defined by following formula:

$$\omega = \frac{2\pi}{T} = 2\pi f \tag{4.2}$$

Oscillations can be divided according to Freymann (2011) in:

- Periodic oscillations
- Harmonic oscillations
- Almost periodic oscillations and
- Transient oscillations.

4.1.1 Periodic oscillations

In case of periodic oscillations the progression of the magnitude repeats in equal recurrent intervals.

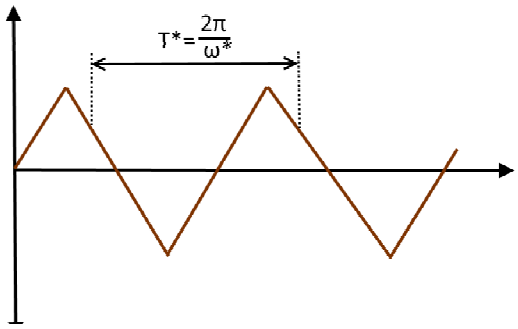

Figure 4-1: Example of a periodic oscillation

4.1.2 Harmonic oscillations

A harmonic oscillation is characterized by a sine- or cosine-shaped figure. Similar to periodic oscillations also harmonic oscillations have equal recurrent intervals.

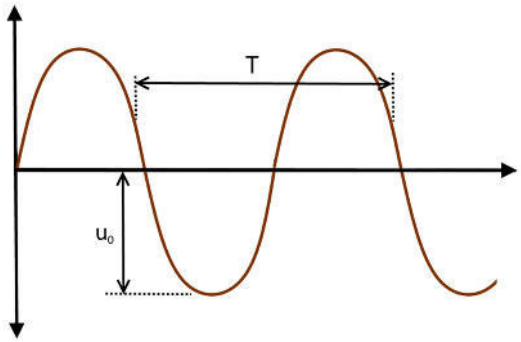

Figure 4-2: Example of a harmonic oscillation

The formula of a harmonic oscillation is with the equations (4.1) and (4.2):

$$u(\mathrm{t}) = u_0 \cos(\omega t + \varphi_0) \tag{4.3}$$

Due to the mathematic relation

$$\cos(\alpha + \beta) = \cos\alpha cos\beta - sin\alpha sin\beta \tag{4.4}$$

the general equation of an harmonic oscillation is:

$$u(\mathrm{t}) = Acos\omega t + Bsin\omega t. \tag{4.5}$$

With:

$$A = u_0 cos\varphi_0 \tag{4.6}$$

$$B = -u_0 sin\varphi_0 \tag{4.7}$$

4.1.3 Almost periodic oscillations

An almost periodic oscillation results out of a superposition of particular harmonic oscillations. This superposition doesn't have to inevitably lead to periodic oscillations, in some cases also almost periodic oscillations are possible. These oscillations have due to their name an almost periodic appearance.

4.1.4 Transient oscillations

Transient oscillations are not subjected any rules regarding their repetition. Their oscillation graph has no visible trend or progression, therefore they are unpredictable.

4.2 Oscillating systems

During an oscillation process potential energy will be transformed into kinetic energy and reversed. Over this process the mass *m* provides due to its inertia the kinetic energy. On the other hand the potential energy will be stored as deformation energy in the spring. (Vöth, 2006)

The damping properties of an oscillator are characterized by the damping force $F_D = c\dot{u}$.

The determination of the oscillation components mass, stiffness and damping can occasionally be difficult. The mass can be easily defined over the density and the volume of the body. Material stiffnesses can normally be found in technical literature. The damping is the most unsteady component. For the damping assumption the literature provides different approaches, which often are based on measurement results and are subjected to uncertainties. (Vöth, 2006)

4.2.1 Classification of oscillating systems

Not every oscillating system is damped and not every system is induced by an external force, therefore oscillations can be differentiated according to Gross, et al. (2012) into free and forced oscillations and damped and undamped oscillations.

The general equation of a two-dimensional oscillating system based on Newton's equation of motion has the formula:

$$m\ddot{u} + c\dot{u} + ku = f(t) \tag{4.8}$$

With:

- the mass component $m\ddot{u}$
- the damping component $c\dot{u}$
- the stiffness component ku
- and the exciting force $f(t)$.

In case of an free oscillation the system is not brought into oscillation by an exciting force so f(t) = 0. Eigen-oscillations of systems can be counted to free oscillations.

Also the damping component only endures in case of damped oscillations. Thereby the amplitude of the oscillation decreases due to the damping component. In the event of an undamped oscillation the amplitude remains steadily because of the missing damping. (Gross, et al., 2012)

4.3 Single-degree-of-freedom system

The single-degree-of-freedom system is the simplest oscillating system in the dynamics. The basics of the single-degree-of-freedom system are taken from Flesch (1993).

The system consists of the mass m, the spring and the damping component. The spring has the spring stiffness k and the damping element possesses the damping coefficient c.

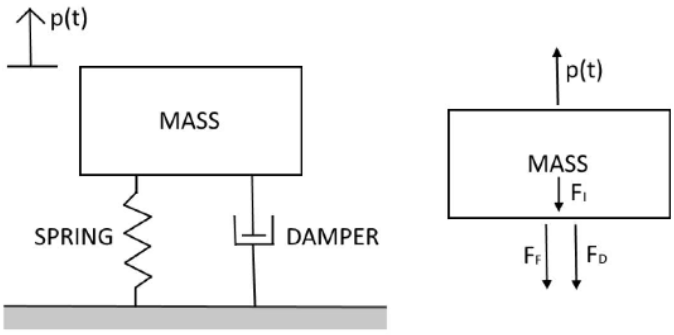

Figure 4-3: Single-degree-of-freedom system

With the inertia force $F_I = m\ddot{u}$ the damping force $F_D = c\dot{u}$ and the spring force $F_S = ku$ the equation of the general equation of a two-dimensional oscillating single-degree-of-freedom system is equal to equation (4.8).

4.3.1 The eigenoscillation of an undamped single-degree-of-freedom system

An oscillating system with one constant mass oscillation and constant amplitude after the release is called undamped single-degree-of-freedom system.

The general approach of a second-order homogeneous differential equation is:

$$u(t) = Ge^{i\omega t}. \tag{4.9}$$

If there is no exciting force acting the general equation of an undamped system is:

$$\ddot{u} + {\omega_0}^2 u = 0. \tag{4.10}$$

The eigenfrequency is defined as:

$$f = \frac{\omega_0}{2\pi}. \tag{4.11}$$

and the angular eigenfrequency is:

$${\omega_0}^2 = \frac{k}{m}. \tag{4.12}$$

With the oscillation period T, the eigenfrequency and the angular eigenfrequency the differential equation of an undamped system can be solved:

$$u(t) = C_1 e^{i\omega_0 t} + C_2 e^{-i\omega_0 t} \tag{4.13}$$

The Euler Equation

$$e^{i\varphi} = \cos\varphi + i\,sin\varphi \tag{4.14}$$

helps to write the final term down in the following way**:**

$$u(t) = B_1 sin\omega_0 t + B_2 cos\omega_0 t \tag{4.15}$$

The two constant terms B1 and B2 can be solved, if the boundary conditions, which are depending on the dynamic system, are known.

4.3.2 The eigenoscillation of a damped single-degree-of-freedom system

An oscillating system with a decreasing mass oscillation and decreasing amplitude after the release is called damped single-degree-of-freedom system.

In case of a damped single-degree-of-freedom system the damping component is added to formula (4.10).

$$\ddot{u} + \frac{c}{m}\dot{u} + {\omega_0}^2 u = 0 \tag{4.16}$$

The general approach of a second-order homogeneous differential equation is:

$$s = -\frac{c}{2m} \pm \sqrt{\left(\frac{c}{2m}\right)^2 - {\omega_0}^2}. \tag{4.17}$$

In consideration of the term under the square root three issues can occur:

- $\frac{c}{2m} = \omega_0 \ldots$ critical damping
- $\frac{c}{2m} > \omega_0 \ldots$ over-critical damping
- $\frac{c}{2m} < \omega_0 \ldots$ under-critical damping

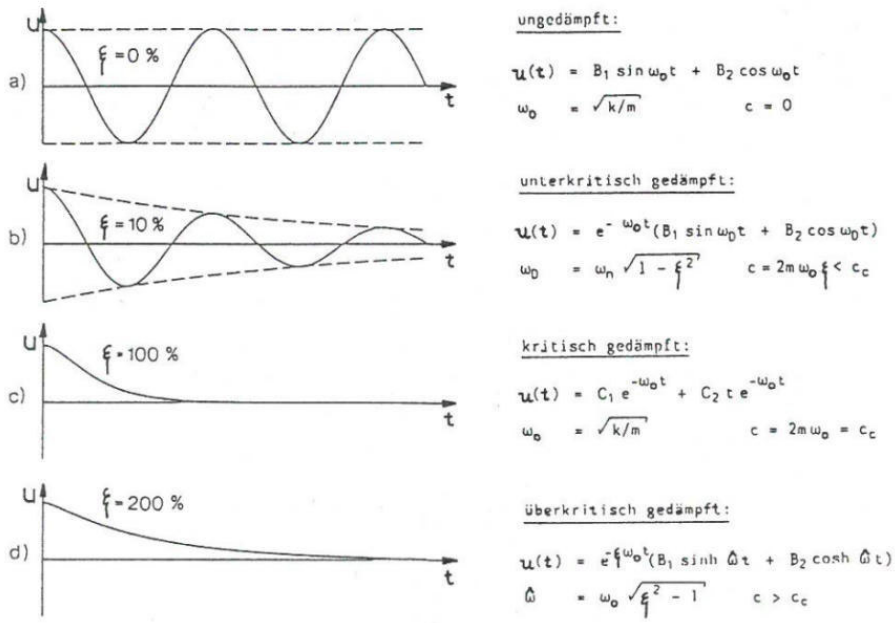

Figure 4-4: Movement distributions for different dampings (Flesch, 1993)

With the components of the three equations the damping factor can be defined as the proportion of the damping coefficient c and two times the product of the mass and the angular eigenfrequency:

$$\xi = \frac{c}{2m\omega_0} = \frac{c}{c_r} \tag{4.18}$$

The case in which the damping is bigger than the critical damping is very unusual in dynamics in civil engineering so the damping factor ξ can be used to simplify the second-order homogeneous differential equation.

Also the damped eigenfrequency:

$$\omega_D = \omega_0\sqrt{1-\xi^2} \tag{4.19}$$

can be integrated into the approach and leads to the simplified equation:

$$s = -\xi\omega_0 \pm i\omega_D. \tag{4.20}$$

It should be mentioned that the damping has almost no effect on the eigenfrequency.

The differential equation of a damped single-degree-of-freedom system can be solved:

$$u(t) = e^{\xi\omega_0 t}(C_1 e^{i\omega_D t} + C_2 e^{-i\omega_D t}) \tag{4.21}$$

With the Euler Equation the final term is:

$$u(t) = e^{\xi\omega_0 t}(B_1 sin\omega_D t + B_2 cos\omega_D t). \tag{4.22}$$

4.4 Multiple-degree-of-freedom system

A multiple-degree-of-freedom system has several masses in different positions. Each mass gets a horizontal degree of freedom for the translation u_j assigned. Following essentials of the multiple-degree-of freedom system are predicated in Flesch (1993).

With the equation of motion the differential equations for each mass can be formed:

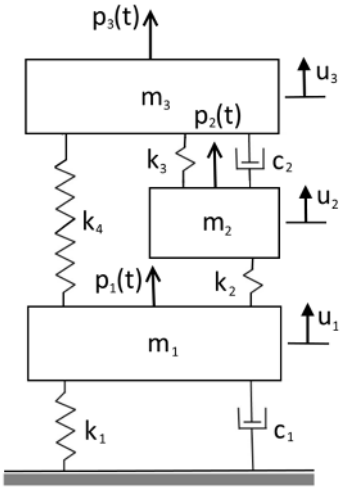

Figure 4-5: Multiple-degree-of-freedom system

$$
\begin{aligned}
m_1\ddot{u}_1 + \sum_{i=1}^{n} c_{1j}\dot{u}_j + \sum_{i=1}^{n} k_{1j}\dot{u}_j &= p_1(t) \\
m_2\ddot{u}_1 + \sum_{i=1}^{n} c_{2j}\dot{u}_j + \sum_{i=1}^{n} k_{2j}\dot{u}_j &= p_2(t) \\
\vdots \qquad\quad \vdots \qquad\quad \vdots \qquad\quad & \vdots \\
m_n\ddot{u}_1 + \sum_{i=1}^{n} c_{nj}\dot{u}_j + \sum_{i=1}^{n} k_{nj}\dot{u}_j &= p_n(t)
\end{aligned}
\tag{4.23}
$$

The components of the equations can be summarized and transformed into matrix notation:

$$[M]\{\ddot{U}\} + [C]\{\dot{U}\} + [K]\{U\} = \{P(t)\} \tag{4.24}$$

With:

- $[M]\ldots$ mass matrix
- $[K]\ldots$ stiffness matrix
- $[C]\ldots$ damping matrix
- $\{U\}, \{\dot{U}\}, \{\ddot{U}\}\ldots$ motion vectors
- $\{P(t)\}\ldots$ load vector.

4.4.1 The eigenoscillation of an undamped multiple-degree-of-freedom system

In case of an undamped multiple-degree-of-freedom system the several masses oscillate constantly with constant amplitude.

The general equation for a free oscillating system has the following form:

$$[M]\{\ddot{U}\} + [K]\{U\} = \{0\}. \tag{4.25}$$

With the approach:

$$\{U\} = \{\overline{U}\}\sin(\omega t + \varphi) \tag{4.26}$$

the homogeneous system of differential equations result:

$$([K] - \omega^2[M])\{\overline{U}\} = \{0\} \tag{4.27}$$

The resulting homogeneous system of equations is solvable if its determinant disappears.

After the disappearance of the determinant the equation:

$$([K] - \omega^2[M]) = \{0\} \tag{4.28}$$

leads to a n-degree polynomial function with n eigenmodes.

For this polynomial function several eigenmodes ω_i, called angular eigenfrequencies are possible.

The results of the system of equations belonging to each ω_i can only be described as ratio. Correlating to each eigenvalue the relative deflection of the mass for each eigenfrequency can be determined. These ratio value form the eigenvalue i.

The eigenmodes can be summarized in the modal matrix:

$$[\psi] = [\{\psi_1\}\{\psi_2\} \dots \{\psi_n\}] \tag{4.29}$$

In the modal matrix the eigenmodes are arranged in order of size, whereby the eigenvalue, which belongs to the smallest eigenfrequency, is defined as base oscillation mode.

A requirement for the system is the orthogonality between the eigenmodes $[\psi_i]$ and $[\psi_j]$:

$$\{\psi_i\}^T[M]\{\psi_j\} = 0 \quad for\ i \neq j \tag{4.30}$$

$$\{\psi_i\}^T[K]\{\psi_j\} = 0 \quad for\ i \neq j \tag{4.31}$$

To calculate the undamped oscillation of the system the displacement $U(\mathrm{t})$ can be constituted as linear combination:

$$\{U(\mathrm{t})\} = \sum_{i=1}^{n} \{\psi_i\} Y_i(t) = [\psi]\{Y(t)\} \tag{4.32}$$

By substituting into the general equation (4.25) and by consideration of the orthogonality relations the differential equation of an undamped multiple-degree-of-freedom system can be written as:

$$\{\psi_i\}^T[M]\{\psi_i\}\{\ddot{Y}(t)\} + \{\psi_i\}^T[K]\{\psi_i\}\{Y(t)\} = \{0\}. \tag{4.33}$$

With the orthogonality relations the system can be separated into several single-degree-of-freedom systems with their specific eigenfrequencies.

4.4.2 The damped multiple-degree-of-freedom system

For the consideration of a damped multiple-degree-of-freedom system also for the damping matrix the orthogonality between the eigenmodes have to exist:

$$\{\psi_i\}^T[C]\{\psi_j\} = 0 \quad for\ i \neq j \tag{4.34}$$

This orthogonality is only an assumption, because the damping-matrix is fully filled, compared to the mass- and the stiffness-matrix which are diagonal matrices.

To avoid complex eigenmodes for the case of a damped multiple-degree-of-freedom system at first the equation for the undamped case has to be solved. After that the damping component can be integrated and leads to a resulting equation for the damped multiple-degree-of-freedom system:

$$\{\psi_i\}^T[M]\{\psi_i\}\{\ddot{Y}(t)\} + \{\psi_i\}^T[C]\{\psi_i\}\{\dot{Y}(t)\} + \{\psi_i\}^T[K]\{\psi_i\}\{Y(t)\} = \{0\} \tag{4.35}$$

4.5 Consideration of damping

For the determination of the mass the density of the material is often known. Additionally the Young's modulus could be determined for nearly every material. Only for the damping no specific parameter for an exact description exists. Due to this fact the Rayleigh-Damping is a common way to consider the damping of a system. According to escoaet (2015) the Rayleigh-Damping is based on the assumption of an orthogonality relation between the eigenvalues of equation (4.34) and hence on the linear combination of the mass matrix and the stiffness matrix:

$$[C] = \alpha[M] + \beta[K] \tag{4.36}$$

Thereby the α −value and the β −value are the unknown parameters. The αM −term is defined as the external damping. It is responsible for the mass proportional damping which occurs at low eigenfrequencies. The βK −term can be specified as the internal damping or as stiffness proportional damping. It has a big influence on high eigenfrequencies. (escoaet, 2015).

Due to the modal viscose damping of the i-nd eigenmode:

$$2\xi\omega_i = \{\psi_j\}^T [C]\{\psi_i\} \tag{4.37}$$

the relation between α, β and the damping factor ξ according to Flesch (1993) can be displayed:

$$\xi_i = \frac{\alpha}{2\omega_i} + \frac{\beta}{2}\omega_n = \frac{c_i}{c_{krit}}. \tag{4.38}$$

The Rayleigh-Damping guarantees a specific damping-factor only in two eigenmodes. The other eigenmodes arise as a result of an interpolation between the two points (Flesch, 1993).

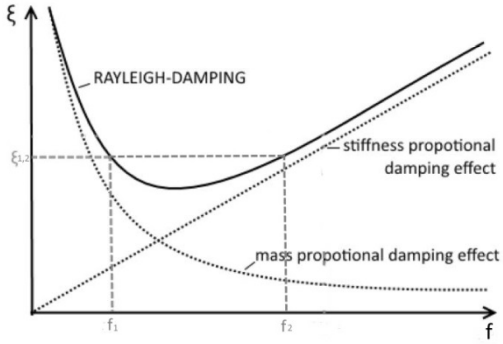

Figure 4-6: Rayleigh-Damping (Pagger, 2014)

In the frequency range between the two eigenmodes a constant damping factor can be formed (escoaet, 2015):

$$\alpha = \frac{\omega_1\omega_2 2\xi}{\omega_1 + \omega_2} = \frac{4\pi f_1 f_2 \xi}{(f_1 + f_2)} \tag{4.39}$$

$$\beta = \frac{2\xi}{\omega_1 + \omega_2} = \frac{\xi}{\pi(f_1 + f_2)} \tag{4.40}$$

5 Hydromechanical basics

The understanding of the equilibrium and the motion of fluids are the main objectives of the hydromechanics. The following pages serve as a short introduction into the essentials of this subject and are based on Gross, et al. (2009).

5.1 General hydro mechanical basics

5.1.1 Properties of fluids

In the event of a deformation of the static fluid without changing the volume only very low resistance forces acting against this, so a static fluid can take any shape while it retains the volume. This acting resistance forces are called shearing forces.

Fluids suffer only slight volume changing anyway so they can be regarded as incompressible.

Newton determined due to experiments on moving fluids a linear correlation between the dynamic viscosity η and the time-based change of the angle γ for shearing forces:

$$\tau = \eta \frac{\partial v}{\partial z} = \eta \dot{\gamma} \tag{5.1}$$

Fluids with this correlation are called Newtonian fluids or viscous fluids.

Ideal fluids are frictionless (η = 0 Pas) as well as incompressible (V = const.).

5.1.2 Hydrostatics

The hydrostatics considers fluids in their static state. A static fluid has special behaviors compared to solid bodies. These behaviors are responsible for the pressure conditions in fluids. The pressure itself is defined as proportion between the force F and the area A:

$$p = \frac{F}{A} \tag{5.2}$$

The unity of the pressure is 1 Pascal (Pa) or 1 N/m². Also 1bar is often used, whereat 1 bar is equal to 10^5 Pascal.

Heavy fluids are fluids with an occurring dead load. The pressure of these fluids increases with the depth.

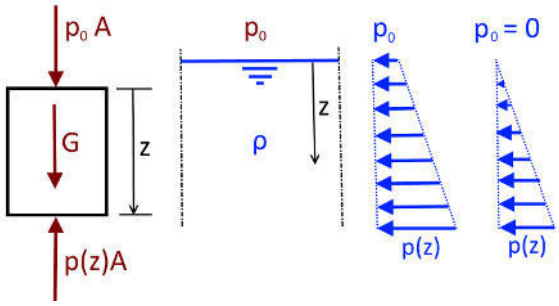

Figure 5-1: Hydrostatic pressure of heavy fluids

$$p(z) = p_0 + \rho g z \tag{5.3}$$

For the case of the fluid water with surrounding atmospheric pressure the term can be written as:

$$p(z) = \rho g z. \tag{5.4}$$

Another specific property of a fluid is the direction independence of the pressure in any depth. Blaise Pascal found out that the pressure of a fluid in each direction has the same value:

$$p = p_x = p_y = p_z \tag{5.5}$$

Hence the pressure p only depends on its location:

$$p = p(x, y, z) \tag{5.6}$$

Due to the not-acting shearing forces only normal stresses occur and the stress tensor can be defined as:

$$\sigma = \begin{bmatrix} -p & 0 & 0 \\ 0 & -p & 0 \\ 0 & 0 & -p \end{bmatrix}. \tag{5.7}$$

5.1.3 The Euler equation for hydrodynamics

The movement of frictionless fluids can be described via the mathematic model of Euler. It's a first order differential equation and a special case of the Navier-Stokes Equation. For the approach an infinitesimal cube is cut out of the fluid, a volume force f is set and the equilibrium equation is established.

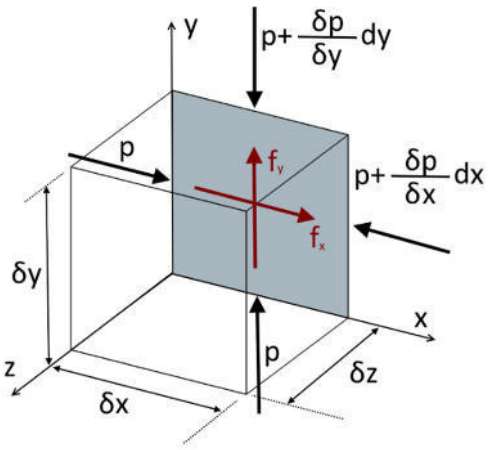

Figure 5-2: Infinitesimal cube for the Euler equation

The equilibrium of forces of the x-y-plane is figured out.

The volume force f is acting on the x-y-plain.

Due to the dependence of the pressure on the location on the two sides of the plane different pressures occur. The force equilibriums in all three directions lead to:

$$pdydz + f_x dxdydz - \left(p + \frac{\partial p}{\partial x} dx\right) dydz = 0 \tag{5.8}$$

$$pdxdz + f_y dxdydz - \left(p + \frac{\partial p}{\partial y} dy\right) dxdz = 0 \tag{5.9}$$

$$pdxdy + f_z dxdydz - \left(p + \frac{\partial p}{\partial z} dz\right) dxdy = 0. \tag{5.10}$$

Out of the equations the correlations result:

$$\frac{\partial p}{\partial x} = f_x = \rho a_x \tag{5.11}$$

$$\frac{\partial p}{\partial y} = f_y = \rho a_y \tag{5.12}$$

$$\frac{\partial p}{\partial z} = f_z = \rho a_z \tag{5.13}$$

The parts can be summarized to:

$$dp = \frac{\partial p}{\partial x} dx + \frac{\partial p}{\partial y} dy + \frac{\partial p}{\partial z} dz. \tag{5.14}$$

The extension of the equation (5.8) with the inertia force leads to:

$$pdydz + f_x dxdydz - \left(p + \frac{\partial p}{\partial x} dx\right) dydz - \frac{dv_x}{dt} \rho \, dxdydz. \tag{5.15}$$

This also can be done for the two other directions.

After division following formula arises:

$$\frac{dv_x}{dt} = a_x - \frac{1}{\rho} \frac{\partial p}{\partial x} \tag{5.16}$$

Summarized the total derivation, containing a local and a convective part, can be written as:

$$\frac{dv_x}{dt} = \frac{\partial v_x}{\partial t} + v_x \frac{\partial v_x}{\partial x} + v_y \frac{\partial v_x}{\partial y} + v_z \frac{\partial v_x}{\partial z}. \tag{5.17}$$

For all three directions the Euler Equation for incompressible, frictionless fluids in vector notation is:

$$\vec{a} = \frac{d\vec{v}}{dt} + (\vec{v} \cdot \nabla)\vec{v} + \frac{1}{\rho} \nabla p \tag{5.18}$$

5.1.4 Hydrostatic pressure on plain surfaces

A static fluid stresses surrounding structures by the hydrostatic pressure. For the mathematical approach of this pressure a specific area of the surface must be taken. This area A is inclined by the angle α.

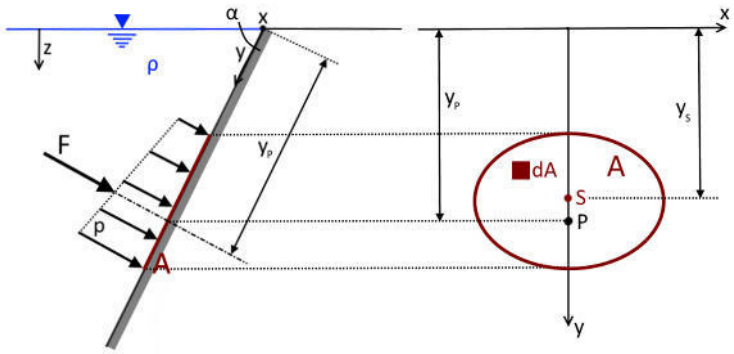

Figure 5-3: Hydrostatic pressure on plain surfaces based on Gross, et al. (2009)

The resulting water load F on the surface can be calculated by integration over the area A by:

$$F = \int_A p \, dA. \tag{5.19}$$

The pressure p results out of the simple formula:

$$p = \rho g z \tag{5.20}$$

by neglecting the atmospheric pressure p_0. In Figure 5-3 the correlation between the depth z and the value y by the sine-function is obvious and leads to:

$$p = \rho g y sin\alpha. \tag{5.21}$$

The insertion of equation p into equation F defines the water load F more precisely:

$$F = \rho g sin\alpha \int_A y\, dA \tag{5.22}$$

With the formula:

$$\int_A y\, dA = y_s A \tag{5.23}$$

and the angle relation:

$$z_s = y_s sin\alpha \tag{5.24}$$

the water pressure *F* on a plain surface can be written as:

$$F = \rho g z_S A. \tag{5.25}$$

Now the magnitude of the orthogonally acting water pressure on the plain surface is known, but the location of the centre of the pressure is already unknown.

With the water pressure *F* and its reaction force an equation of the moments can be formed:

$$F * y_P = \int_A yp\, dA = \rho g sin\alpha \int_A y^2\, dA \tag{5.26}$$

The area moment of inertia:

$$I_X = \int_A y^2\, dA \tag{5.27}$$

and the static moment:

$$S_x = \int_A y\, dA \tag{5.28}$$

helps to form the formula to calculate the y-component of the centre of the pressure:

$$y_P = \frac{I_x}{S_x} = \frac{I_x}{y_S A}. \tag{5.29}$$

For non-symmetric areas the x-component can also be calculated over moment relations around the y-axis:

$$Fx_P = \int_A xp\, dA \tag{5.30}$$

and results in:

$$x_P = -\frac{I_{xy}}{S_x} = \frac{I_{xy}}{y_s A}. \tag{5.31}$$

5.1.5 Hydrostatic pressure on curved surfaces

For the calculation of the hydrostatic pressure F on the curved surface the splitting of the force into its components is necessary.

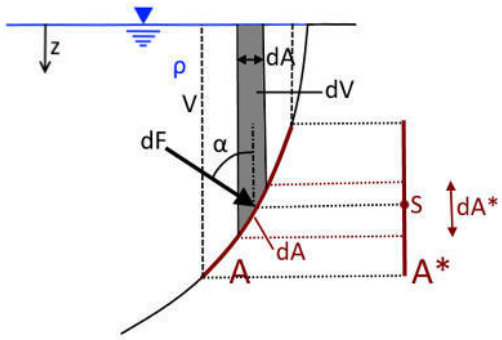

Figure 5-4: Hydrostatic pressure on curved surfaces
based on Gross, et al. (2009)

The components can be written as:

$$dF_H = p\, dA sin\alpha = pdA^* \tag{5.32}$$

$$dF_V = p\, dA cos\alpha = \rho g z\, d\bar{A} = \rho g\, dV. \tag{5.33}$$

The integrations over the volume V and the area $A*$ lead to the two forces:

$$F_H = \int p\, dA^* = \rho g \int z\, dA^* \rightarrow \tag{5.34}$$

$$F_H = \rho g z_s A^* \tag{5.35}$$

$$F_V = \rho g \int dV \rightarrow \tag{5.36}$$

$$F_V = \rho g V \tag{5.37}$$

The centre of the orthogonally acting water pressure F on curved surfaces can be calculated over the same formulas as in the case of a plain surface. The horizontal force component acts in the centre of the vertical projected surface and the vertical force component occurs in the centre of the horizontal projected surface.

5.1.6 Uplift

The uplift force of a static fluid equates to the dead load of the replaced fluid.

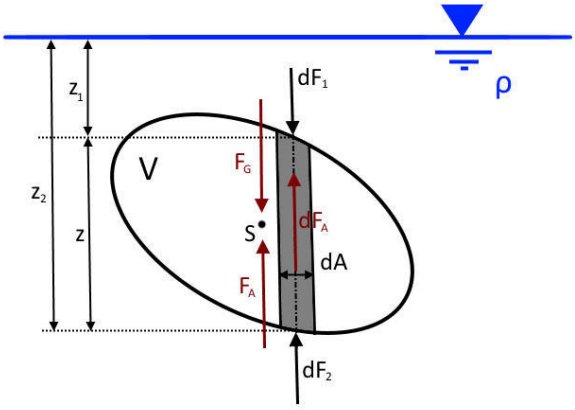

Figure 5-5: Uplift force of a fluid based on Gross, et al. (2009)

The forces dF_1 and dF_2 acting on the body:

$$dF_1 = \rho g z_1 dA \tag{5.38}$$

$$dF_2 = \rho g z_2 dA \tag{5.39}$$

$$dF_A = dF_2 - dF_1 = \rho g V dA = \rho g (z_2 - z_1) dA \tag{5.40}$$

The resulting uplift force F_A can be calculated by integration over the volume V:

$$F_A = \int_V \rho g \, V \tag{5.41}$$

5.2 Hydrostatic pressure on radial gates

Radial gates are stressed during their lifetime by different forces. In case of an open gate the structure can be underflowed or overflowed. If one of these two cases happens hydrodynamic forces occur in the flow area. Also operation forces by lifting and lowering the gate can appear. Due to the fact that steel is a good head conductor also temperature loads can strain the gate. Similar to the load on a gravity dam also a radial gate can be stressed by floating debris or ice. The common loading case is a combination of the hydrostatic load on the radial gate and the dead load of the steel structure. In case of an impulse in consequence of an earthquake also additional dynamic loads can act in terms of accelerations.

The following rudiments based on Erbisti (2004) supply the water load on the structure and the bearing forces in the pivot of the radial gate.

The geometry of the gate has a big influence on the angle and the magnitude of the resulting water load. The following calculation procedure is for the case of a vertical position of the pivot between the upper and lower end of the gate. To locate the pivot point the heights h_1 and h_2 as well the angles α_1 and α_2 are necessary. The height h, the radius R and the width b of the gate define the rough geometry.

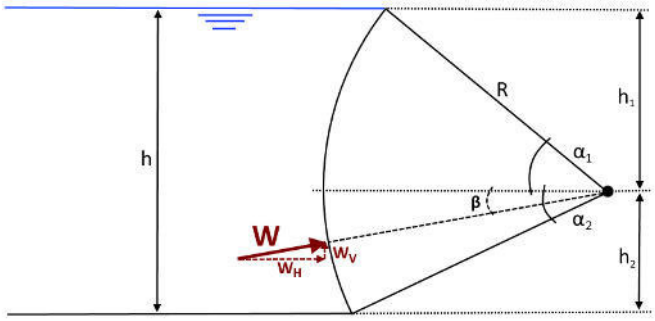

Figure 5-6: Geometry definitions for the calculation of the water load and the bearing forces

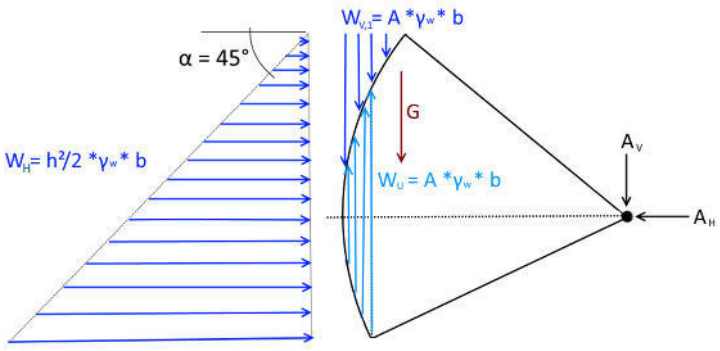

Figure 5-7: Horizontal and vertical components of the water load and the bearing force

With the simple equation $\sum F_H = 0$ the horizontal bearing force A_H results out of:

$$A_H = W_H = \frac{h^2}{2}\gamma_W b \tag{5.42}$$

Also the vertical bearing force can be calculated over the equation $\sum F_V = 0$:

The uplift force W_u acts against the dead weight of the gate G and the vertical water load component $W_{v,1}$.

$$A_V = W_V = W_U - G - W_{V,1} \tag{5.43}$$

$$A_V = W_V = A_6\gamma_W b - G - A_5\gamma_W b \tag{5.44}$$

The variables A_5 and A_6 are defined as these areas:

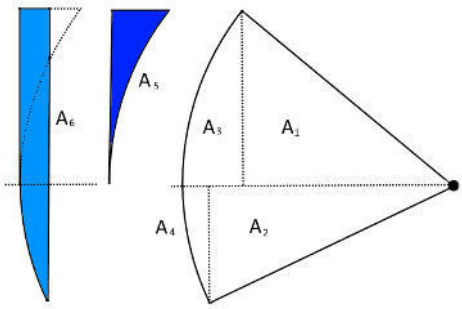

Figure 5-8: Definition of the uplift section and the vertical water load section

Finally the resulting water load on the radial gate with the angle β can be calculated with:

$$W = \sqrt{{W_H}^2 - {W_V}^2} \tag{5.45}$$

$$\beta = arctan\left(\frac{W_V}{W_H}\right). \tag{5.46}$$

The resulting bearing force A have to be divided by 2 to get the bearing force on each abutment pier.

5.3 Static loads on gravity dams

Different static loads can occur on a gravity dam simultaneously. In addition to the gravity load and the upstream water pressure also the downstream hydrostatic water pressure, the silt load and the uplift load can arise. Especially on gravity dams often loads due to temperature have to be considered too. Due to an earthquake event or bounce forces of floating solid bodies like debris and ice also dynamic forces can stress the structure.

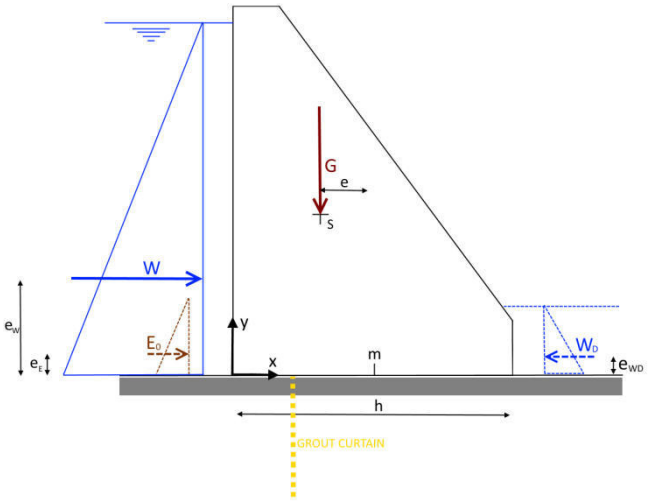

Figure 5-9: Static loads on a gravity dam

The stability analysis of a gravity dam can simply be done with the rigid-body-method consisting of a two-dimensional triangular dam on a rigid foundation with a rough contact path with the friction angle φ. Therefore the structural safety, the stability of the foundation and the sliding stability have to be proofed.

The following approaches are used for the analytical stability analysis of a gravity dam (Institut für Wasserbau und Wasserwirtschaft, 2012):

At first the mass center and the section modulus of the two-dimensional structure must be calculated:

$$x_s = \frac{\sum A_i x_i}{\sum A_i} \tag{5.47}$$

$$y_s = \frac{\sum A_i y_i}{\sum A_i} \tag{5.48}$$

$$W = \frac{bh^2}{6} \tag{5.49}$$

The following graphics show common stress distributions in the contact path of a gravity dam. Beside the figures the formulas for the different loads are summarized.

The stresses in the contact path can be calculated with:

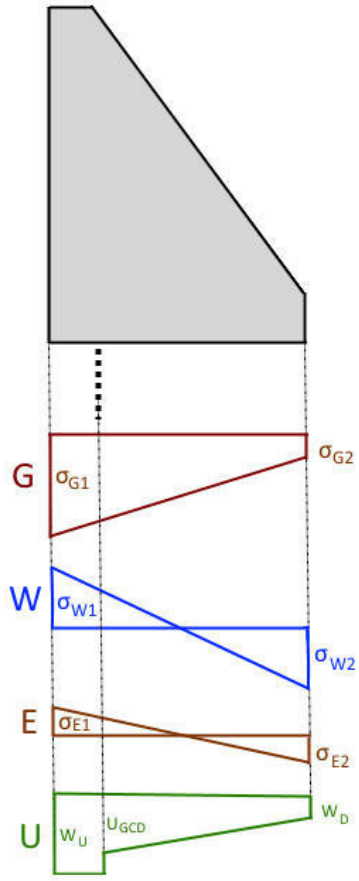

Figure 5-10: Common stress distributions in the contact path of a gravity dam

$$\sigma_{1,2} = \frac{N}{A} \pm \frac{M}{W}. \tag{5.50}$$

Dead Load *G*:

$$G = A\gamma_c \tag{5.51}$$

$$M_G = Ge \tag{5.52}$$

The distance *e* for the calculation of the moment M_G is defined in Figure 5-9 .

Water load upstream W_u:

$$w_u = h_{wu}\gamma_W \tag{5.53}$$

$$W_u = \frac{{h_{wu}}^2}{2}\gamma_W \tag{5.54}$$

$$M_W = W_u \frac{h_{wu}}{3} \tag{5.55}$$

Water load downstream W_d:

$$\sigma_{1,2} = \frac{N}{A} \pm \frac{M}{W}. \tag{5.56}$$

$$w_d = h_{wd}\gamma_W \tag{5.57}$$

Earth pressure at rest *E*:

$$K_0 = 1 - sin\varphi \tag{5.58}$$

$$e_{0,g,H} = \gamma' z(1 - sin\varphi) \tag{5.59}$$

$$E_{0,g,H} = \gamma'(1 - sin\varphi)\frac{{h_S}^2}{2} \tag{5.60}$$

$$M_{E_{0,g,H}} = E_{0,g,H}\frac{h_S}{3} \tag{5.61}$$

Uplift *U*:

$$u_{GCD} = \frac{2}{3} w_u \tag{5.62}$$

$$U = \int_A u(x)\, dx \tag{5.63}$$

The dynamic loads on the structure due to an earthquake can be assumed over the pseudo-static method with equivalent static forces. These additional water and dead loads result from following formulas:

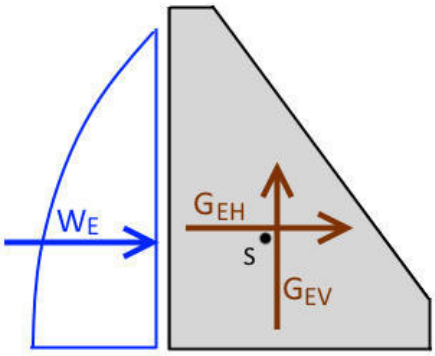

Figure 5-11: Equivalent static loads due to the seismic loading

$$a_{eff} = 0.7 a_{max} \tag{5.64}$$

$$a_H = a_{eff} g;\ a_V = \frac{2}{3}\, a_H \tag{5.65}$$

$$W_E = \frac{7}{8} \rho_W A_W \sqrt{h_W z_i}\, a_{eff} \tag{5.66}$$

$$G_{EH} = a_{eff} A_G \rho_G \tag{5.67}$$

$$G_{EV} = \frac{2}{3} G_{EH} \tag{5.68}$$

The DIN 19700-11 (2004) standardizes in addition to the normal operation case two loading conditions, for which a sliding safety analysis have to be done:

Normal operation:

$$s_{nop} = \frac{(G - 0.85U) tan\varphi + bc}{W + E_{0,g,H}} \geq 1.5 \tag{5.69}$$

OBE (operating basis earthquake):

$$s_{spl} = \frac{(G - 0.85U - G_{EV}) tan\varphi + bc}{W + E_{0,g,H} + W_E + G_{EH}} \geq 1.3 \tag{5.70}$$

MCE (maximum credible earthquake):

$$s_{spl} = \frac{(G - 0.85 * U - G_{EV}) tan\varphi + bc}{W + E_{0,g,H} + W_E + G_{EH}} \geq 1.2 \tag{5.71}$$

In the formulas (5.69), (5.70) and (5.71) the uplift is reduced by 85 % due to the Austrian approach.

The US Army Corps of Engineers defines in the guideline EM 1110-2-2000 (1995) other safety factors for the usual, the unusual and the extreme earthquake event.

Sliding Safety Requirements			
		DIN 19700-11	US Army Corps of Engineers EM 1110-2-2200
Load Case	Usual	1.5	2.0
	Unusual	1.3	1.5
	Extreme	1.2	1.1

Table 5-1: Sliding safety requirements

6 Modelling and calculation methods for dynamic simulations

6.1 Calculation methods for dynamic simulations

For the dynamic simulation of structures different methods can be used which differ from each other due to their accuracy.

Depending on the structure type according to Flesch (1993) in dynamic simulations different interactions have to be considered:

- building – foundation
- building – installed facilities
- building – surrounding medium

The knowledge of the occurring loads and their properties are of interest. Thereby different parameters can be necessary depending on the required accuracy. Sometimes the knowledge about the maxima of the oscillation (accelerations, displacements, etc.) are enough information for the calculation, otherwise for complex simulations the whole time history or the frequency content is needed to get comprehensive results. (Flesch, 1993)

For the modelling of structures in civil engineering Flesch (1993) mentions the frequently requirement of multiple-degree-of-freedom systems with mass-, stiffness- and damping matrices. The results of the system of equations can be approximated via different calculation methods.

Methods		Modelling of			Field of Application
		Reservoir	Foundation	Dam	
Static	Pseudo Static	Added Mass	Rigid	Linear	Concrete Dams of secondary importance and Embankment Dams
Dynamic	Appr. Dynamic	Added Mass	Rigid	Linear	Concrete Dams of secondary importance and Embankment Dams
	Modal Analysis Response Spectrum	Added Mass	FEM, Massless	Linear	Concrete Dams and Embankment Dams, Standard Method for Linear Analysis
	Modal Analysis Time History	Added Mass	FEM, Massless	Linear	Concrete Dams and Embankment Dams, Standard Method for Linear Analysis
	Frequency Domain	FEM / BEM	BEM	Linear	Concrete Dams to consider Radiation Damping
	Direct Integration	Added Mass	FEM, Massless	Nonlinear	Concrete Dams and Embankment Dams to consider Nonlinerarities

Figure 6-1: Calculation methods for dynamic simulations (Österreichische Staubeckenkommission, 2001)

For the dynamic simulation for structures in civil engineering a range of commercial and open-sourced computer programs exist.

The introduction of the different methods is based on Flesch (1993) and Österreichische Staubeckenkomission (2001).

6.1.1 Pseudo-static method

The pseudo-static method is the simplest way to consider seismic loads on a structure. With the assumption of a time-independent equivalent static load the system can be simplified. This equivalent static load results out of the product of the seismic coefficient ε and the dead load of the structure.

Three different versions for the determination of the equivalent static load are common:

- Constant acceleration distribution due to the earthquake over the height of the structure
- More detailed calculation of the accelerations by comprehension of the first eigenmode of the structure
- Determination of the acceleration with the first eigenmode and the first eigenfrequency as base.

This method can be used for dams of secondary importance, because the calculation leads in rare cases to conservative results. Due to this fact strict criteria for the stability analysis must be achieved.

6.1.2 Dynamic approximation

The dynamic approximation is a way to consider the seismic accelerations on a structure with a pseudo-static method. Therefore common methods according to Chopra, Newmark or Makdisi/Seed, which are based on parameter studies, can be used. Chopra applies in his method for gravity dams a mass distribution based on the first eigenoscillation, a rigid foundation and added masses according to Westergaard.

6.1.3 Modal analysis with the response spectra method

In the first step of a modal analysis the system has to be split up into several independent single-degree-of-freedom systems. These single-degree-of-freedom systems possess different eigenfrequencies and dampings. After this the response of each system can be calculated by determination of the maximum displacements, oscillation velocities and accelerations for each eigenfrequency. By plotting the maximum values dependent on the eigenfrequencies the response spectra can be built.

Due to the fact that the simultaneous occurrence of the maximum values of each mode is unlikely and an exact result of a multiple-degree-of-freedom system specific superposition procedures have to be implemented.

There are several superposition methods described in literature, the most common methods are mentioned on the following page.

The common formula for the superposition is the SRRS (Square-Root-of-Sum-of-Square):

$$N = \sqrt{\sum_{i=1}^{n} N_i} \tag{6.1}$$

With:

N… Total value of a random displacement value

Ni… Ratio of the eigenmode i on the displacement value

The SRRS – formula is the standard superposition formula for these purposes.

In case of a system with small intervals between the eigenfrequencies the maximum response can be underestimated. For these cases the CQC-method (Complete quadratic combination) is common. It avoids the problem of underestimation but the computing time is longer.

$$\mathrm{N} = \sqrt{\sum_{i=1}^{n}\sum_{j=1}^{n} N_i \varrho_{ij} N_J} \tag{6.2}$$

With:

N… Total value of a random displacement value

Ni… Ratio of the eigenmode i on the displacement value

Nj… Ratio of the eigenmode j on the displacement value

ϱ_{ij}... Factor of interpendency

The added mass technique according to Westergaard and the approach of the foundation as massless finite elements are possible for modal analyses with the response spectra method.

6.1.4 Modal analysis with the time history method

The time integration of each mode due to the acceleration time histories is essential for this modal analysis method. Thereby the results are superposed mode by mode to get time histories for the total structure response. This method has the advantage that time histories can be computed, not only maximum values as with the response spectra method.

6.1.5 Calculation within the frequency domain

With the calculation within the frequency domain the differential equations are solved by integral transformations. At first the loads have to be transferred from the time domain into the frequency domain. After that the equations can be solved in the frequency domain. Here each frequency can be computed by a simple static calculation with a complex stiffness matrix. At last the results must be transferred back into the frequency domain.

For the integral transformation different algorithm exist. This method is often used for a more precise consideration of fluid-structure interactions, but it is only applicable to linear simulations.

6.1.6 Direct time integration method

The direct time integration method is the most exact way for seismic simulations, but also the most complex one. A time discretization is necessary for this method. For the time integration the finite difference method is used in case of an explicit method. The method according to Newmark is common for implicit solutions. For the direct integration method the whole time history of the earthquake event is needed.

The advantage of this method is the possibility of the computation of nonlinear problems. A disadvantage is the big computing time especially in case of nonlinear problems.

The solution of nonlinear problems can be done with an implicit or an explicit method. The differences of these solution methods are figured out according to Bathe (2002).

- **Explicit solution:**
  In case of an explicit solution the conditions of the timestep t_n are used between the timestep t_n and the timestep t_{n+1}. These conditions are extrapolated from the previous step to the subsequent step. With increasing time steps the explicit method leads to increasing deviations. More accuracy can be achieved by choosing smaller increment steps. Less computing time for each step is necessary.

- **Implicit solution:**
  Based on the timestep t_n the equation of motion for the step t_{n+1} is getting constructed and solved. The iterations must be done until convergence is reached. A big computing time is necessary for implicit solutions due to the iteration processes but bigger time increments are possible compared to the explicit method.

6.2 Essentials for the dynamic simulation of gravity dams

Earthquakes occur in the solid earth due to volcanic, tectonic or artificially initiated stimulation. Tectonic earthquakes are the heaviest and the most common one. These quakes arise by plate movements and fractions in the earth crust. The centers of tectonic earthquakes are in depths between 70 and 720 kilometers, there waves and as result accelerations originate and propagate through different layers to the earth surface (Wieland, 1978).

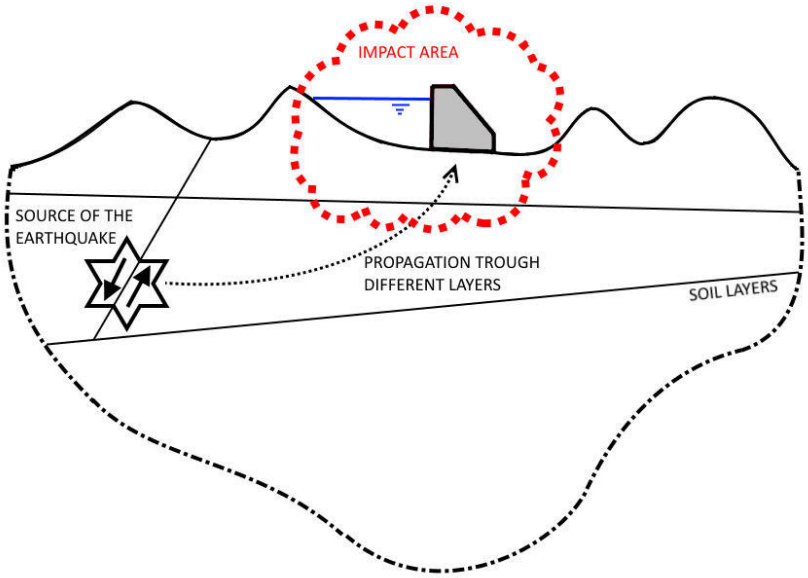

Figure 6-2: Modelling scheme of seismic simualtions based on Meskouris, et al. (2011)

The basement naturally has “infinite” dimensions. For simulation boundaries have to be defined in most cases. The difficulty of the assumption of these model borders is to hold the influence of the limits on the dynamic behavior as little as possible. Due to the big decreasing of the displacements over the depth of the foundation the influence of the model limits in numeric simulations is small in cases of conservative geometry assumptions (Österreichische Staubeckenkommission, 2001).

In cases of dams of secondary importance or in case of earth- or rock fill dams with low stiffnesses compared to the surrounding foundation the dam can be directly supported by rigid bearings. (Österreichische Staubeckenkommission, 2001) For the simulation of taller concrete dams the numerical model has to consist of following parts:

- gravity dam
- foundation
- reservoir

A common modelling technique for the foundation is the definition as massless, limited, linear elastic structure. Due to the fixation in all three directions there is no space for the movement of the rock mass due to a seismic stimulation. This circumstance and the uncertainties of the rock properties lead to a simplified assumption of the foundation as massless rock. The damping behavior can be assumed with

the damping values of the gravity dam due to the similar material properties of the concrete and the rock. The bottom boundary and the vertical boundaries can be defined as rigid bearings. The flexibility of the contact path of the gravity dam can be considered in this way however the radiation damping of the foundation has to be neglected so the earthquake may be overrated (Österreichische Staubeckenkommission, 2001).

Conventional stability analyses of gravity dams can be done with a two-dimensional plain strain model. For more precise considerations of specific parts in most cases a three-dimensional model is more accurate.

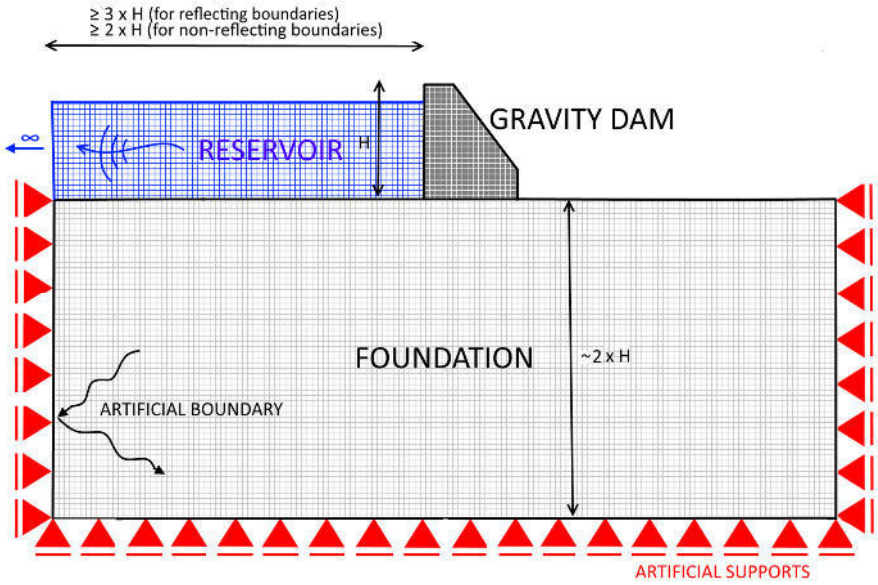

Figure 6-3: Common two-dimensional model for seismic simulations of gravity dams

As a rule of thumb the height of the foundation can be assumed as 2 times the height of the dam. The length of the reservoir and the horizontal length between the downstream end of the dam and the vertical boundary should be at least three times the height of the dam for models with reflecting reservoir boundaries. In case of a definition of the reservoir's back boundary as non-reflecting a length of 2 times the dam height is sufficed. (Österreichische Staubeckenkommission, 2001).

The stimulation of the system due to the stress of an earthquake can arise in various ways depending on the calculation method. In case of the direct integration method the vertical accelerations are applied on the horizontal boundary and the horizontal accelerations are appointed on the vertical boundaries. Thereby the same magnitude on every node can be chosen as simplification. In case of modal analyses global horizontal and vertical accelerations or response spectra has to be defined. Another assumption is the simultaneous appearance of the accelerations on each node.

Different material parameters are necessary to correctly take the dynamic behavior of the parts into consideration. For the concrete of the gravity dam and the foundation the density, the Young's modulus and the Poisson's ration are important. The water can be considered by Westergaard's added mass technique or with compressible acoustic finite elements. For acoustic elements the density and the bulk modulus have to be defined.

In coincidence with the modelling following regions and interactions have to be surveyed:

- dam-foundation – interaction
- dam-reservoir – interaction
- reservoir-foundation – interaction
- water surface
- reservoir boundaries
- possibly symmetric conditions

The interaction between the foundation and the dam can be supposed as nonpositive connection. (Österreichische Staubeckenkommission, 2001) Also between the dam and the reservoir's acoustic elements a tie constraint can be assumed. On the water surface the pressure has to be declared as zero. To avoid the water wave reflection due to the earthquake on the back vertical boundary the surface must be defined as non-reflecting.

In the following point the ways to consider the interaction between the reservoir and the dam in seismic simulations is professed in more detail.

6.2.1 Consideration of the hydrodynamic pressure on the structure

There are different possibilities to consider the hydrodynamic pressure on structures. For fluid-structure-interaction simulations the approaches can be separated into analytical procedures and modelling procedures via finite elements or finite volumes.

The following consideration opportunities according to Institut für Wasserbau und Wasserwirtschaft (2013) for fluids exist:

- Added mass techniques
    - Added masses by Westergaard
    - Added masses by Zangar
- Acoustic Elements
- Fluid Elements
- Eulerian Finite Elements
- Lagrangian Finite Elements
- Smoothed Particle Hydrodynamics

Due to the used methods in the simulation only the added mass technique according Westergaard and the acoustic elements are declared in detail.

6.2.1.1 Westergaard's added mass technique

The added mass technique by Westergaard is a classic, analytical way to consider the hydrodynamic pressure on structures. The mass of the reservoir is replaced by mass points on the structure's surface. The mass points are located in the interacting surface nodes of the elements of the structure. The value of these masses depends on the surface area of the elements. In case of this procedure no discretization of the water is necessary and surface waves of the water are neglected. The limits of these methods are the consideration of only horizontal movements and the negligence of resonance effects (Österreichische Staubeckenkommission, 2001).

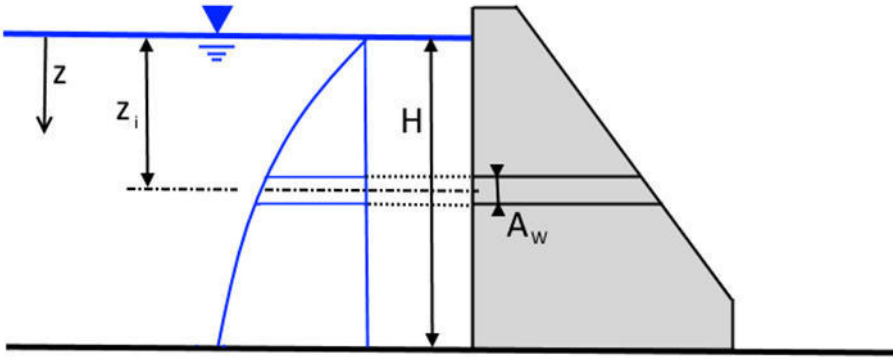

Figure 6-4: Westergaard's added mass technique based on Goldgruber (2011)

The added mass for an element with the area A_W can be calculated with the following formula according to Goldgruber (2011):

$$m_W = \frac{7}{8}\rho A_W \sqrt{H z_i} \tag{6.3}$$

For the most cases the procedure according Westergaard is sufficient and leads to conservative results. In cases of slim structure as arch dams other procedures like acoustic elements better represent the physical behavior of the reservoir. (Institut für Wasserbau und Wasserwirtschaft, 2013).

6.2.1.2 Acoustic elements

The acoustic elements are derived from fluid dynamics. In case of the method with acoustic elements the fluid has to be discretized with finite elements. These finite elements possess only one degree of freedom, namely the pressure. The elements are defined as compressible, frictionless, homogeneous and irrotational with a constant density. (Institut für Wasserbau und Wasserwirtschaft, 2013)

The procedure with acoustic elements is a combination of Newton's law of motion and the continuity equation.

The general equation of motion for an acoustic medium is:

$$\nabla \cdot p + \rho_W \dot{v} = 0 \tag{6.4}$$

The time derviation of formula (6.4) is:

$$\frac{\partial^2 \rho}{\partial t^2} + \rho_W \nabla \cdot \dot{v} = 0 \tag{6.5}$$

The continuity equation is defined as:

$$\frac{\partial p}{\partial t} + \rho_W \nabla \cdot v = 0 \tag{6.6}$$

The constitutive law is:

$$\partial p = {c_W}^2 \partial p \tag{6.7}$$

With the wave propagation speed c_W:

$$c_W = \sqrt{\frac{K}{\rho_W}} \tag{6.8}$$

With the previous formulas the linear acoustic wave equation can be formed:

$$\frac{\partial^2 p}{\partial t^2} - {c_W}^2 \nabla^2 \cdot p = 0 \tag{6.9}$$

7 Numerical simulation of the gravity dam in Abaqus/CAE

For the discretization and simulation the commercial finite-element-analysis software Abaqus/CAE is used. Abaqus supplies different modules for standard implicit or explicit simulations, for computational fluid dynamics or for electromagnet models. It provides a simple interface for the preprocessing operations. Nevertheless the result of the preprocessing work is the generation of an input file to run the job. Also the post processing by evaluation and visualization can be done with Abaqus/CAE. (Dassault Systemes, 2013)

In addition for visualization purposes and evaluation of the results the scripting language Python 2.7 with the packages Numpy and Matplotlib is applied.

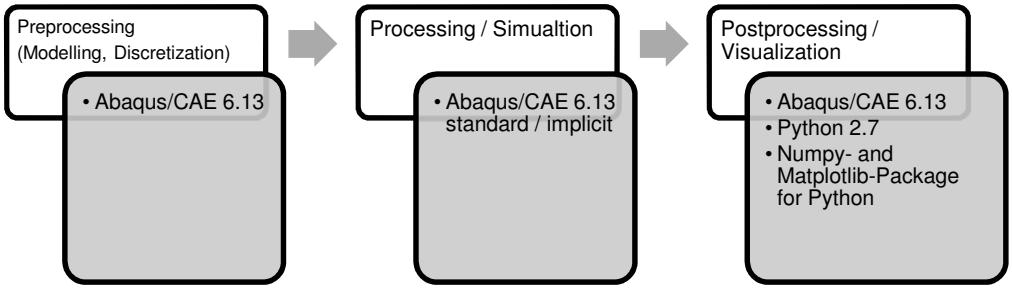

Figure 7-1: Components and tools for the numerical simulation

The base of the model is the geometry of the storage hydro power plant Birecik in Turkey. This hydro power plant consists of a left and a right embankment dam, a powerhouse, the intake concrete structure as well the spillway with stilling basin. For the seismic simulation one section of the 60 meters high spillway part with installed radial gate is cut out.

A three-dimensional model is designed in Abaqus/CAE to incorporate the influences in Y-direction on the abutment of the radial gate.

The three-dimensional numerical model consists of following parts:

- Gravity dam
- Reservoir
- Foundation
- Radial gate

These parts are connected by constraints. Orthogonal to the flow direction symmetry constraints as described in 7.3.1 are defined to prevent motions in this direction.

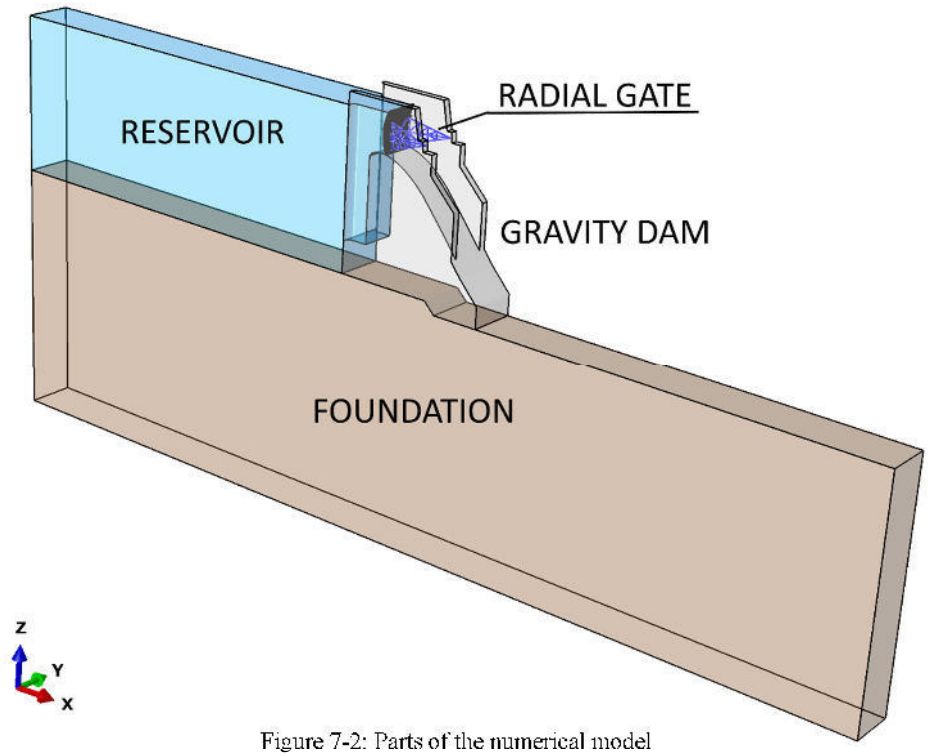

Figure 7-2: Parts of the numerical model

The system is supported by horizontal and vertical bearings at the foundation boundaries.

On the spillway the radial gate with a fitted flap is installed. The installed flap guarantees an exact adjustment of the water level and the discharge of a defined water flow.

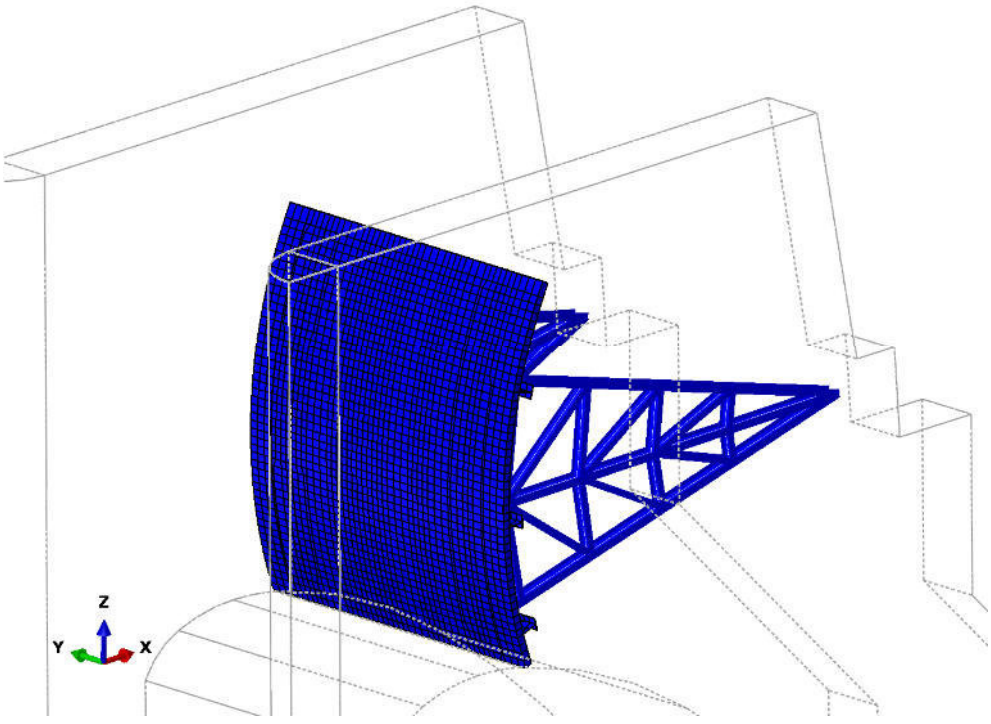

Figure 7-3: Radial gate part

7.1 Geometry

The geometry of the model is caused by the width of the spillway section and the assumption of the artificial boundaries of the reservoir and the foundation.

The height of the gravity dam is settled with 62.50 meters. The stored water reservoir with a height of 58 meters leads to a freeboard of 4.50 meters. The assumed length of the reservoir is about 2.5 times the height of the reservoir. Also the downstream distance of the foundation is about 2.5 times the height of the reservoir. The height of the foundation is 1.5 times the height of the gravity dam. The width of one spillway section is 17.50 meters, whereby the five meters wide piers are cut in the middle.

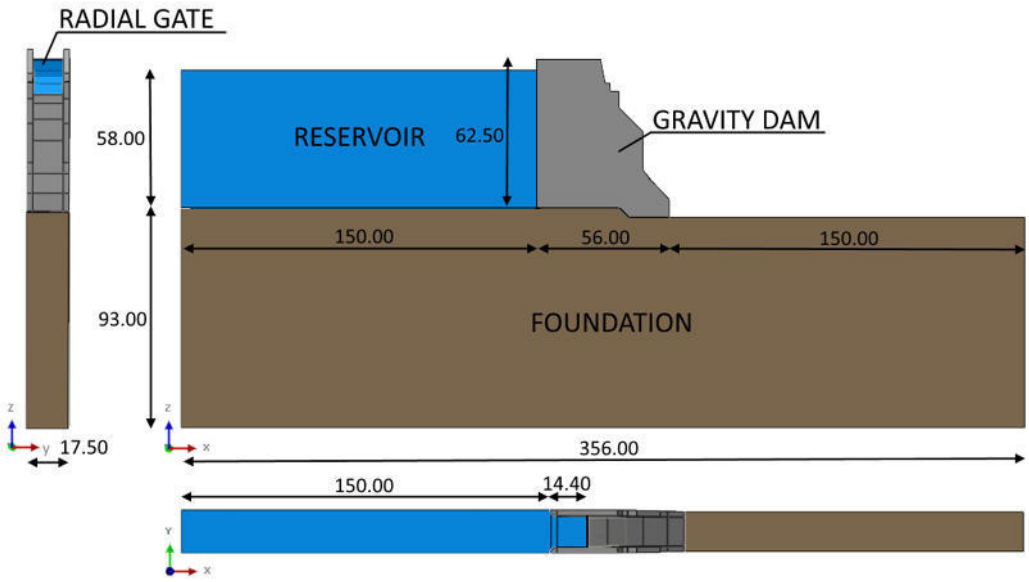

Figure 7-4: Geometry of the general model

The radial gate consists of a curved skin plate with main girders and secondary girders, radial framework arms and diagonal bracings. On both sides the gate is pivoted at the pier's downstream side. The rotation of the gate is assumed as locked.

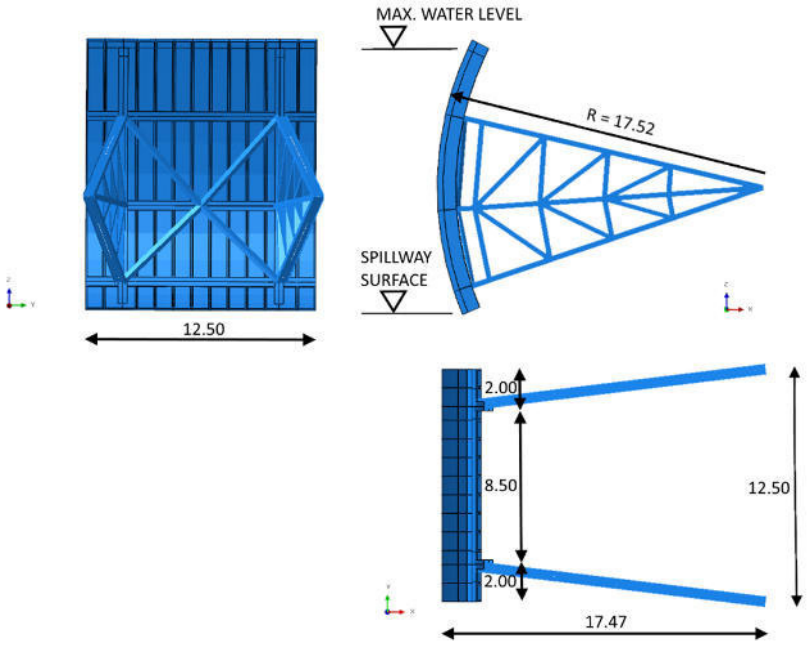

Figure 7-5: Geometry of the radial gate

Due to the lack of schemes for the geometry of the radial gate random cross section dimensions are used.

The width of the gate is 12.50 meters. The radius of the curved skin plate is defined with 17.52 meters. The plate is supported by diagonal bracings. The framework arms are inclined outward to the piers.

7.2 Material definitions

For the right consideration of the mechanical behaviors different materials for each part are defined.

The foundation is assumed as massless, homogeneous material with zero density. For the simulations the radial gate is defined as massless or as steel part with a density of 0.0078 kt/m³. The material properties of the four parts are shown in Table 7-1:

Material properties				
Part	Density [kt/m³]	Young's Modulus [MPa]	Poisson's Ratio [-]	Bulk Modulus [MPa]
Gravity Dam	0.0024	25000	0.17	x
Foundation	0	30000	0.2	x
Reservoir	0.001	x	x	2200
Radial Gate	0 or 0.0078	210000	0.28	x

Table 7-1: Material properties of the parts

7.3 Boundary conditions

7.3.1 Symmetry boundary condition

One spillway section is removed from the residual gravity dam due to symmetry. In case of a cut-out symmetry conditions have to be put on the vertical boundaries. For the numerical model the dam has to be held in y-direction. That means displacements in y-direction are prohibited. Also rotations around the z-axis are inadmissible. Figure 7-6 shows the surfaces for the symmetry boundary condition only on the orthographic right side. The same conditions are set on the left side.

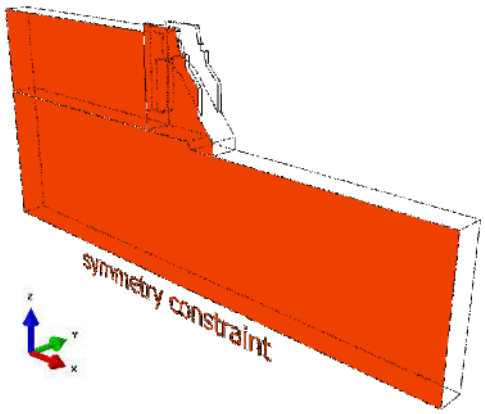

Figure 7-6: Symmetry boundary condition

7.3.2 Tie constraints

The gravity dam is in contact with the reservoir by a tie constraint. Due to the assumed similar material behavior of the gravity dam and the foundation the contact path also can be designed as a tie constraint. The radial gate is installed over a coupled connection on the spillway pier.

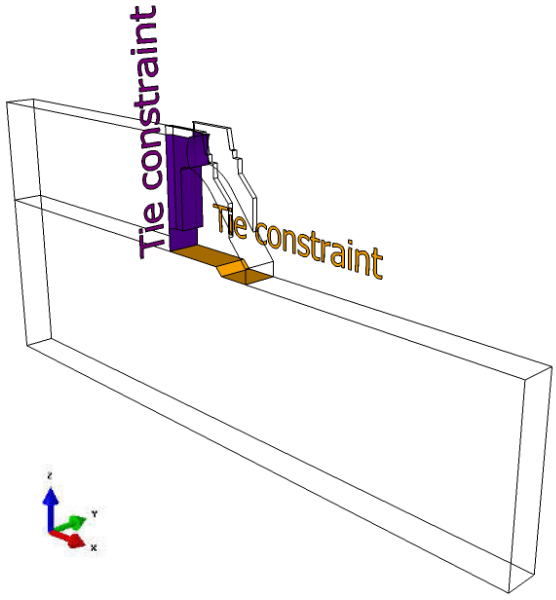

Figure 7-7: Tie constraints in the model

7.3.3 Supporting conditions in static steps

The numerical model is in static steps supported by rigid bearings on the horizontal and vertical artificial boundaries of the foundation. Thereby the movement in x-direction is locked on the vertical borders and the movement in z-direction is avoided on the horizontal border.

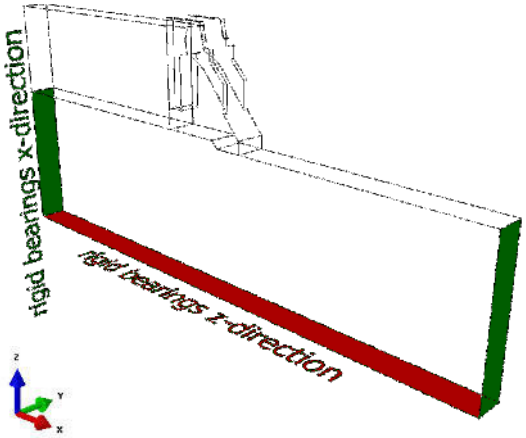

Figure 7-8: Supporting conditions in static steps

7.3.4 Boundary conditions for the acoustic elements

To avoid reflections of the acoustic waves caused by an earthquake on the free field simulated boundary of the reservoir the vertical surface has to be defined as non-reflecting for absorption. In case of using acoustic elements the water surface has to be specified as surface with zero pressure.

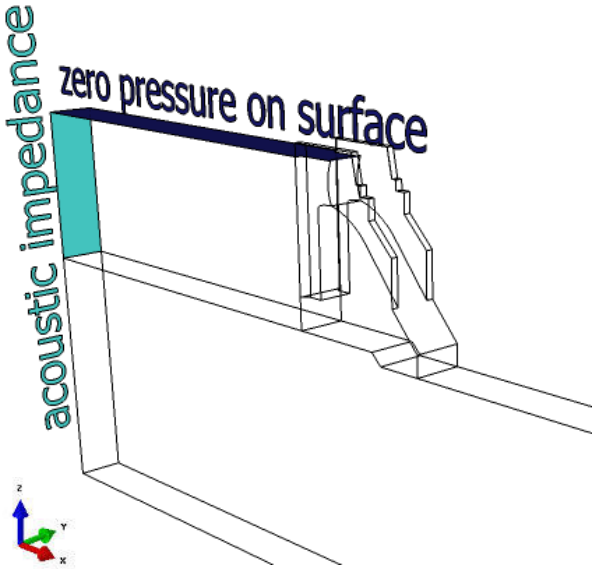

Figure 7-9 Surface conditions for acoustic elements

7.3.5 Stimulating earthquake accelerations

For the earthquake loading two random time histories in x- and z-direction are used. Thereby the x-direction is the flow direction and orthogonal to the dam axis and the z-direction is the vertical direction and orthogonal to the flow direction. The earthquake duration is 20 seconds and the maximum earthquake accelerations go up to 0.1 g. The accelerations are put on the foundation boundaries as shown in Figure 7-10.

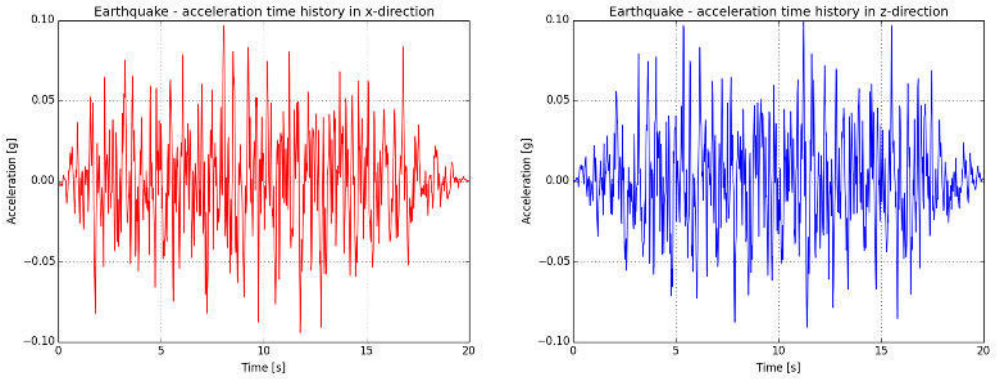

Figure 7-10: Earthquake accelerations in x- and z-direction

The response spectra of the acceleration time histories in x-direction and z-direction are shown in Figure 7-11.

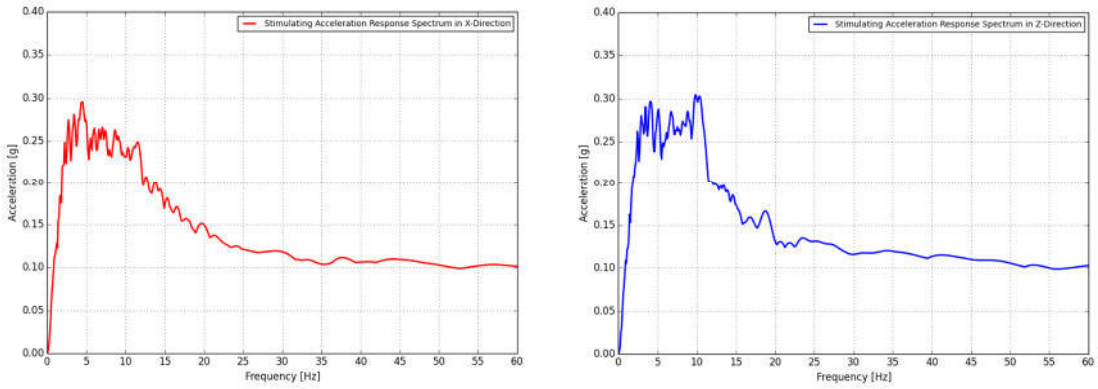

Figure 7-11: Acceleration response spectra in x- and z-direction of the stimulating acceleration time histories

7.4 Simulation steps

The numerical simulation can be divided into a static simulation, the eigenfrequency analysis and the seismic dynamic analysis. The static simulation contains the gravity step with the dead weight of the dam as load and the hydrostatic step with the static water load acting on the structure.

The following calculation steps are computed:

- Initial step
- Static analysis:
    - Gravity step
    - Hydrostatic step
- Eigenfrequency analysis (including pre-deformation from the static analysis)
- Dynamic analysis

7.4.1 Gravity step

The first calculation step is the static gravity step. As load the dead weight of the concrete structure is applied. As results the stresses in the contact path due to the dead load are of interest.

7.4.2 Hydrostatic step

The hydrostatic water pressure on the gravity dam is the decisive load in case of hydraulic structures. The additional load leads to higher deformations in x-direction and higher stresses in the contact path compared to the gravity step.

7.4.3 Eigenfrequency analysis

In the frequency step the eigenoscillations of the structure are computed. As result a maximum of 20 eigenmodes are extracted. With the eigenmodes the dynamic behavior of the structure can be represented. By calculating the Rayleigh Damping coefficients with the eigenfrequencies the damping behavior of the structure can be considered. Abaqus/CAE uses standardly the Lanczos method for iteration of the eigenvalues.

7.4.4 Dynamic step

The seismic dynamic analysis can only be done with the knowledge of the eigenmodes. For the rock mass the damping behavior of the gravity dam can be adopted because of the uncertainties of the material properties. For the dynamic step two different calculation methods are used:

- Modal analysis with the time history method
- Direct integration method.

By using the modal analysis method with time histories the dynamic simulation can be done by superposition. A global stimulation of the system by the two time histories and a global damping parameter with 5 % over the whole 20 modes is defined.

The calculation method of direct time integration uses the two time histories as stimulations on the foundation borders and the Rayleigh coefficients α and β for the consideration of the damping. The

earthquake is simulated over a time period of 20 seconds with a defined maximum increment number of 2000 and an increment size of 0.01 using the Full-Newton method.

7.5 Discretization of the model

For the discretization of the model different element types dependent on the required accuracy are used. The foundation is modelled with linear solid elements. For the gravity dam quadratic solid elements are used. The radial gate is discretized with quadratic shell elements and a rigid body definition or with linear shell elements and quadratic beam elements. The model configurations in which the reservoir is discretized with finite elements use quadratic acoustic elements.

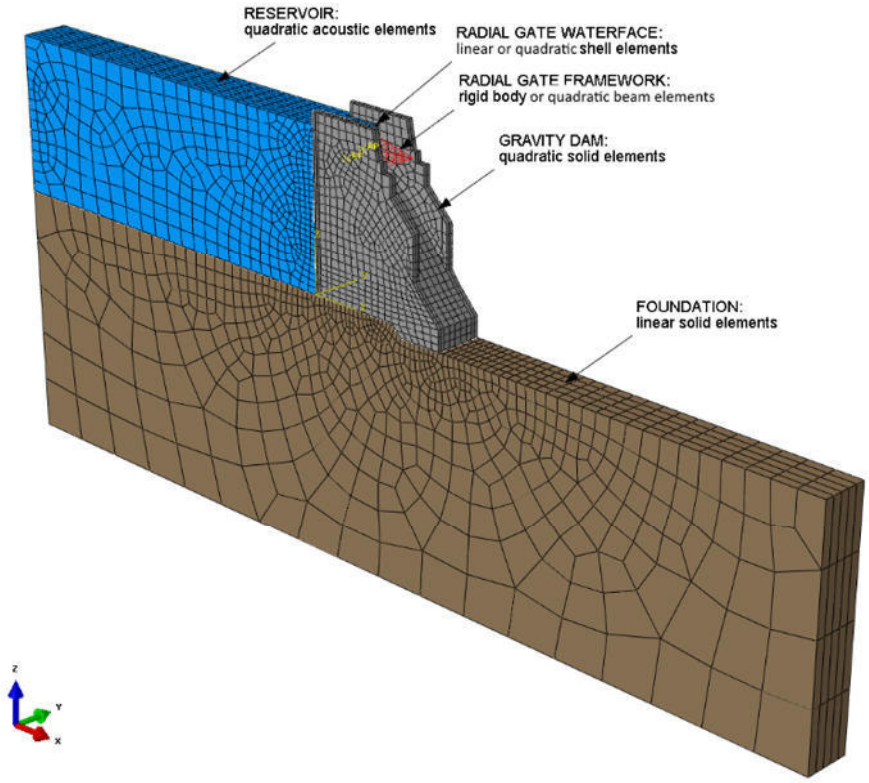

Figure 7-12: Discretization of the model

The following element types with their definitions in Abaqus/CAE are used.

Mesh properties: element types		
gravity dam		
	models with rigid gate	models with deformable gate
element type according Abaqus CAE	C3D20R	
element shape	hexahedral	
element type	quadratic 3D stress	
foundation		
	models with rigid gate	models with deformable gate
element type according Abaqus CAE	C3D8R	
element shape	hexahedral	
element type	linear 3D stress	
reservoir		
	models with rigid gate	models with deformable gate
element type according Abaqus CAE	AC3D20	
element shape	hexahedral	
element type	acoustic medium	
radial gate skin plate		
	models with rigid gate	models with deformable gate
element type according Abaqus CAE	S8R	S8R
element shape	quadrilateral	quadrilateral
element type	quadratic shell	quadratic shell
radial gate framework arms		
	models with rigid gate	models with deformable gate
element type according Abaqus CAE	RB3D2	B32
element shape	line	quadratic
element type	linear discrete rigid	linear beam

Table 7-2: Element definition for the model in Abaqus/CAE

The deformable skin plate of the gate with its complex geometry must be discretized with linear shell elements to keep the node number low.

Due to the more complex geometry of the deformable gate the sum of elements is 15676 and the number of nodes is 44937 for these jobs.

The total number of elements for jobs with rigid gate is 10506 and the total number of nodes is 39623.

Mesh properties: element numbers						
	gravity dam	foundation	reservoir	radial gate skin plate	radial gate arms	Total number of elements
jobs with rigid gate	2888	2720	4568	**90**	**240**	10506
jobs with deformable gate	2888	2720	4568	**5102**	**398**	15676

Table 7-3: Number of elements

Mesh properties: node numbers						
	gravity dam	foundation	reservoir	radial gate skin plate	radial gate arms	Total number of elements
jobs with rigid gate	14270	3618	21213	**313**	**209**	39623
jobs with deformable gate	14270	3618	21213	**5066**	**770**	44937

Table 7-4: Number of nodes

7.6 Static analysis

After the initial step the static analysis is computed. It contains the gravity step and the hydrostatic step.

7.6.1 Gravity step

In the Gravity step only the dead weight of the concrete structure is acting. This loads lead to stresses in the contact path of the dam, which are shown in the following figure.

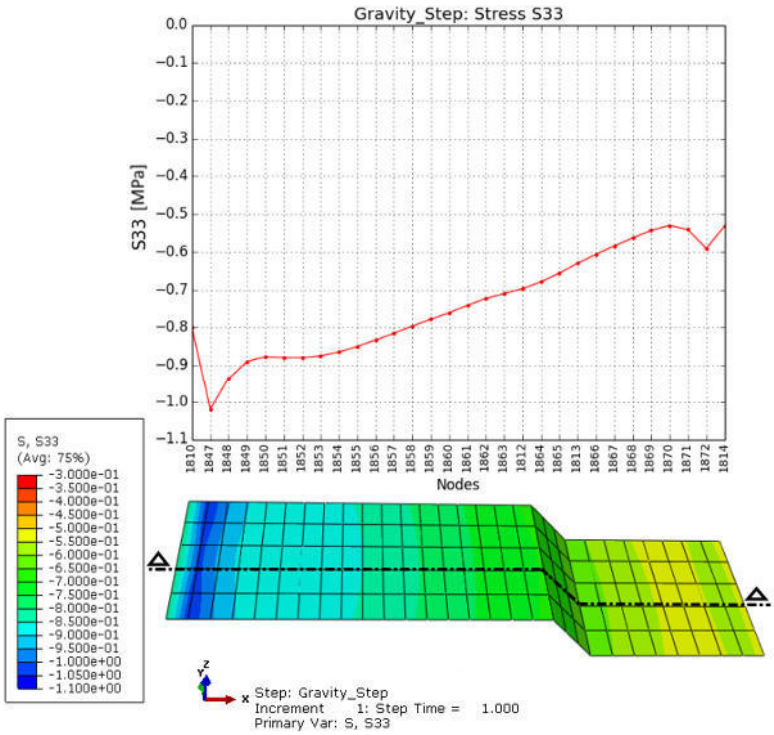

Figure 7-13: Stresses in the contact path of the dam due to the dead weight

The maximum pressure in the contact path is about 1 MPa on the upstream heel of the dam. On the downstream heel of the dam a pressure of about 0.55 MPa occurs. Due to the change in altitude at the nodes 1864, 1865 and 1813 a steeper stress graph is visible in this area.

The peaks in the stress graph at node 1847 and 1872 are caused by typical numerical troubles. The common static stress distribution in the contact path of a gravity dam has a nearly linear form and decreases from upstream to downstream. The analytical way to calculate the stresses is described in 5.3.

7.6.2 Hydrostatic step

In addition to the dead weight of the concrete structure also the hydrostatic water pressure acts on the dam. The hydrostatic pressure distribution is shown in Figure 7-14.

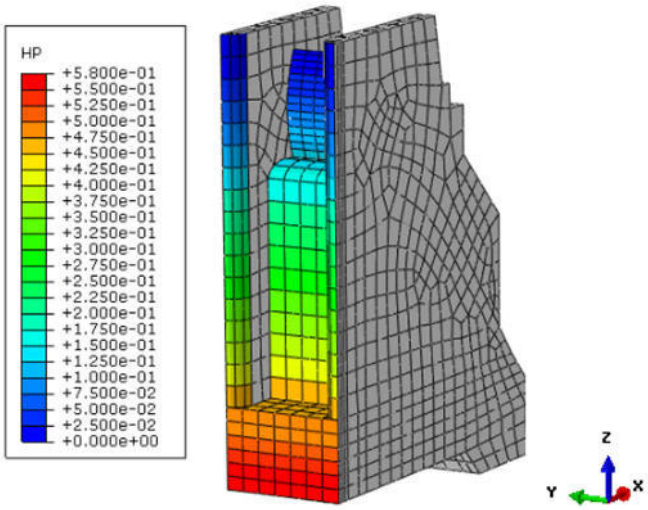

Figure 7-14: Hydrostatic pressure on the gravity dam in MPa

Because of the direction independence of the water the hydrostatic pressure increases with the depth with an inclination of 45 degrees. The two steps in the distribution arise from the horizontal surfaces of the dam. The maximum hydrostatic pressure at the bottom of the dam is 0.58 MPa.

The hydrostatic influence on the structure leads to a different figure of the stresses in the contact path compared with the gravity step.

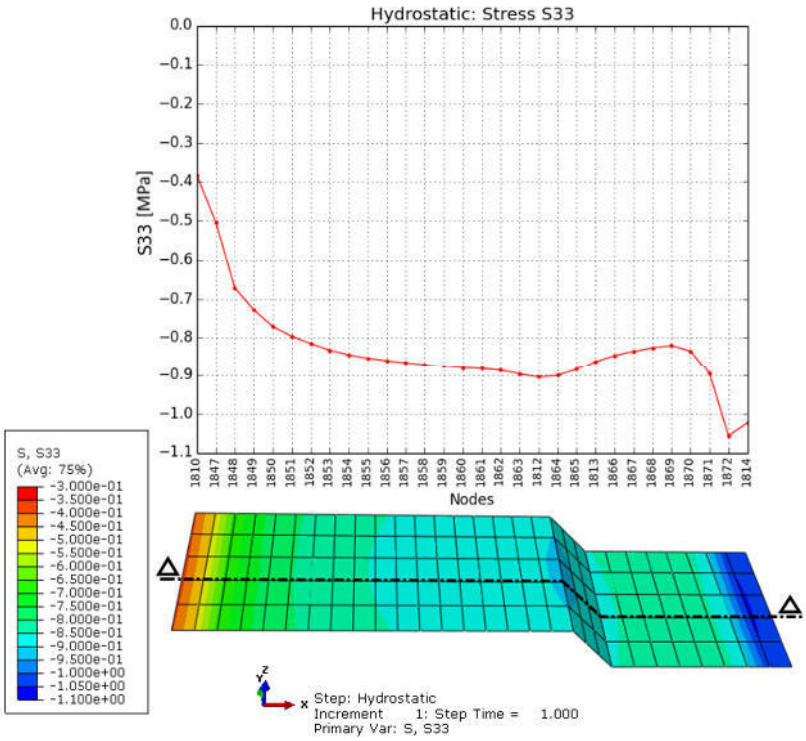

Figure 7-15: Stresses in the contact path of the dam due to the dead weight and the hydrostatic pressure

In contrast to the gravity step the stresses increase from upstream to downstream. A pressure of 0.4 MPa is visible on the upstream heel of the dam. Due to the altitude step in the contact path the stresses decrease between node 1812 and 1869 before they rise again. A maximum pressure in the contact path of 1.05 MPa at the downstream heel is visible.

7.6.2.1 Resulting hydrostatic water load and bearing forces of the gate

The bearing forces of the gate can be figured out by a so called “Free Body Cut” in Abaqus/CAE. The obtained results are compared with the analytical calculation.

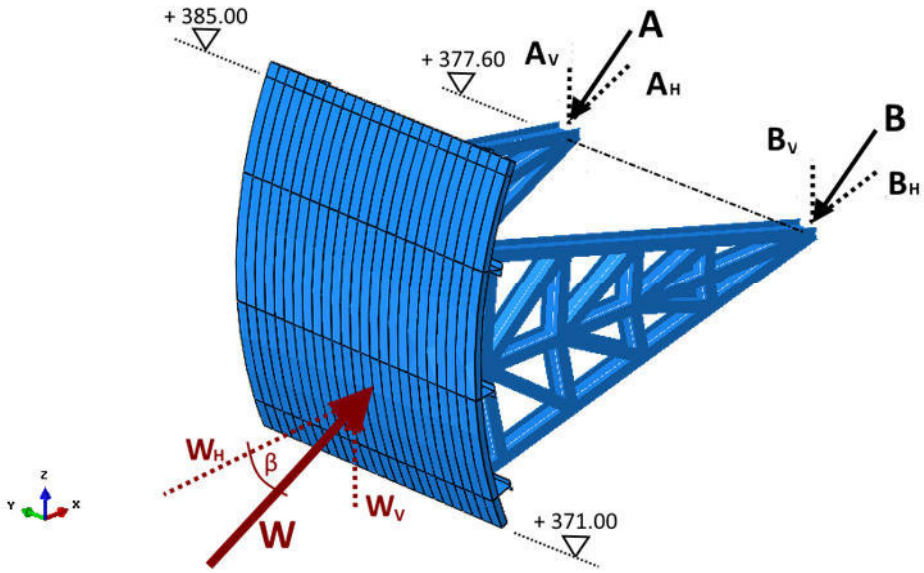

Figure 7-16: Resulting hydrostatic water load with its direction and static bearing forces A and B

The analytical calculation is done with a developed Python-Script attached in appendix A and results in following forces:

$$A = B = 6.17\ MN \tag{7.1}$$

$$W = 12.33\ MN \tag{7.2}$$

The influence of the Y-direction in the numerical model leads to slightly higher bearing forces.

The direction of the resulting bearing forces is the orientation of the framework arms.

$$A_{num} = B_{num} = 6.4\ MN \tag{7.3}$$

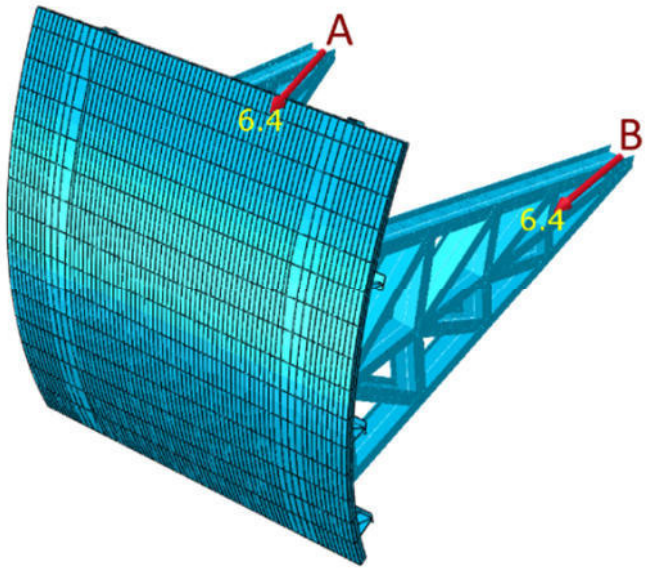

Figure 7-17: Numerical results of the static bearing forces of the radial gate

7.7 Dynamic analysis

Different configurations of the model are chosen and compared for the numerical, dynamic simulation. These differences are caused by different reservoir loading conditions, different masses of the radial gate, different reservoir modelling methods and different stiffnesses of the radial gate. In the following figure the compared jobs with their specifications are pictured in the mentioned order.

		RESERVOIR CASE	RADIAL GATE STIFFNESS	RADIAL GATE MASS	RESERVOIR MODELLING	CALCULATION METHOD
7.7.3	Comparison regarding calculation methods and reservoir consideration methods	Full Reservoir Full Reservoir Full Reservoir	Rigid Gate Rigid Gate Rigid Gate	Massless Gate Massless Gate Massless Gate	Acoustic Elements Westergaard Westergaard	Direct Time Integration Direct Time Integration Modal Analysis with Time History
7.7.4	Comparison regarding empty or full reservoir	Full Reservoir Empty Reservoir Empty Reservoir	Rigid Gate Rigid Gate Rigid Gate	Massless Gate Massless Gate Massless Gate	Acoustic Elements - -	Direct Time Integration Direct Time Integration Modal Analysis With Time History
7.7.5	Comparison regarding the mass of the gate	Full Reservoir Full Reservoir Full Reservoir Full Reservoir	Rigid Gate Rigid Gate Deformable Gate Deformable Gate	Massless Gate 100 t Gate Massless Gate 100 t Gate	Acoustic Elements Acoustic Elements Acoustic Elements Acoustic Elements	Direct Time Integration Direct Time Integration Direct Time Integration Direct Time Integration
7.7.6	Comparison regarding the stiffness of the radial gate	Full Reservoir Full Reservoir Full Reservoir Full Reservoir	Rigid Gate Deformable Gate Rigid Gate Deformable Gate	100 t Gate 100 t Gate 100 t Gate 100 t Gate	Acoustic Elements Acoustic Elements Westergaard Westergaard	Direct Time Integration Direct Time Integration Direct Time Integration Direct Time Integration
7.7.7	Comparison of Westergaard's added masses and acoustic elements	Full Reservoir Full Reservoir	Deformable Gate Deformable Gate	100 t Gate 100 t Gate	Acoustic Elements Westergaard	Direct Time Integration Direct Time Integration

Figure 7-18: Configurations of the model for the comparisons

The reservoir is modelled with acoustic elements or with point masses according to Westergaard. For jobs with Westergaard's added mass technique point masses are set on the nodes of the upstream gravity dam and radial gate surface. Jobs with this method are computed with the user element subroutine by Goldgruber (2011).

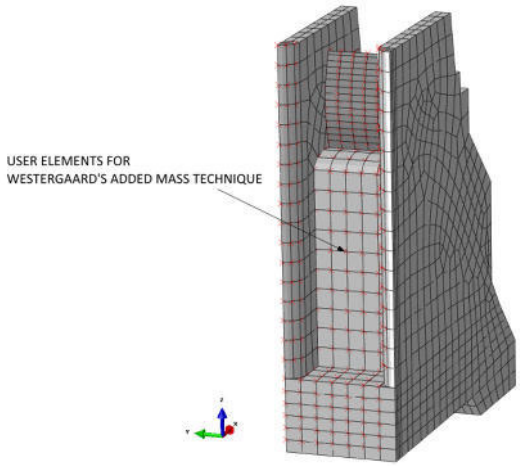

Figure 7-19: Point mass definitions for Westergaard's added mass technique

The dynamic simulation contains the eigenfrequency analysis and the dynamic analysis with the dynamic, implicit direct time integration method or the modal analysis with time history method. With the calculated eigenfrequencies the damping behavior of the structure can be considered. On the following pages the different configurations are compared concerning eigenmodes, accelerations and displacements and acceleration response spectra are created. These response spectra graphs show the calculated accelerations belonging to each eigenfrequency A Python script is developed to calculate these accelerations and plot them in a chart.

For a better clarity each configuration has a different color as visible in Figure 7-18.

The analyzed nodal point is the left abutment of the radial gate on the pier.

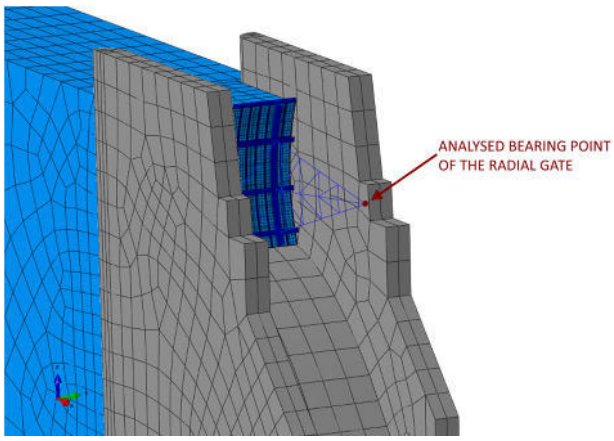

Figure 7-20: Analyzed nodal point of the dynamic simulation

7.7.1 Eigenfrequencies and eigenmodes of the radial gate

The eigenfrequency analysis of the radial gate results in the following eigenmodes and eigenfrequencies. The first four eigenmodes are shown in Figure 7-21.

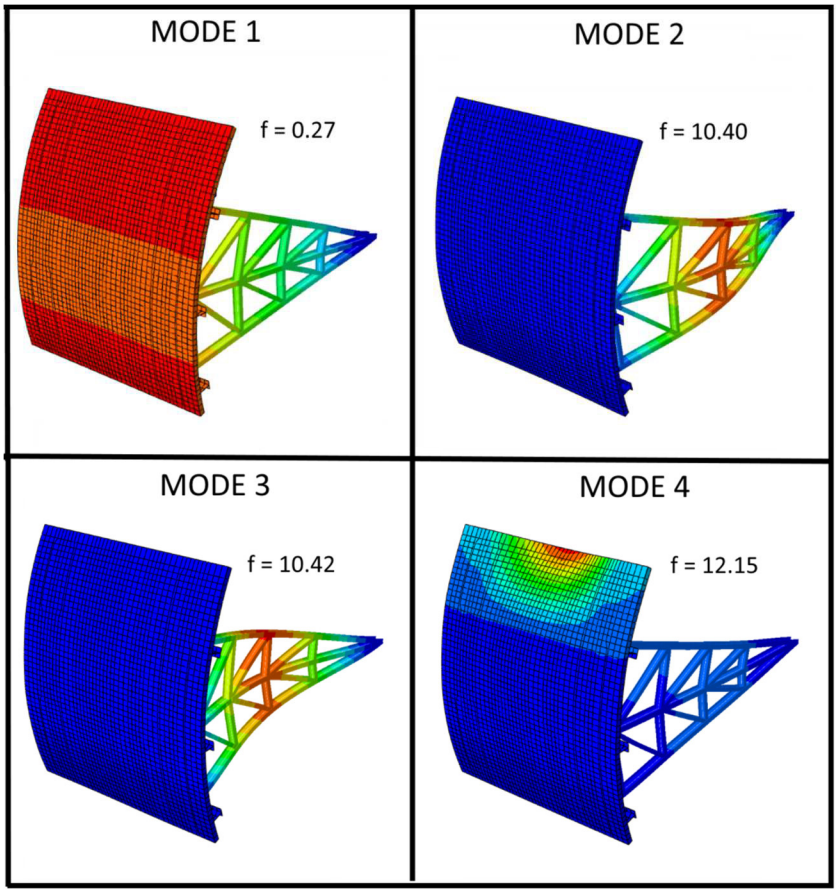

Figure 7-21: Eigenmodes of the radial gate

	Deformable Radial Gate				
	Eigenfrequency	EMx		EMz	
		[kt]	[%]	[kt]	[%]
Total Mass	-	0.1000	100	0.1000	100
Modes					
1	0.2720	0.0000	0.00	0.0851	85.10
2	10.4009	0.0002	0.24	0.0000	0.00
3	10.4201	0.0000	0.00	0.0000	0.00
4	12.1481	0.0159	15.88	0.0049	4.92
5	12.5943	0.0002	0.22	0.0001	0.06
6	12.6498	0.0000	0.00	0.0000	0.00
7	14.9637	0.0000	0.00	0.0000	0.00
8	14.9638	0.0000	0.00	0.0000	0.00
9	15.0370	0.0000	0.00	0.0000	0.00
10	15.0370	0.0000	0.00	0.0000	0.00
11	15.0645	0.0000	0.00	0.0000	0.00
12	15.0646	0.0000	0.00	0.0000	0.00
13	16.8666	0.0000	0.00	0.0000	0.00
14	17.1293	0.0024	2.37	0.0045	4.49
15	17.3012	0.0000	0.00	0.0000	0.00
16	17.3014	0.0000	0.00	0.0000	0.00
17	18.8212	0.0000	0.00	0.0000	0.00
18	18.8213	0.0000	0.00	0.0000	0.00
19	20.0691	0.0694	69.43	0.0015	1.53
20	20.0833	0.0000	0.00	0.0000	0.00

Table 7-5: Eigenfrequencies and effective masses in x-and z-direction of the radial gate

7.7.2 Eigenmodes of the entire model

Also for the whole model the eigenmodes are pictured whereby the gravity dam structure with the radial gate is cut out for better illustration. For the first mode a movement in positive x-direction and for the modes two, three and four a movement in the negative x-direction is identifiable.

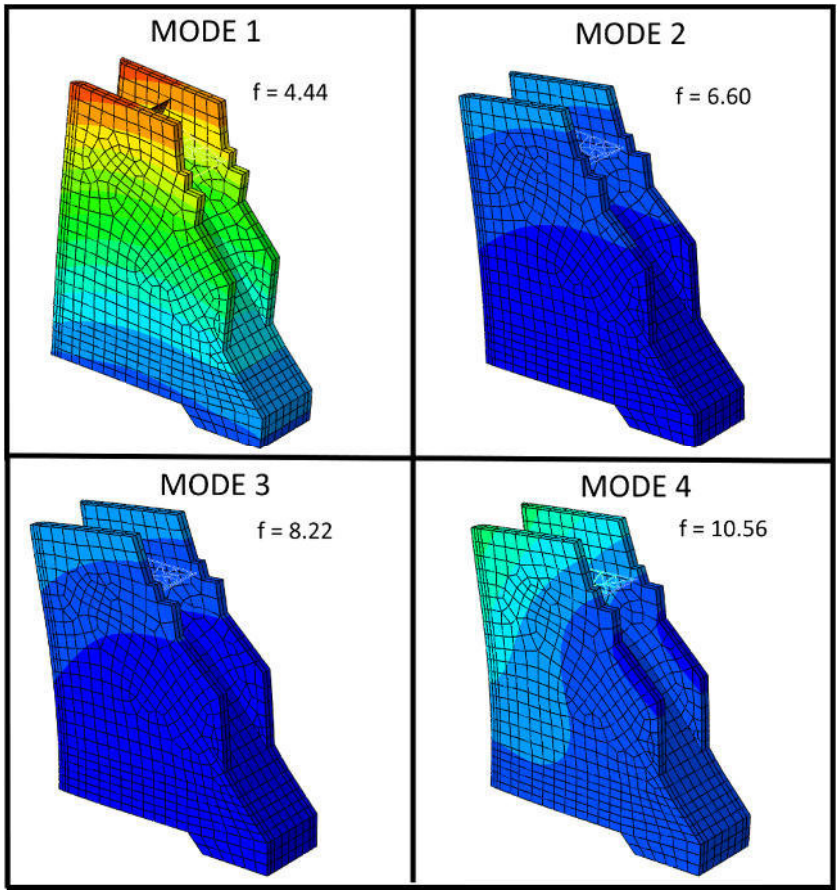

Figure 7-22: Eigenmodes of the entire structure

7.7.3 Comparison of the reservoir considerations and the calculation methods

7.7.3.1 Eigenfrequency analysis

Three different jobs with full reservoir and rigid, massless gate are compared. The simulation with acoustic elements is done with the time integration method (green). The consideration with the added mass technique according Westergaard is computed with the direct time integration method (darkblue) as well with the modal analysis with time histories (lightblue).

In Figure 7-23 only the two configurations with direct time integration are compared because the calculation method has no influence on the eigenfrequencies and effective masses.

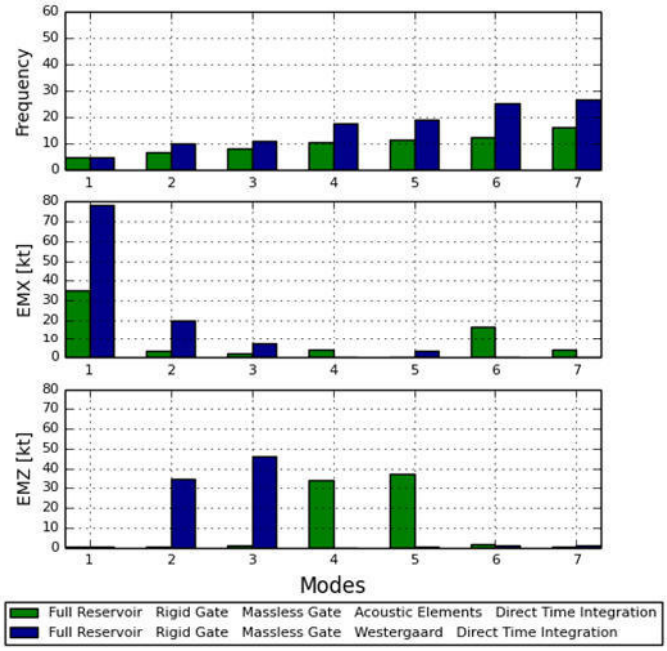

Figure 7-23: Eigenfrequencies and effective masses in x- and z-direction of the modes 1 to 7 of the comparison regarding the reservoir consideration technique and the calculation method

Full Reservoir Rigid Gate Massless Gate Acoustic Elements				Full Reservoir Rigid Gate Massless Gate Westergaard			
Modes	Eigenfrequency	EMx	EMz	Modes	Eigenfrequency	EMx	EMz
1	4.7043	35.0861	0.1579	1	4.6469	78.5766	0.5437
2	6.6085	3.5458	0.1523	2	10.0932	19.7553	34.4281
3	8.2364	2.1705	1.2003	3	11.1847	7.2270	46.1859
4	10.5925	4.2537	33.9575	4	17.6164	0.0003	0.0000
5	11.5652	0.2947	37.3101	5	19.2857	3.7327	0.2231
6	12.6128	16.5834	1.5330	6	25.3775	0.0387	0.9210
7	16.0885	4.3049	0.0703	7	26.8732	0.0719	0.9831

Table 7-6: Eigenfrequencies and effective masses in x- and z-direction of the modes 1 to 7 of the comparison regarding the reservoir consideration technique and the calculation method

The assessed α- and β-values are shown in Table 7-7. For the modal analysis a global damping factor of $\xi = 0.05$ is chosen.

Rayleigh Damping: Used Frequencies, α- and β-Values										
$\alpha = \omega_1 * \omega_2 * \beta = 4 * \pi * f_1 * f_2 * \beta$										
$\beta = 2 * \xi / (\omega_1 + \omega_2) = \xi / (\pi * (f_1 + f_2)$										
Calculation Method	Reservoir Case	Reservoir Consideration	Gate Stiffness	Gate Mass [t]	1st used Mode	2nd used Mode	f_1	f_2	α	β
Direct Integration	full	Acoustic Elements	rigid	0	1	10	4.7043	19.5576	2.3827	0.0007
Direct Integration	full	Westergaard's added Masses	rigid	0	1	7	4.6469	26.8732	2.4893	0.0005
Modal Analysis	full	Westergaard's added Masses	rigid	0	1	20	ξ = 0,05			

Table 7-7: Calculation of the Rayleigh damping coefficients of the comparison regarding the reservoir consideration technique and the calculation method

7.7.3.2 Resulting accelerations in the abutment

The highest accelerations are visible at the direct time integration method with Westergaard's added masses. The lowest amplitudes can be pointed out at the direct time integration method with acoustic elements however the maximum values of this method are higher than the maxima of the modal analysis due to the constant damping of 0.05 for all nodes.

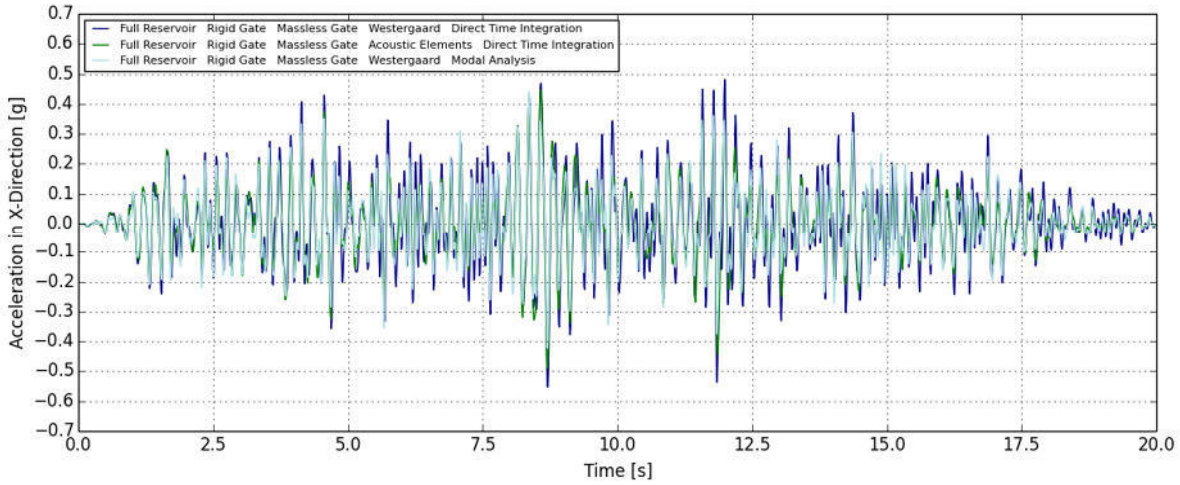

Figure 7-24: Resulting accelerations in x-direction in the abutment of the comparison regarding the reservoir consideration technique and the calculation method

7.7.3.3 Resulting displacements in the abutment

The displacement time histories of the two direct time integration methods are nearly similar whereby the higher displacements on the peaks belong to the consideration with the added mass technique by Westergaard. The resulting displacements of the modal analysis are smaller over the whole time history.

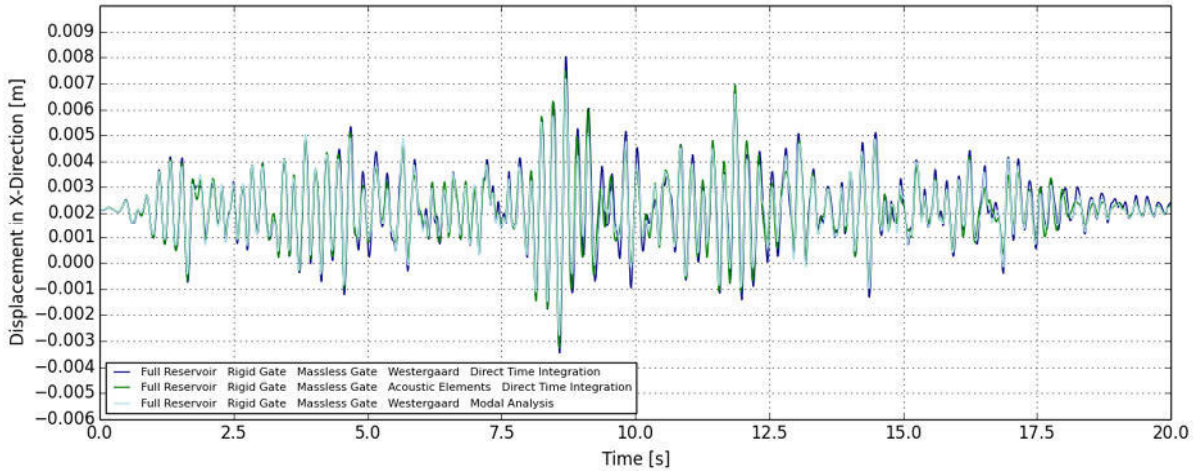

Figure 7-25: Resulting displacements in x-direction in the abutment of the comparison regarding the reservoir consideration technique and the calculation method

7.7.3.4 Acceleration response spectra

The maximum value of the stimulating acceleration time history is visible at a frequency of 4.5 Hz.

In the upper right graph the occurring accelerations of the different configurations at a frequency of 4.5 Hz are shown.

Slight frequency shifts between the three configurations and the stimulating time history are visible.

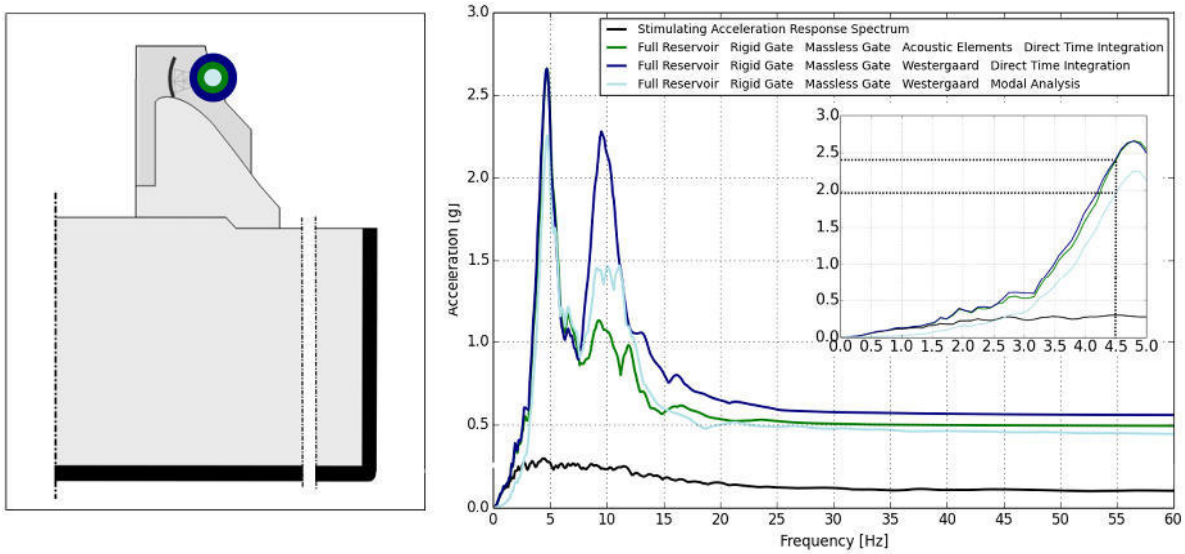

Figure 7-26: Acceleration response spectra of the comparison regarding the reservoir consideration technique and the calculation method

7.7.4 Comparison of the full and empty reservoir case

7.7.4.1 Eigenfrequency analysis

The empty reservoir case simulated by the direct time integration method or the modal analysis method and the full reservoir case with acoustic elements and the direct time integration method are compared. Figure 7-27 shows the eigenfrequencies and effective masses of the full reservoir model compared with the empty reservoir case independent on the calculation method.

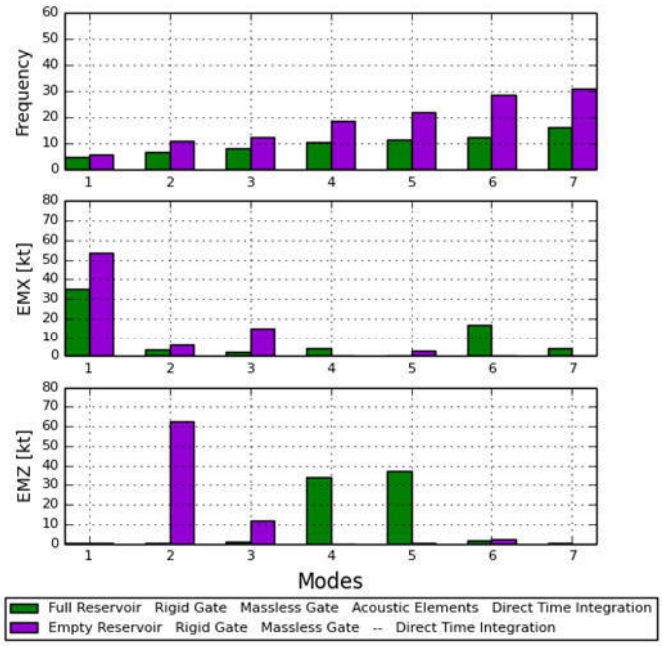

Figure 7-27: Eigenfrequencies, and effective masses in x- and z-direction of the modes 1 to 7 of the comparison regarding the reservoir case

For the full reservoir case (green) the modes 1 and 10 are used for the Rayleigh damping. In case of the empty reservoir (violet) the used modes are 1 and 7.

Full Reservoir Rigid Gate Massless Gate Acoustic Elements				Empty Reservoir Rigid Gate Massless Gate -			
Modes	Eigenfrequency	EMx	EMz	Modes	Eigenfrequency	EMx	EMz
1	4.7043	35.0861	0.1579	1	5.5834	53.8139	0.5126
2	6.6085	3.5458	0.1523	2	10.9115	5.9977	62.5959
3	8.2364	2.1705	1.2003	3	12.4107	14.7414	12.0704
4	10.5925	4.2537	33.9575	4	18.5685	0.0000	0.0000
5	11.5652	0.2947	37.3101	5	22.0665	3.0282	0.3980
6	12.6128	16.5834	1.5330	6	28.5847	0.0547	2.0631
7	16.0885	4.3049	0.0703	7	30.9350	0.0000	0.0000

Table 7-8: Eigenfrequencies and effective masses in x- and z-direction of the modes 1 to 7 of the comparison regarding the reservoir case

Rayleigh Damping: Used Frequencies, α- and β-Values										
$\alpha = \omega_1 * \omega_2 * \beta = 4 * \pi * f_1 * f_2 * \beta$										
$\beta = 2 * \xi / (\omega_1 + \omega_2) = \xi / (\pi * (f_1 + f_2)$										
Calculation Method	**Reservoir Case**	**Reservoir Consideration**	**Gate Stiffness**	**Gate Mass [t]**	**1st used Mode**	**2nd used Mode**	**f_1**	**f_2**	**α**	**β**
Direct Integration	full	Acoustic Elements	rigid	0	1	10	4.7043	19.5576	**2.3827**	**0.0007**
Direct Integration	empty	-	rigid	0	1	7	5.5834	30.935	**2.9718**	**0.0004**
Modal Analysis	empty	-	rigid	0	1	20	**ξ = 0,05**			

Table 7-9: Calculation of the Rayleigh damping coefficients of the comparison regarding the reservoir case

7.7.4.2 Resulting accelerations in the abutment

Smaller amplitudes of the empty reservoir case with direct time integration method are visible. The biggest maximum and minimum accelerations are calculated for the full reservoir case. The full reservoir case has a completely different response acceleration time history in contrast to the empty reservoir case.

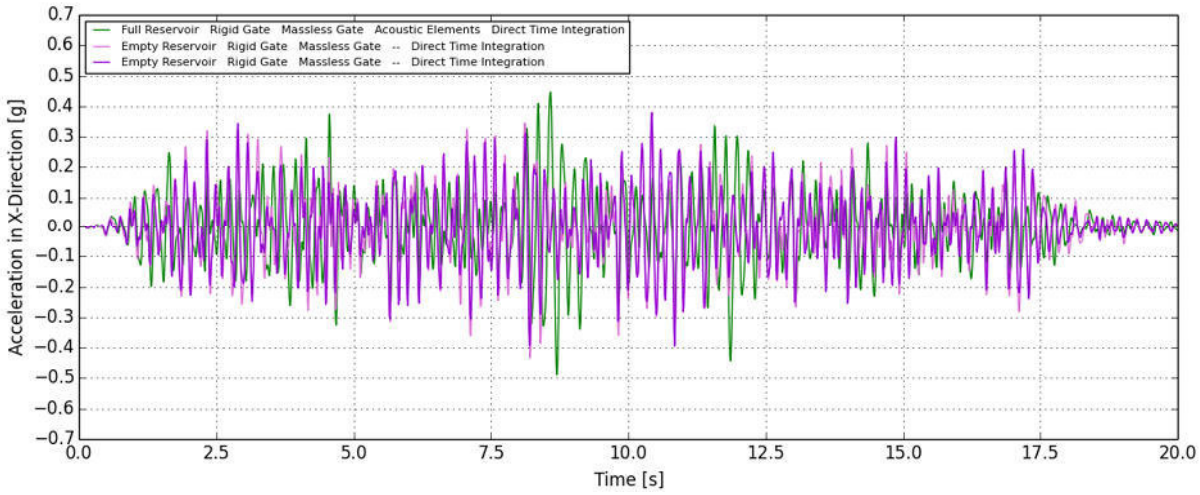

Figure 7-28: Resulting accelerations in x-direction in the abutment of the comparison regarding the reservoir case

7.7.4.3 Resulting displacements in the abutment

The direct time integration method for the full reservoir case leads to larger displacements in positive x-direction over the 20 seconds of the earthquake compared to the empty reservoir case. Displacements in negative x-direction, caused by absence of the hydrostatic pressure for the empty reservoir case, are visible. The modal analysis (rosy) has the smallest displacements again.

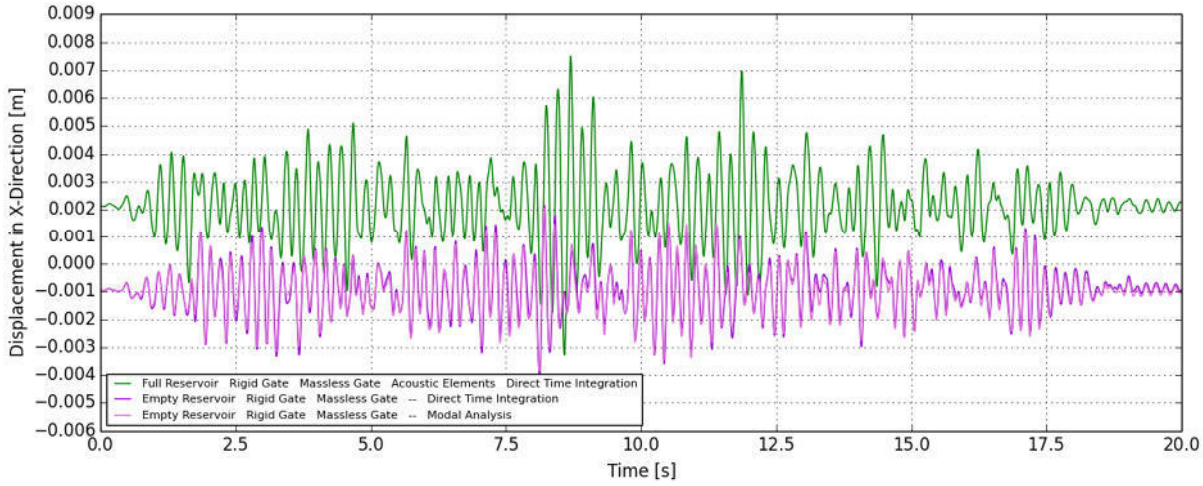

Figure 7-29: Resulting displacements in x-direction in the abutment of the comparison regarding the reservoir case

The reason of the smaller resulting values in case of the modal analysis in the two comparisons can be the global damping factor of 5 % over the whole 20 seconds in contrast to the direct time integration method with the Rayleigh damping coefficients whereby the system is underdamped between the two used modes and overdamped for the remaining modes.

7.7.4.4 Acceleration response spectra

Also at the comparison of the full reservoir case and the empty reservoir case changes in the response frequencies are identifiable whereby the peaks of the empty reservoir case occur at higher frequencies.

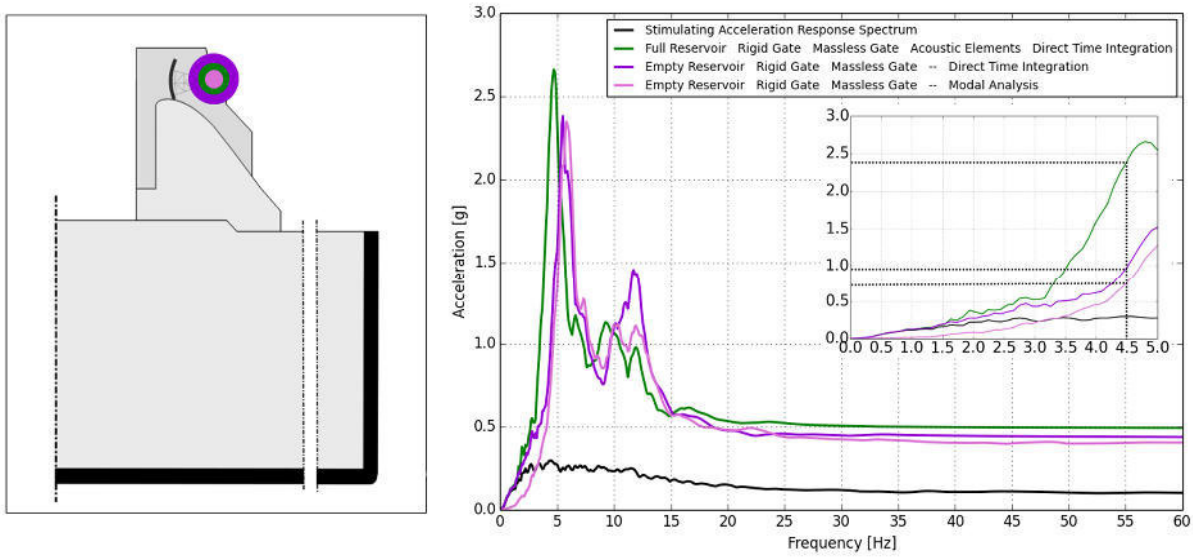

Figure 7-30: Acceleration response spectra of the comparison regarding the reservoir case

7.7.5 Comparison regarding the mass of the gate

The rigid radial gate consists of a rigid body for the framework arms and a stiff shell with a very high Young's Modulus. The mass for the dynamic simulation is considered as point mass in the mass center of the gate. According to formula 3.3 and the approach by Strobl & Zunic (2006) the oscillating mass of the gate is assumed with 100 t. For the deformable radial gate random beam sections are chosen to reach the mass of 100 t over the steel volume and the density for significant comparisons.

7.7.5.1 Eigenfrequency analysis

In case of the rigid gate only small differences between the eigenfrequencies and the effective masses of the model with the massless gate (green) and the model with the gate mass of 100 t (orange) occur.

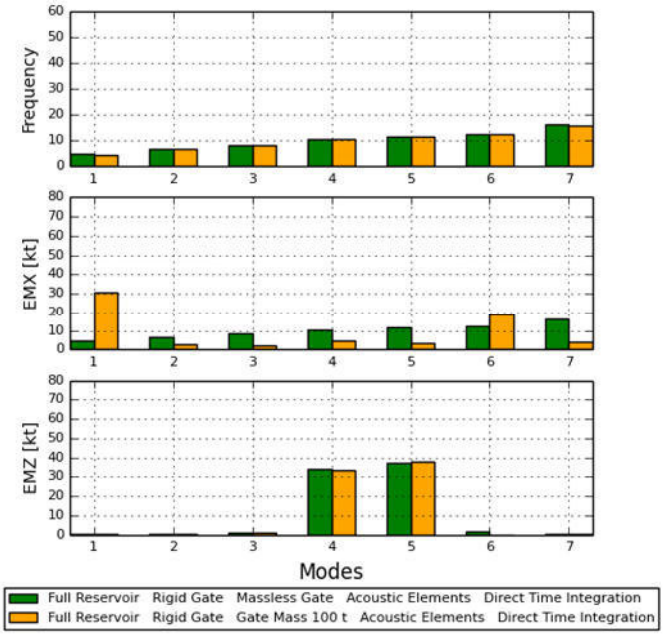

Figure 7-31: Eigenfrequencies and effective masses in x- and z-direction of the modes 1 to 7 of the rigid gate case for the comparison regarding the mass of the gate

Full Reservoir Rigid Gate Massless Gate Acoustic Elements				Full Reservoir Rigid Gate Gate Mass 100 t Acoustic Elements			
Modes	Eigenfrequency	EMx	EMz	Modes	Eigenfrequency	EMx	EMz
1	4.7043	35.0861	0.1579	1	4.4391	30.8563	0.1083
2	6.6085	3.5458	0.1523	2	6.6012	3.0408	0.1422
3	8.2364	2.1705	1.2003	3	8.2222	1.9378	1.2118
4	10.5925	4.2537	33.9575	4	10.5572	4.6580	33.1260
5	11.5652	0.2947	37.3101	5	11.3828	3.1681	37.9311
6	12.6128	16.5834	1.5330	6	12.3714	18.4527	0.0008
7	16.0885	4.3049	0.0703	7	15.9472	3.9001	0.3294

Table 7-10: Eigenfrequencies and effective masses in x- and z-direction of the modes 1 to 7 of the rigid gate case for the comparison regarding the mass of the gate

Higher eigenfrequencies of the model with massless gate (red) compared to the model with the gate mass of 100 t (brown) are visible due to the mass difference in case of a deformable gate. In contrast to the rigid gate case the values of the eigenfrequencies are smaller.

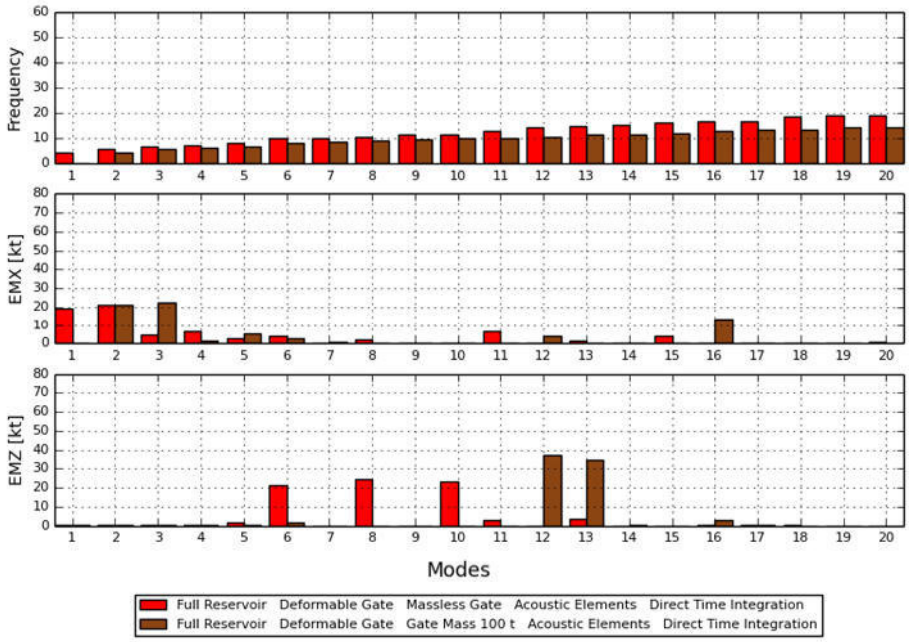

Figure 7-32: Eigenfrequencies and effective masses in x- and z-direction of the deformable gate case for the comparison regarding the mass of the gate

Full Reservoir Deformable Gate Massless Gate Acoustic Elements				Full Reservoir Deformable Gate Gate Mass 100 t Acoustic Elements			
Modes	Eigenfrequency	EMx	EMz	Modes	Eigenfrequency	EMx	EMz
1	4.2657	19.6115	0.1193	1	0.2944	0.0000	0.0874
2	5.6753	21.2439	0.4093	2	4.2090	21.3174	0.1117
3	6.6108	4.9536	0.2112	3	5.6053	22.7322	0.3454
4	7.2659	6.7660	0.2654	4	6.4671	1.3306	0.0867
5	8.2452	2.6226	1.3644	5	6.6465	5.2600	0.1945
6	10.0688	4.2123	21.6374	6	8.2332	2.4914	1.4088
7	10.1670	0.0000	0.0012	7	8.7269	0.6390	0.0110
8	10.5944	1.8794	24.6445	8	9.2606	0.0000	0.0000
9	11.5883	0.0000	0.0008	9	9.7333	0.0189	0.0025
10	11.6442	0.0001	23.3089	10	9.9197	0.0000	0.0000
11	12.7482	6.7827	2.6053	11	10.1791	0.0000	0.0000
12	14.1966	0.0000	0.0000	12	10.5841	3.7788	37.1099
13	15.0579	1.6177	3.7650	13	11.6412	0.0001	34.5770
14	15.4608	0.0022	0.0021	14	11.6990	0.0069	0.2849
15	16.1158	3.8727	0.0542	15	11.9481	0.0000	0.0000
16	16.6182	0.0134	0.2631	16	12.7451	13.6208	2.6095
17	16.8978	0.1557	0.4295	17	13.4986	0.0206	0.2137
18	18.7448	0.0511	0.4899	18	13.6084	0.0001	0.0011
19	18.9548	0.0022	0.0018	19	14.1885	0.0000	0.0000
20	19.1453	0.7481	0.0089	20	14.2679	0.0063	0.0000

Table 7-11: Eigenfrequencies and effective masses in x- and z-direction of the deformable gate case for the comparison regarding the mass of the gate

Rayleigh Damping: Used Frequencies, α- and β-Values										
$\alpha = \omega_1 * \omega_2 * \beta = 4 * \pi * f_1 * f_2 * \beta$										
$\beta = 2 * \xi / (\omega_1 + \omega_2) = \xi / (\pi * (f_1 + f_2)$										
Calculation Method	Reservoir Case	Reservoir Consideration	Gate Stiffness	Gate Mass [t]	1st used Mode	2nd used Mode	f_1	f_2	α	β
Direct Integration	full	Acoustic Elements	rigid	0	1	10	4.7043	19.5576	**2.3827**	**0.0007**
Direct Integration	full	Acoustic Elements	rigid	100	1	10	4.4391	18.5810	**2.2513**	**0.0007**
Direct Integration	full	Acoustic Elements	deformable	0	1	16	4.2657	16.6182	**2.1328**	**0.0008**
Direct Integration	full	Acoustic Elements	deformable	100	2	16	4.2090	12.7451	**1.9880**	**0.0009**

Table 7-12: Calculation of the Rayleigh damping coefficients of the comparison regarding the mass of the gate

7.7.5.2 Resulting accelerations in the abutment

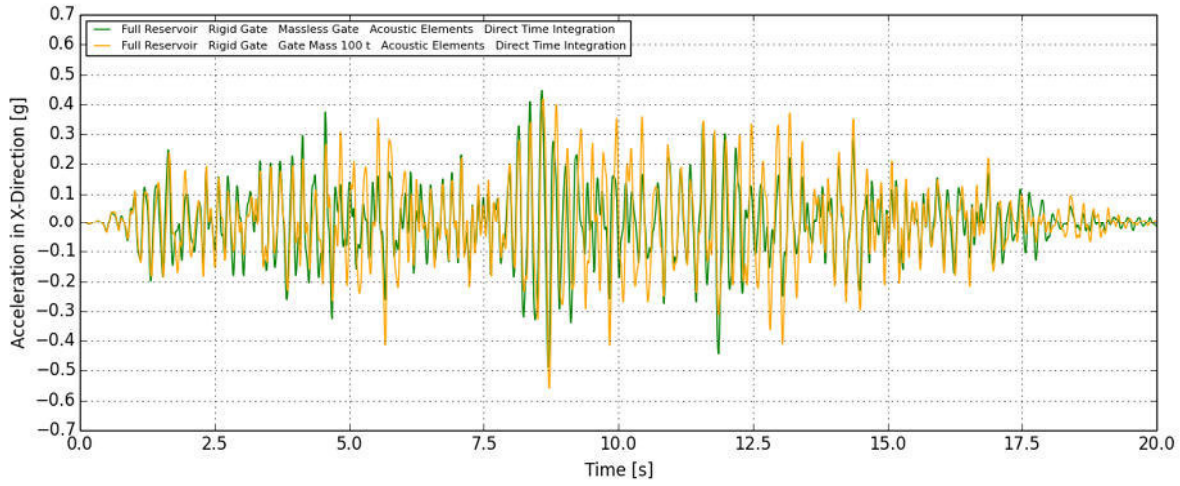

Figure 7-33: Resulting accelerations in x-direction in the abutment of the rigid gate case of the comparison regarding the mass of the gate

Higher amplitudes of the model with the gate mass of 100 t, especially between 4 and 15 seconds are visible for the rigid radial gate case. A slight phase shift is recognizable whereby the time history of the model with the gate mass of 100 t is a little delayed.

In case of a deformable gate higher accelerations of the massless model are visible whereby the amplitudes and the peaks of the two models are quiet similar.

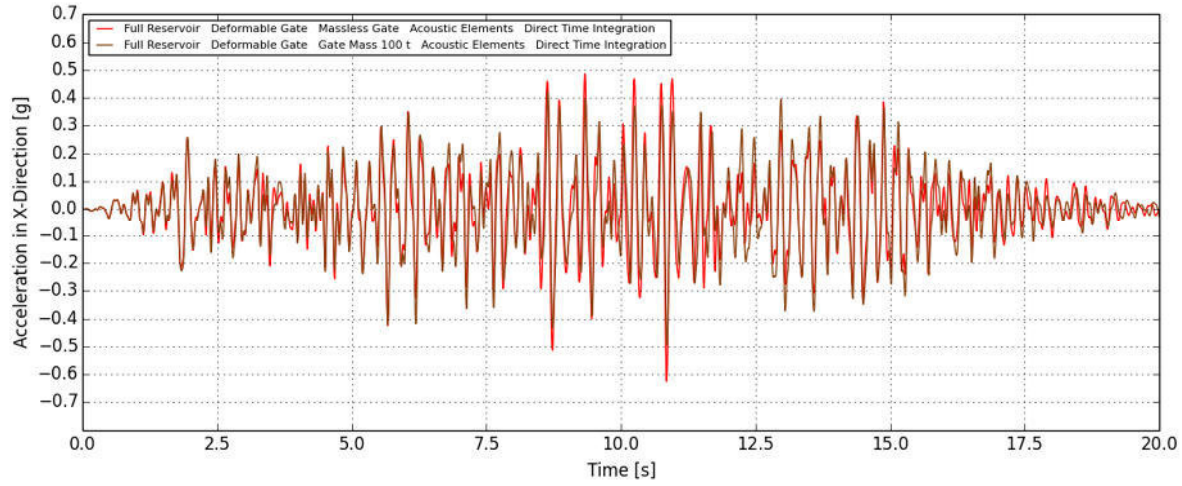

Figure 7-34: Resulting accelerations in x-direction in the abutment of the deformable gate case of the comparison regarding the mass of the gate

7.7.5.3 Resulting displacements in the abutment

Higher amplitudes of the rigid gate with a mass of 100 t are identifiable. Also the maximum displacements are seeable for the model with a rigid mass of 100 t. Also in the displacement time history for this comparison slight phase shifts are visible.

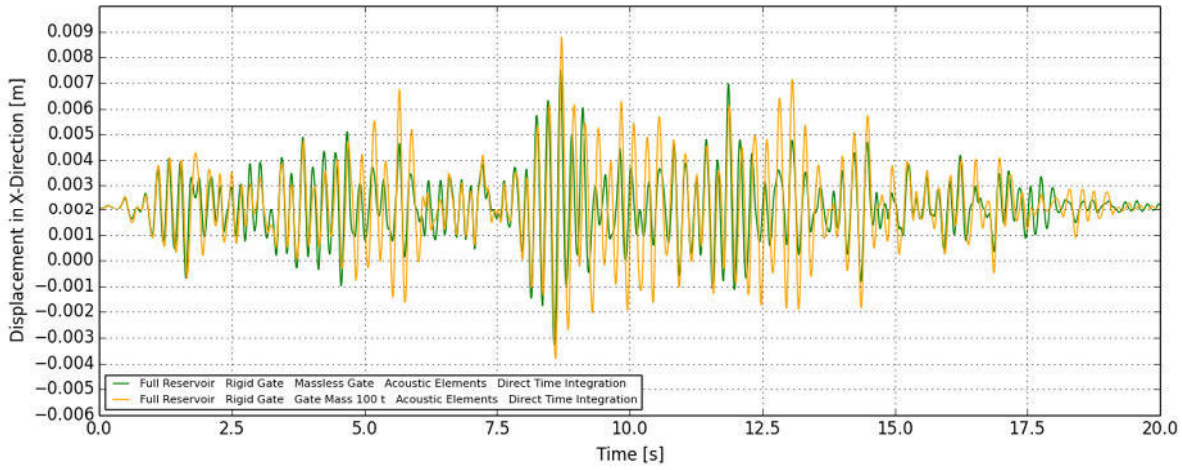

Figure 7-35: Resulting displacements in x-direction in the abutment of the rigid gate case of the comparison regarding the mass of the gate

The influence of the mass is visible for the model with a deformable gate at the maximum accelerations. They occur for the model with the massless, deformable gate otherwise the amplitudes are higher in case of a deformable gate with a gate mass of 100 t.

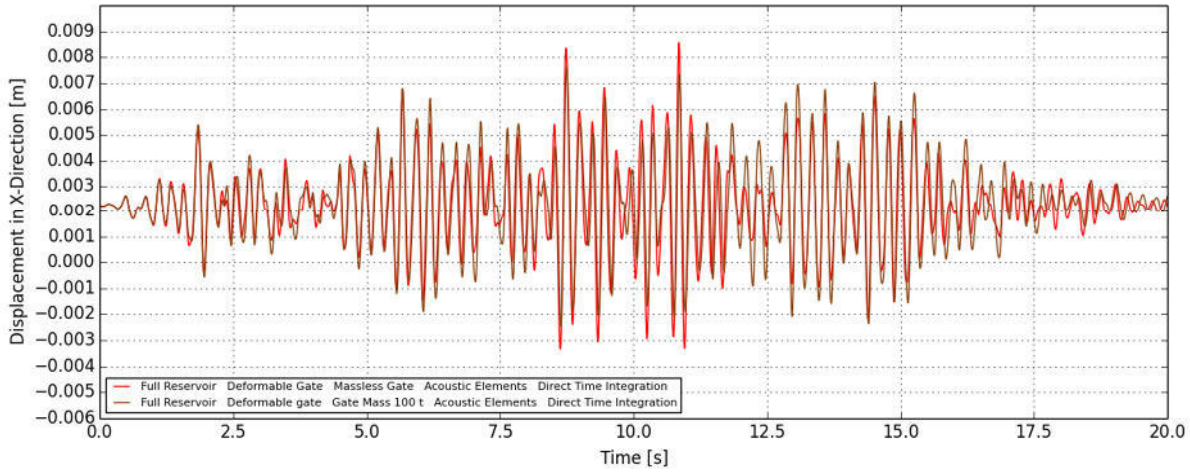

Figure 7-36: Resulting displacements in x-direction in the abutment of the deformable gate case of the comparison regarding the mass of the gate

7.7.5.4 Acceleration response spectra

Not only between the stimulating accelerations and the resulting accelerations of the configurations frequency shifts are visible, also between the model with the massless gate and the model with a gate mass of 100 t in case of a rigid gate a shifting arises.

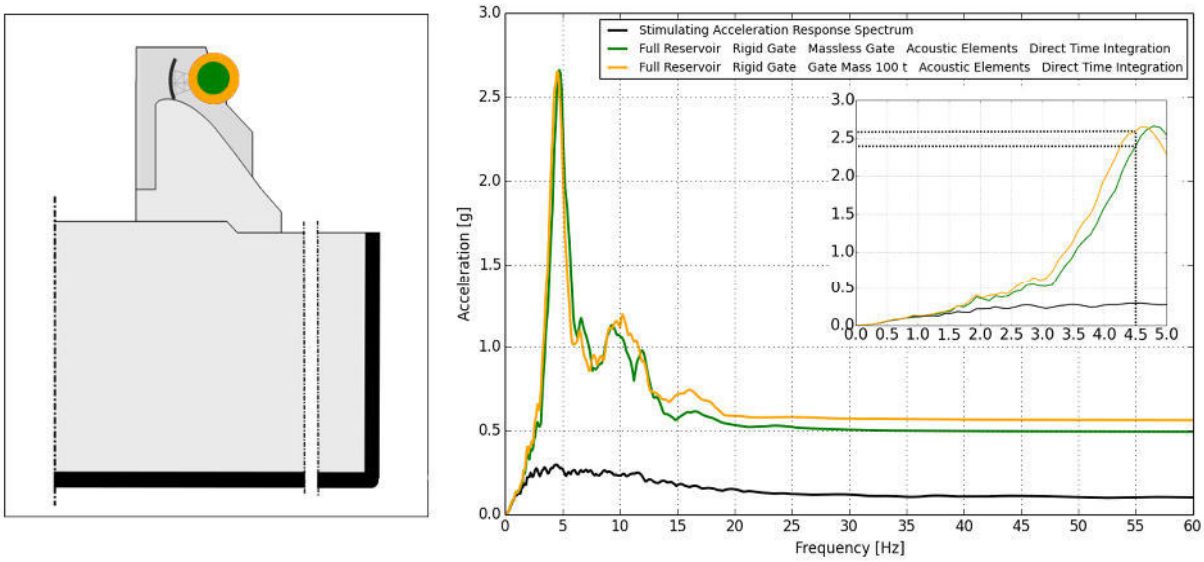

Figure 7-37: Acceleration response spectra of the rigid gate case of the comparison regarding the mass of the gate

Like the acceleration time history also at the response spectra shows higher accelerations of the massless, deformable gate compared to the deformable gate with a gate mass of 100 t.

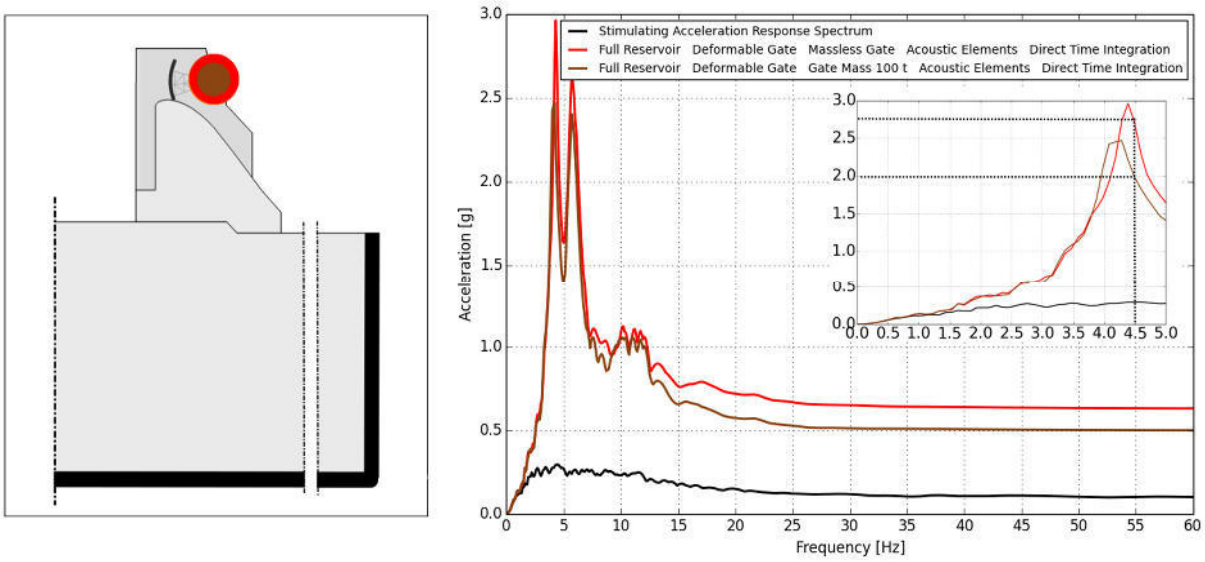

Figure 7-38: Acceleration response spectra of the deformable gate case of the comparison regarding the mass of the gate

7.7.6 Comparison regarding the stiffness of the gate

Four different models are created to match the results of the dynamic simulation of the model with the rigid gate with the model of the deformable gate. A rigid body is defined in Abaqus/CAE with an infinitely high Young's Modulus. The deformable gate has normal steel material properties.

The full reservoir case with acoustic elements or Westergaard's added masses and a rigid or deformable radial gate with a mass of 100 t are compared.

7.7.6.1 Eigenfrequency analysis

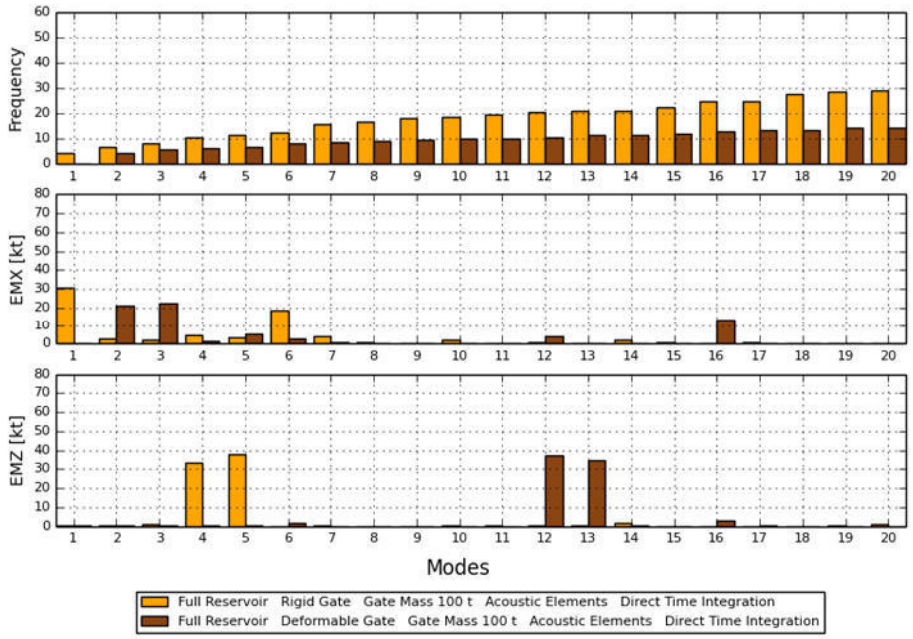

Figure 7-39: Eigenfrequencies and effective masses in x- and z-direction in case of using acoustic elements of the comparison regarding the stiffness of the gate

Full Reservoir Rigid Gate Gate Mass 100 t Acoustic Elements				Full Reservoir Deformable Gate Gate Mass 100 t Acoustic Elements			
Modes	Eigenfrequency	EMx	EMz	Modes	Eigenfrequency	EMx	EMz
1	4.4391	30.8563	0.1083	1	0.2944	0.0000	0.0874
2	6.6012	3.0408	0.1422	2	4.2090	21.3174	0.1117
3	8.2222	1.9378	1.2118	3	5.6053	22.7322	0.3454
4	10.5572	4.6580	33.1260	4	6.4671	1.3306	0.0867
5	11.3828	3.1681	37.9311	5	6.6465	5.2600	0.1945
6	12.3714	18.4527	0.0008	6	8.2332	2.4914	1.4088
7	15.9472	3.9001	0.3294	7	8.7269	0.6390	0.0110
8	16.5745	0.6977	0.0087	8	9.2606	0.0000	0.0000
9	18.4284	0.0002	0.0001	9	9.7333	0.0189	0.0025
10	18.5810	2.1292	0.6655	10	9.9197	0.0000	0.0000
11	19.4109	0.3296	0.0949	11	10.1791	0.0000	0.0000
12	20.3439	0.8813	0.2632	12	10.5841	3.7788	37.1099
13	20.8431	0.0078	0.2919	13	11.6412	0.0001	34.5770
14	21.1130	1.8622	1.3428	14	11.6990	0.0069	0.2849
15	22.6646	0.9371	0.0384	15	11.9481	0.0000	0.0000
16	24.6382	0.0725	0.0030	16	12.7451	13.6208	2.6095
17	24.9016	1.0824	0.0111	17	13.4986	0.0206	0.2137
18	27.5152	0.0137	0.0081	18	13.6084	0.0001	0.0011
19	28.8372	0.3683	0.3629	19	14.1885	0.0000	0.0000
20	29.2757	0.2932	1.1456	20	14.2679	0.0063	0.0000

Table 7-13: Eigenfrequencies and effective masses in x- and z-direction in case of using acoustic elements of the comparison regarding the stiffness of the gate

The model with the rigid radial gate (orange) has higher eigenfrequencies and effective masses compared to the model with the deformable gate (brown) for the case of acoustic elements.

A bigger difference of the eigenfrequencies between the model with the rigid radial gate (cyan) and the deformable radial gate (lightgreen) for the model with Westergaard's added masses is discernible in contrast to the model with acoustic elements.

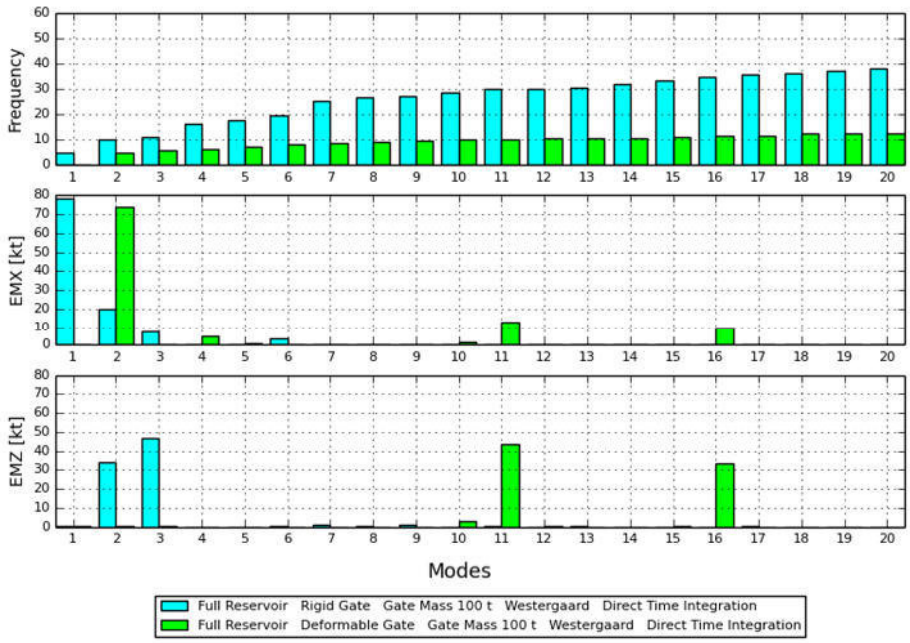

Figure 7-40: Eigenfrequencies and effective masses in x- and z-direction in case of using Westergaard's added masses of the comparison regarding the stiffness of the gate

For the models with the rigid radial gate the 1st and the 7th mode for the calculation of the Rayleigh damping coefficients are used. Due to the bigger effective masses occurring at higher modes in case of a deformable gate it is necessary to choose the 2nd and the 17th mode for the Rayleigh damping.

Full Reservoir Rigid Gate Gate Mass 100 t Westergaard				Full Reservoir Deformable Gate Gate Mass 100 t Westergaard			
Modes	Eigenfrequency	EMx	EMz	Modes	Eigenfrequency	EMx	EMz
1	4.6384	78.5279	0.5532	1	0.2725	0.0000	0.0999
2	10.0589	19.9179	33.9168	2	4.7394	73.8128	0.5042
3	11.1756	7.0934	46.7267	3	6.0301	0.3931	0.1015
4	16.4125	0.3517	0.0317	4	6.4673	4.7799	0.0022
5	17.6164	0.0003	0.0000	5	7.1527	0.6548	0.0271
6	19.3872	3.4975	0.2512	6	8.3383	0.0001	0.0039
7	25.4280	0.0402	1.1471	7	8.4923	0.0000	0.0000
8	26.9694	0.3406	0.3246	8	9.2300	0.0000	0.0000
9	27.0961	0.4027	0.7422	9	9.7831	0.0000	0.0000
10	28.6835	0.0003	0.0001	10	10.0947	1.4678	3.0818
11	29.9756	0.0070	0.5468	11	10.2441	12.7607	43.8635
12	30.3270	0.0019	0.0010	12	10.4411	0.0081	0.1399
13	30.6602	0.0957	0.0668	13	10.4435	0.0027	0.0466
14	31.8181	0.0002	0.0001	14	10.6748	0.0000	0.0003
15	33.6207	0.0354	0.0064	15	11.2522	0.0030	0.1067
16	35.0166	0.0009	0.0009	16	11.4574	9.7816	33.2620
17	35.9267	0.1207	0.0695	17	11.5082	0.0011	0.0018
18	36.2721	0.0160	0.0005	18	12.4055	0.0000	0.0000
19	37.3373	0.0058	0.0114	19	12.6671	0.0036	0.0081
20	38.2278	0.0035	0.0013	20	12.6889	0.0000	0.0000

Table 7-14: Eigenfrequencies and effective masses in x- and z-direction in case of using Westergaard's added masses of the comparison regarding the stiffness of the gate

Rayleigh Damping: Used Frequencies, α- and β-Values										
$\alpha = \omega_1 * \omega_2 * \beta = 4 * \pi * f_1 * f_2 * \beta$										
$\beta = 2 * \xi / (\omega_1 + \omega_2) = \xi / (\pi * (f_1 + f_2)$										
Calculation Method	Reservoir Case	Reservoir Consideration	Gate Stiffness	Gate Mass [t]	1st used Mode	2nd used Mode	f_1	f_2	α	β
Direct Integration	full	Acoustic Elements	rigid	100	1	10	4.4391	18.5810	2.2513	0.0007
Direct Integration	full	Acoustic Elements	deformable	100	2	16	4.2090	12.7451	1.9880	0.0009
Direct Integration	full	Westergaard's added masses	rigid	100	1	7	4.6384	25.4280	2.4648	0.0005
Direct Integration	full	Westergaard's added masses	deformable	100	2	17	4.7394	11.5082	2.1092	0.0010

Table 7-15: Calculation of the Rayleigh damping coefficients of the comparison regarding the stiffness of the gate

7.7.6.2 Resulting accelerations in the abutment

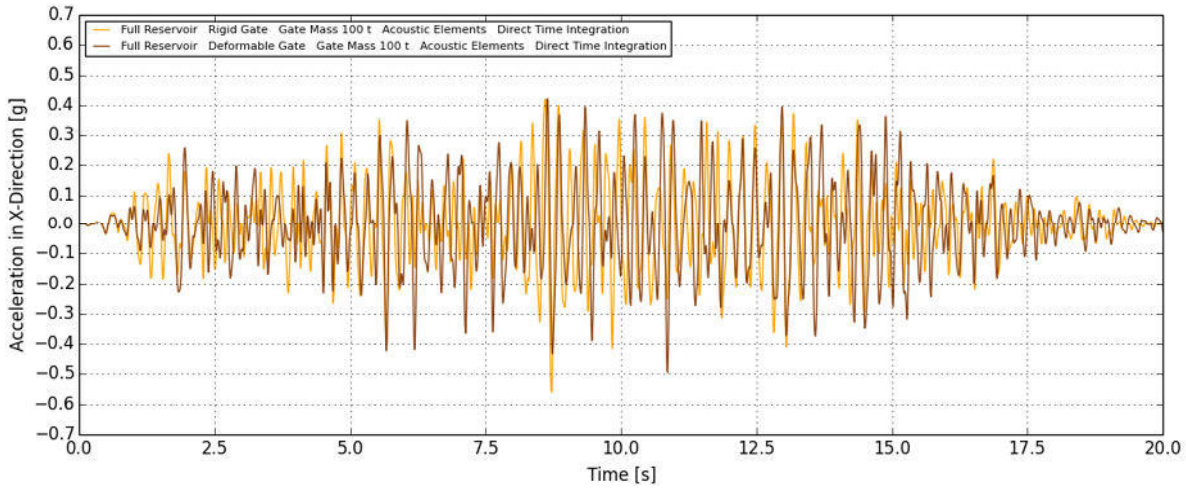

Figure 7-41: Resulting accelerations in x-direction in the abutment in case of using acoustic elements of the comparison regarding the stiffness of the gate

In the comparison of the resulting accelerations of the models with a rigid radial gate and a deformable radial gate by using acoustic elements no significant differences in the amount of the accelerations are visible. A small phase shift is recognizable whereby the model with the deformable gate is a little delayed.

Higher amplitudes of the model with a deformable radial gate arise in case of the modelling of the reservoir according to Westergaard. The maximum occurs at the rigid gate case and the minimum acceleration belongs to the deformable gate case.

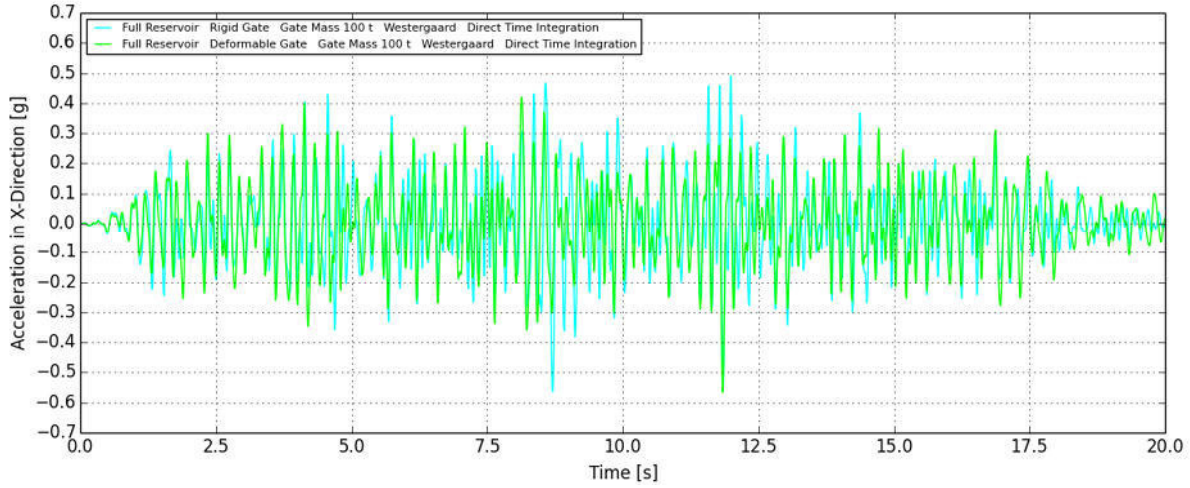

Figure 7-42: Resulting accelerations in x-direction in the abutment in case of using Westergaard's added masses of the comparison regarding the stiffness of the gate

7.7.6.3 Resulting displacements in the abutment

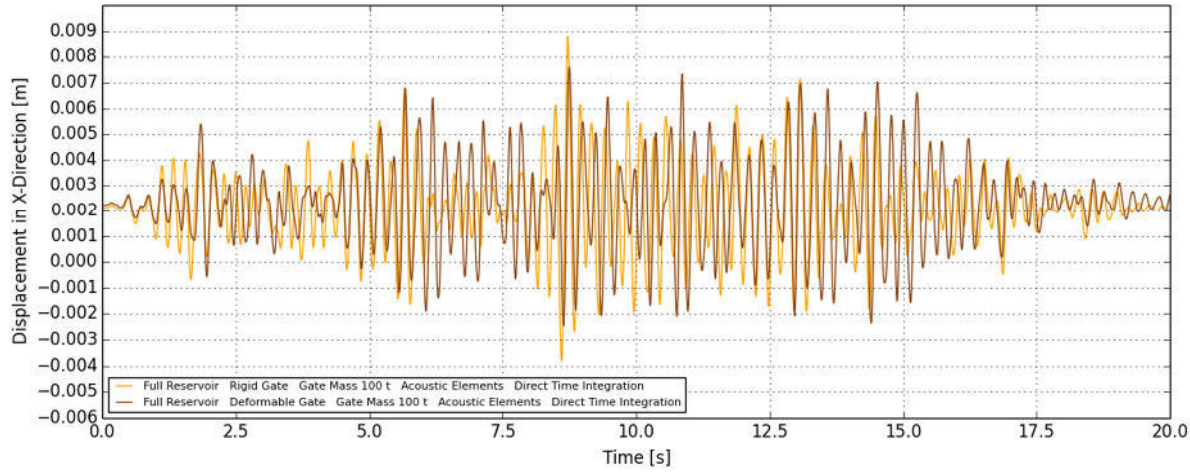

Figure 7-43: Resulting displacements in x-direction in the abutment in case of using acoustic elements of the comparison regarding the stiffness of the gate

Like the acceleration time history also at the displacements a small phase shift is seeable in case of acoustic elements. The minimum and maximum displacements belong to the rigid gate.

Also at the displacement time histories higher amplitudes of the deformable gate case in case of using Westergaard are visible. The maximum displacement belongs to the rigid gate case and the minimum displacement belongs to the deformable gate.

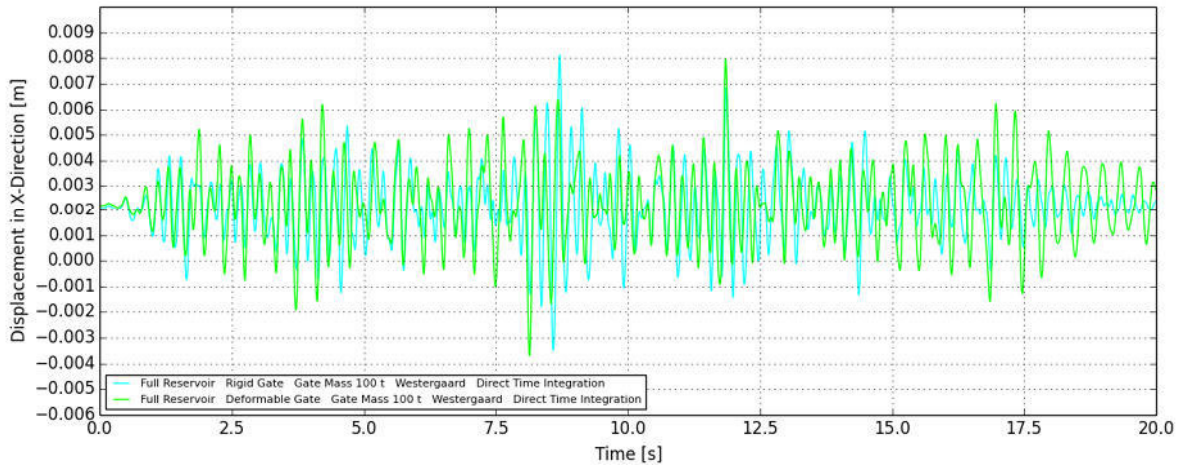

Figure 7-44: Resulting displacements in x-direction in the abutment in case of using Westergaard's added masses of the comparison regarding the stiffness of the gate

7.7.6.4 Acceleration response spectra

In the two acceleration response spectra the maximum accelerations of the models with deformable gates occur at frequencies smaller 4.5 Hz. The maximum accelerations of the models with a rigid gate are between 4.5 and 5 Hz.

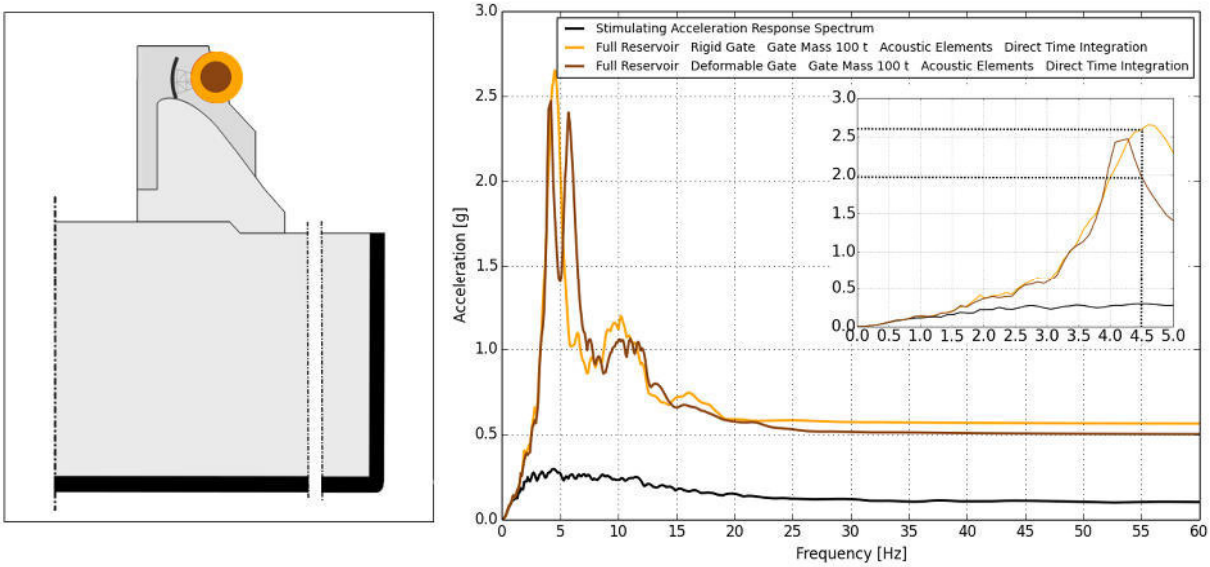

Figure 7-45: Acceleration response spectra in case of using acoustic elements of the comparison regarding the stiffness of the gate

In case of modelling with Westergaard's added masses the two response spectra of the rigid and the deformable gate with a mass of 100 t are quite similar whereby the distribution of the rigid gate is a little higher. A slight change in response frequency occurs.

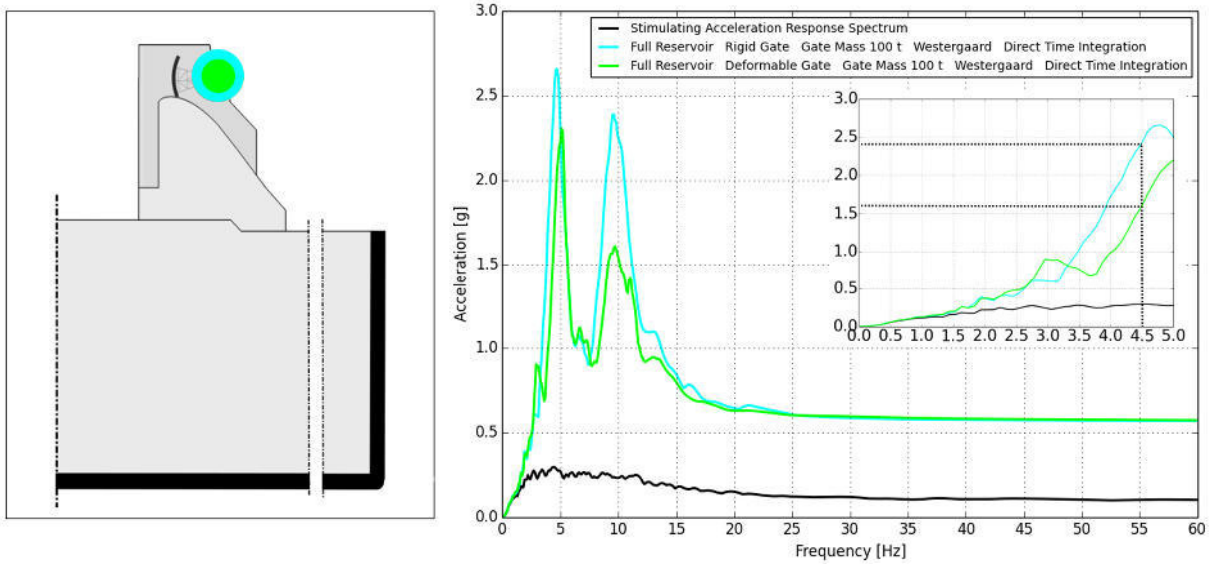

Figure 7-46: Acceleration response spectra in case of using Westergaard's added masses of the comparison regarding the stiffness of the gate

7.7.7 Comparison of Westergaard's added mass technique and acoustic elements

7.7.7.1 Eigenfrequency analysis

The eigenfrequency comparison of the two reservoir modelling techniques shows slightly higher frequencies of the acoustic elements case (lightgreen) and the case of using Westergaard's added masses (brown).

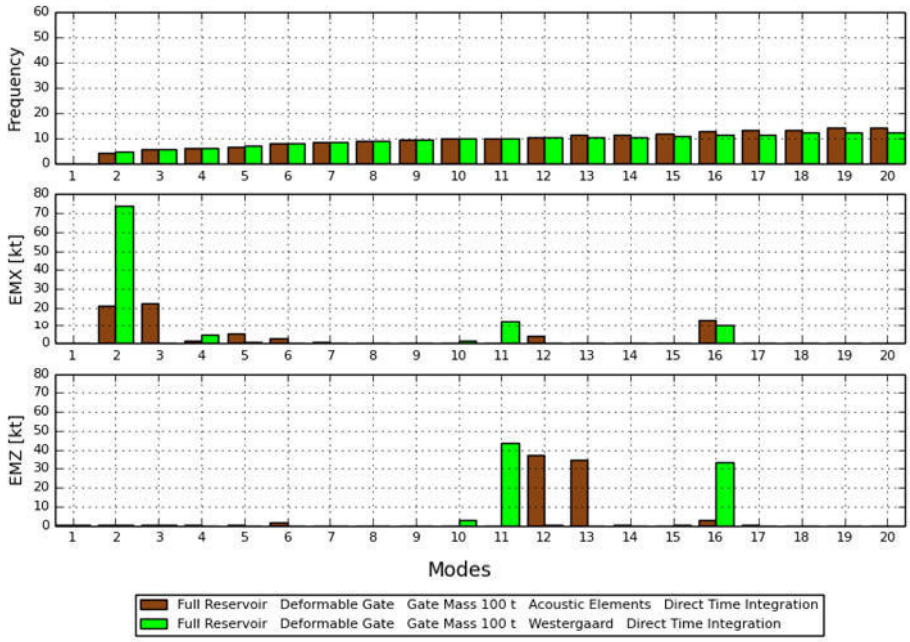

Figure 7-47: Eigenfrequencies and effective masses in x- and z-direction of the comparison of the reservoir modelling technique

Full Reservoir Rigid Gate Gate Mass 100 t Westergaard				Full Reservoir Deformable Gate Gate Mass 100 t Westergaard			
Modes	Eigenfrequency	EMx	EMz	Modes	Eigenfrequency	EMx	EMz
1	0.2944	0.0000	0.0874	1	0.2725	0.0000	0.0999
2	4.2090	21.3174	0.1117	2	4.7394	73.8128	0.5042
3	5.6053	22.7322	0.3454	3	6.0301	0.3931	0.1015
4	6.4671	1.3306	0.0867	4	6.4673	4.7799	0.0022
5	6.6465	5.2600	0.1945	5	7.1527	0.6548	0.0271
6	8.2332	2.4914	1.4088	6	8.3383	0.0001	0.0039
7	8.7269	0.6390	0.0110	7	8.4923	0.0000	0.0000
8	9.2606	0.0000	0.0000	8	9.2300	0.0000	0.0000
9	9.7333	0.0189	0.0025	9	9.7831	0.0000	0.0000
10	9.9197	0.0000	0.0000	10	10.0947	1.4678	3.0818
11	10.1791	0.0000	0.0000	11	10.2441	12.7607	43.8635
12	10.5841	3.7788	37.1099	12	10.4411	0.0081	0.1399
13	11.6412	0.0001	34.5770	13	10.4435	0.0027	0.0466
14	11.6990	0.0069	0.2849	14	10.6748	0.0000	0.0003
15	11.9481	0.0000	0.0000	15	11.2522	0.0030	0.1067
16	12.7451	13.6208	2.6095	16	11.4574	9.7816	33.2620
17	13.4986	0.0206	0.2137	17	11.5082	0.0011	0.0018
18	13.6084	0.0001	0.0011	18	12.4055	0.0000	0.0000
19	14.1885	0.0000	0.0000	19	12.6671	0.0036	0.0081
20	14.2679	0.0063	0.0000	20	12.6889	0.0000	0.0000

Table 7-16: Eigenfrequencies and effective masses in x- and z-direction of the comparison of the reservoir modelling techniques

Rayleigh Damping: Used Frequencies, α- and β-Values										
$\alpha = \omega_1 * \omega_2 * \beta = 4 * \pi * f_1 * f_2 * \beta$										
$\beta = 2 * \xi / (\omega_1 + \omega_2) = \xi / (\pi * (f_1 + f_2)$										
Calculation Method	Reservoir Case	Reservoir Consideration	Gate Stiffness	Gate Mass [t]	1st used Mode	2nd used Mode	f_1	f_2	α	β
Direct Integration	full	Acoustic Elements	deformable	100	2	16	4.2090	12.7451	**1.9880**	**0.0009**
Direct Integration	full	Westergaard's added Masses	deformable	100	2	17	4.7394	11.5082	**2.1092**	**0.0010**

Table 7-17: Calculation of the Rayleigh damping coefficients of the comparison regarding the reservoir modeling technique

7.7.7.2 Resulting accelerations in the abutment

Higher amplitudes of the model with Westergaard's added masses are visible but the maximum and maximum acceleration belongs to the acoustic elements.

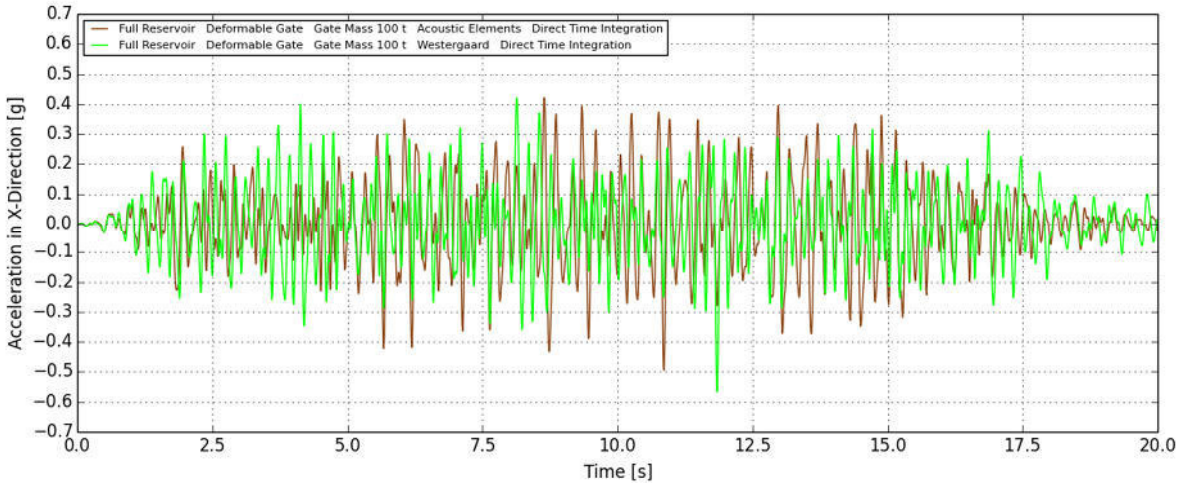

Figure 7-48: Resulting accelerations in x-direction in the abutment of the comparison regarding the reservoir modelling technique

7.7.7.3 Resulting displacements in the abutment

Also in the displacement time histories bigger amplitudes of the model with added masses are identifiable. The maximum and minimum displacements are also visible in case of Westergaard.

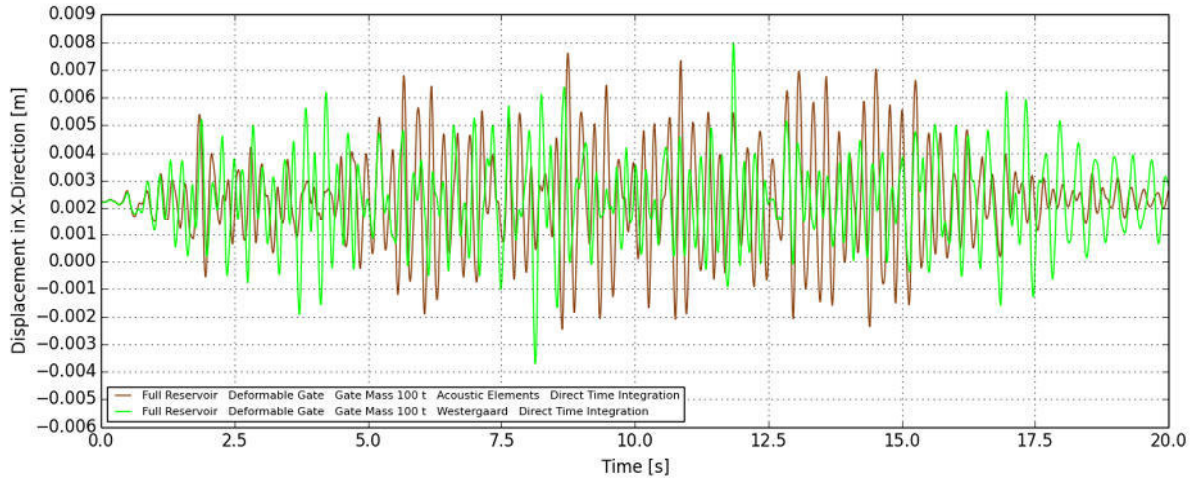

Figure 7-49: Resulting displacements in x-direction in the abutment of the comparison regarding the reservoir modelling technique

7.7.7.4 Acceleration response spectra

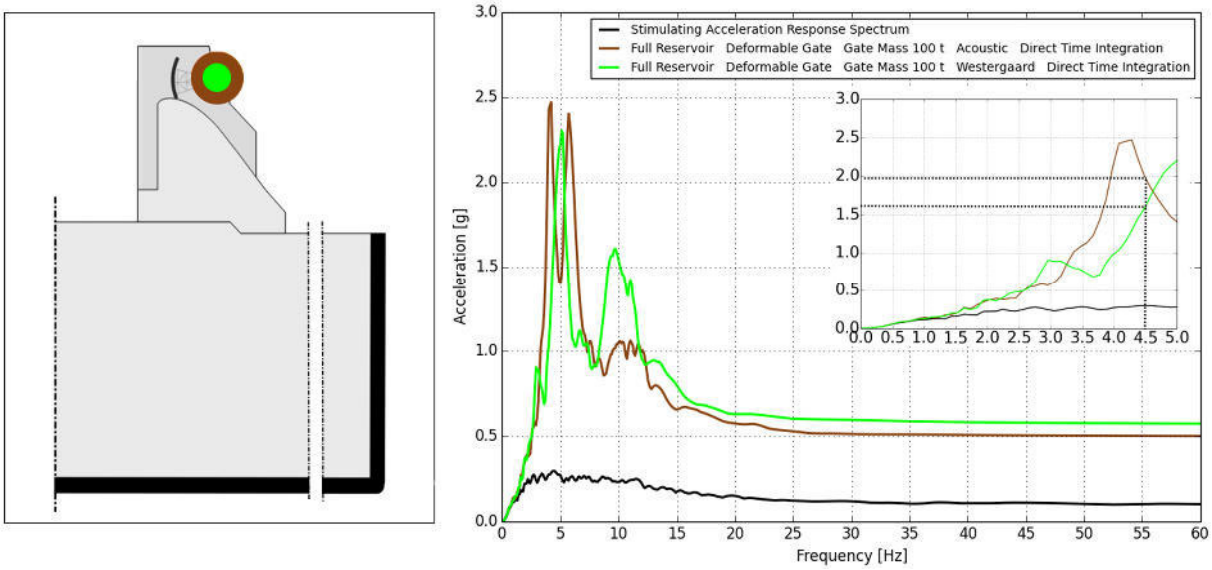

Figure 7-50: Acceleration response spectra of the comparison regarding the reservoir modelling technique

Higher maximum accelerations for the case of using acoustic elements are shown in the response spectra for the comparison of the reservoir modelling technique. A frequency shift is visible and a pronounced second peak at about 10 Hz in case of using Westergaard is identifiable.

7.7.8 Minimum and maximum accelerations and displacements of the different configurations

In the following table the maximum and minimum accelerations of the configurations are summarized. The models are sorted by the minimum acceleration value.

The minimum acceleration is visible at the full reservoir case with massless, deformable gate using the direct time integration method and acoustic elements. The maximum acceleration occurs at the model with rigid gate with a mass of 100 t and Westergaard's added mass technique. The maximum displacement belongs to the full reservoir case with rigid, massless gate, acoustic elements and direct time integration and the minimum displacement occurs in case of an empty reservoir and a rigid, massless gate using the modal analysis.

Maximum and minimum Accelerations and Displacements								
Calculation Method	Reservoir Case	Reservoir Consideration	Gate Stiffness	Gate Mass [t]	Accelerations [g]		Displacements [m]	
					Maximum	Minimum	Maximum	Minimum
Direct Integration	full	Acoustic Elements	deformable	-	0.485	**-0.625**	0.0086	-0.0035
Direct Integration	full	Westergaard	deformable	100	0.420	-0.567	0.0080	-0.0037
Direct Integration	full	Westergaard	rigid	100	**0.491**	-0.564	0.0081	-0.0035
Direct Integration	full	Acoustic Elements	rigid	100	4.107	-0.559	**0.0088**	-0.0038
Direct Integration	full	Westergaard	rigid	-	0.481	-0.553	0.0080	-0.0035
Direct Integration	full	Acoustic Elements	deformable	100	0.421	-0.495	0.0076	-0.0025
Direct Integration	full	Acoustic Elements	rigid	-	0.447	-0.489	0.0075	-0.0033
Direct Integration	empty	-	rigid	-	0.345	-0.433	0.0022	-0.0040
Modal Analysis	full	-	rigid	-	0.441	-0.423	0.0050	**-0.0049**
Modal Analysis	empty	-	rigid	-	0.380	-0.396	0.0038	-0.0038

Table 7-18: Maximum and minimum accelerations and displacements in the abutment in x-direction

7.7.9 Acceleration amplification factor of the different configurations at a frequency of 4.5 Hz in the Response Spectra

The maximum acceleration of the stimulating time history in x-direction occurs in the response spectra at a frequency of 4.5 Hz. Due to the seismic loading higher accelerations at 4.5 Hz occur in the abutment of the radial gate. The amplification factor of the accelerations in the abutment compared to the stimulating accelerations at the foundation boundaries are pointed out.

In Figure 7-51 and Figure 7-52 the order of the models is the same as in Table 7-18.

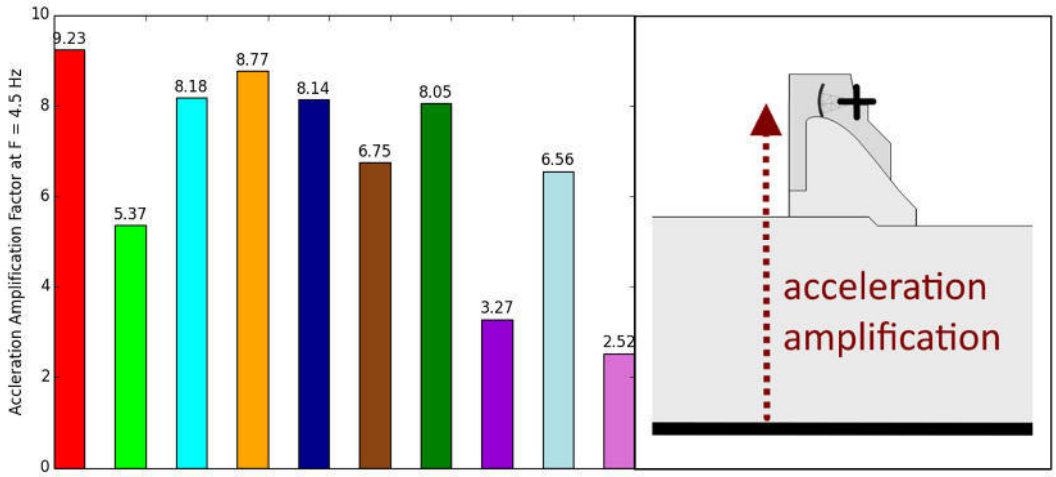

Figure 7-51: Acceleration amplification factor in the abutment at 4.5 Hz

Acceleration Amplification Factor at F = 4.5 Hz							
Calculation Method	Reservoir Case	Reservoir Consideration	Gate Stiffness	Gate Mass [t]	Maximum stimulating Acceleration (F	Acceleration at F = 4.5 Hz [g]	Amplification Factor [-]
Direct Time Integration	full	Acoustic Elements	deformable	-	0.295	2.72	9.23
Direct Time Integration	full	Westergaard	deformable	100		1.58	5.37
Direct Time Integration	full	Westergaard	rigid	100		2.41	8.18
Direct Time Integration	full	Acoustic Elements	rigid	100		2.59	8.77
Direct Time Integration	full	Westergaard	rigid	-		2.40	8.14
Direct Time Integration	full	Acoustic Elements	deformable	100		1.99	6.75
Direct Time Integration	full	Acoustic Elements	rigid	-		2.37	8.05
Direct Time Integration	empty	-	rigid	-		0.96	3.27
Modal Analysis	full	-	rigid	-		1.94	6.56
Modal Analysis	empty	-	rigid	-		0.74	2.52

Table 7-19: Acceleration amplification factor in the abutment at 4.5 Hz

7.7.10 Maximum acceleration amplification factor of the different configurations in the Response Spectra

In addition to the developed acceleration amplification factor at a frequency of 4.5 Hz also the maximum occurring accelerations of each model and the maximum acceleration of the stimulating acceleration in the response spectra are compared.

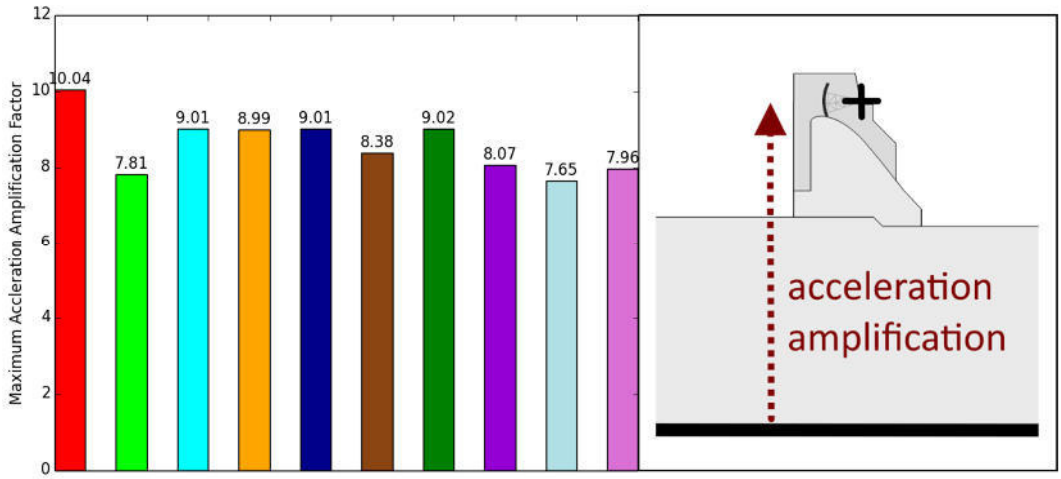

Figure 7-52: Maximum acceleration amplification factor in the abutment

Maximum Acceleration Amplification Factor							
Calculation Method	Reservoir Case	Reservoir Consideration	Gate Stiffness	Gate Mass [t]	Maximum stimulating Acceleration [g]	Maximum Acceleration	Amplification Factor [-]
Direct Time Integration	full	Acoustic Elements	deformable	-	0.295	2.96	10.04
Direct Time Integration	full	Westergaard	deformable	100		2.30	7.81
Direct Time Integration	full	Westergaard	rigid	100		2.66	9.01
Direct Time Integration	full	Acoustic Elements	rigid	100		2.65	8.99
Direct Time Integration	full	Westergaard	rigid	-		2.66	9.01
Direct Time Integration	full	Acoustic Elements	deformable	100		2.47	8.38
Direct Time Integration	full	Acoustic Elements	rigid	-		2.66	9.02
Direct Time Integration	empty	-	rigid	-		2.38	8.07
Modal Analysis	full	-	rigid	-		2.26	7.65
Modal Analysis	empty	-	rigid	-		2.35	7.96

Table 7-20: Maximum acceleration amplification factor in the abutment

7.7.11 Dynamic forces in the abutment

The static calculation results in a bearing force of 6.4 MN in the connection between the radial gate arms and the concrete pier due to equation 7.3. These forces increase in case of oscillating masses due to accelerations. The resulting dynamic forces are figured out by Abaqus/CAE's "Free Body Cut" function and plotted in charts. Figure 7-53 shows the resulting dynamic force in the abutment after 8.30 seconds of the earthquake for the models with deformable gate with a gate mass of 100 t.

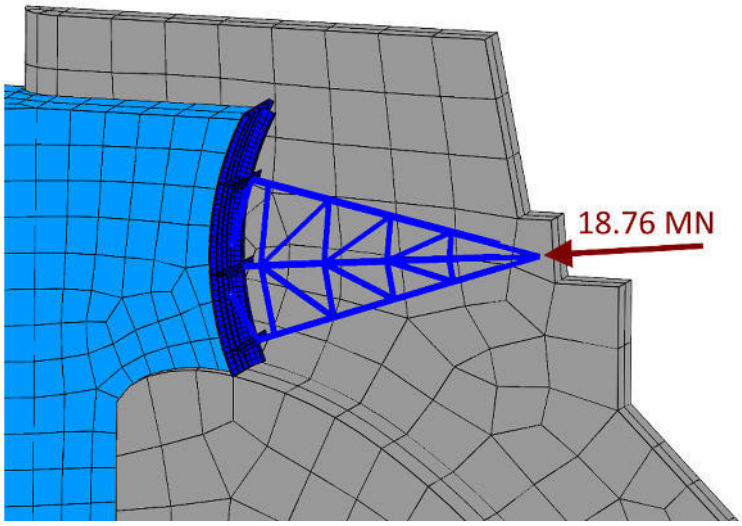

Figure 7-53: Dynamic force in the abutment at 8.3 seconds for the model with acoustic elements

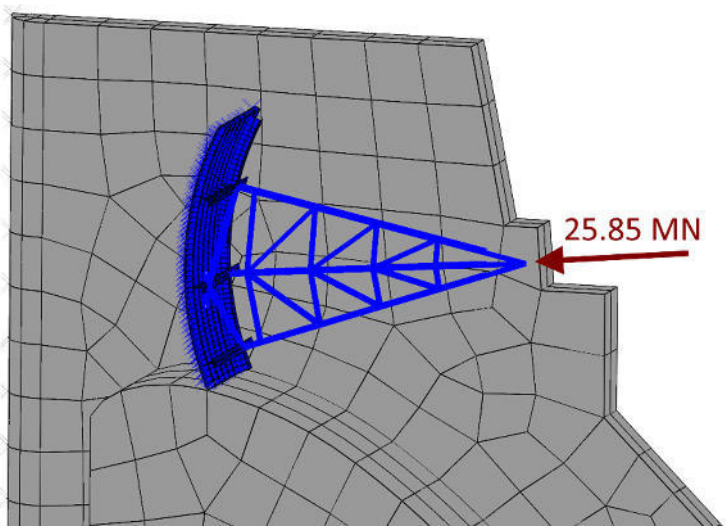

Figure 7-54: Dynamic force in the abutment at 8.3 seconds for the model with Westergaard's added masses

Both maxima occur after 8.30 seconds of the earthquake. The maximum force for the model with acoustic elements is 18.76 MN and the maximum force for the model with added masses is 25.85 MN.

7.7.12 Pseudostatic method for the calculation of the dynamic force in the abutment

The resulting maximum forces of the numerical simulation in the abutment can be compared with the result of the pseudostatic method. Therefore the added masses according to Westergaard have to be calculated by using formula (6.3).

$$m_W = \frac{7}{8} \cdot 0.001 \cdot 14 \cdot 12.5 \cdot \sqrt{14 \cdot 7} = 1.516\ kt \tag{7.4}$$

The addition of the mass of the radial gate and the calculated added mass results in a total mass of:

$$m = 1.616\ kt \tag{7.5}$$

The multiplication of the resulting mass with the maximum accelerations of about 25 m/s in the response spectra of the comparison of acoustic elements and Westergaard (Figure 7-50) leads to the resulting water load on the radial gate and furthermore to the dynamic force in the abutment.

$$W = m \cdot a = 1.616 \cdot 25 = 40.40\ MN \tag{7.6}$$

$$A = B = \frac{W}{2} = 20.20\ MN \tag{7.7}$$

The pseudostatic method results in a dynamic bearing force of 20.20 MN. It's between the result of the of the model with acoustic elements and the result of the model using Westergaard's added masses

Resulting dynamic Bearing Force	
Calculation Method	Results [MN]
Numerical Simulation with Acoustic Elements	18.76
Numerical Simulation with Westergaard	25.85
Pseudostatic Method	20.20

Table 7-21: Resulting dynamic bearing force in the abutment of the radial gate

7.7.12.1 Time histories of the forces in the abutment of the radial gate

The highest dynamic forces occur between 5 and 15 seconds. For a better readability this period is illustrated more precisely.

Higher amplitudes of the model with Westergaard's added masses are visible especially in the graph of the forces in z-direction. The maximum forces occur at the same time.

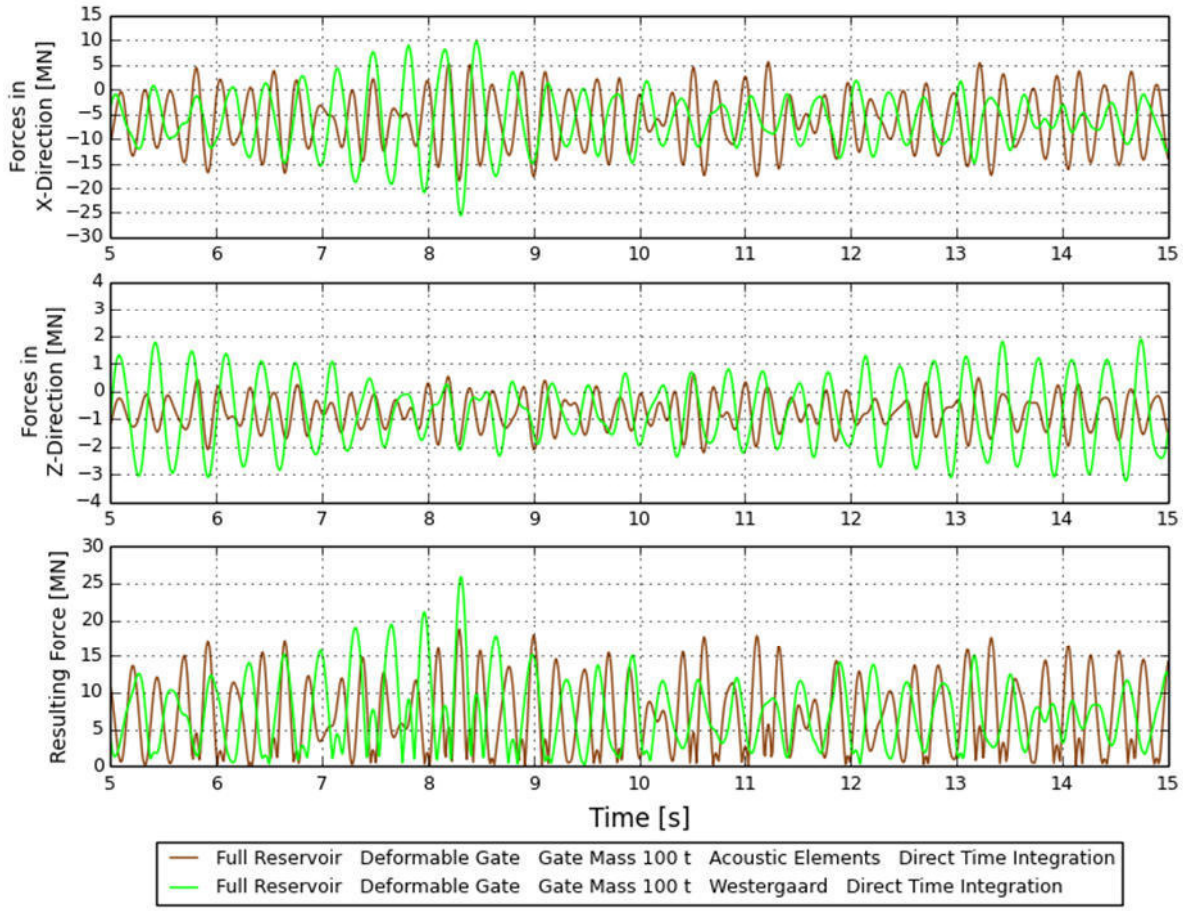

Figure 7-55: Dynamic force time histories in the abutment of the radial gate

The seismic stimulation of the system leads to a threefold magnification of the forces in the abutment of the model with acoustic elements and a force increasing with the factor of four for the model with Westergaard's added mass technique.

7.8 Discussion and summary of the results

7.8.1 Static analysis

The maximum pressure in the contact path of the gravity dam caused by the dead weight of the concrete structure is about 1 MPa and occurs on the upstream heel of the dam (Figure 7-13). The addition of the hydrostatic pressure leads to a mirroring of the stress distribution and a maximum of 1 MPa on the downstream end of the contact path (Figure 7-15). The amount of the hydrostatic water pressure on the bottom of the reservoir is 0.58 MPa (Figure 7-14).

The hydrostatic water loading results in forces of 6.4 MN in the abutment of the radial gate (Figure 7-16, Figure 7-17). Due to the oscillating masses caused by seismic loading the forces increase up to 18.76 MN (Figure 7-55). That is about 3 times the force of the hydrostatic step.

7.8.2 Dynamic analysis

In the framework of the dynamic numerical simulation different model configurations are compared.

Comparison regarding the reservoir modelling technique and calculation the method:
At first the models with a rigid, massless radial gate are matched whereby the modelling of the reservoir with Westergaard's added mass technique yields the highest accelerations and displacements over the 20 seconds. The modal analysis results in the smallest values (Figure 7-24, Figure 7-25). The eigenfrequencies of the model with added masses and the model with acoustic elements with a massless rigid gate are similar (Figure 7-23). In the response spectra graphs frequency shifts occur and the peaks of the resulting distributions at about 4.7 Hz are delayed compared with the stimulating acceleration at 4.5 Hz (Figure 7-26). The acceleration amplification factor at 4.5 Hz is for the model with acoustic elements 8.05 and for the model with Westergaard's added masses 8.14 and therefore nearly the same (Figure 7-51). Also the maximum amplification factor by comparing the maximum peaks of the resulting response spectra and the maximum peak of the response spectrum of the stimulating acceleration time history is very similar (Figure 7-52).

Comparison regarding the reservoir case:
The comparison of the reservoir cases with the rigid and massless gate show clear differences in the eigenfrequency due to the difference of the acting model masses (Figure 7-27). Higher accelerations and bigger amplitudes of the model with full reservoir are visible in the acceleration time histories (Figure 7-28). The displacements of the full reservoir case are mainly positive whereas the displacements of the empty reservoir are mostly negative (Figure 7-29). The lower results of the modal analysis are probably caused by the higher global damping assumption with a constant damping coefficient of 5% in contrast to the Rayleigh damping assumption of the direct time integration whereby the system is underdamped between the two used modes and overdamped for the remaining modes. The response spectra of this comparison show a change in response frequency whereby the peaks of the two empty reservoir cases occur at frequencies bigger than 5 Hz (Figure 7-30). The amplification factors of the empty reservoir cases are with 3.27 and 2.52 are significantly smaller than the amplification factor of the full reservoir case (Figure 7-51). The comparisons of the maximum amplification factors show smaller differences (Figure 7-52).

Comparison regarding mass of the radial gate:
The slight influence of the gate mass on the eigenfrequencies is visible at the comparison of the models with massless, rigid or deformable gate and models with a gate mass of 100 t (Figure 7-31, Figure 7-32). The amplitudes in the acceleration time histories in case of a rigid gate as well in case of a deformable gate are higher for models with a gate mass of 100 t. The maximum acceleration occurs for the rigid gate at the massless case and for the deformable gate at the 100 t case (Figure 7-33, Figure 7-34). The maximum and minimum displacements belong to the massless gate models independent on the stiffness of the gate (Figure 7-35, Figure 7-36). The response spectra show small frequency shifts whereby the distributions of the models with a massless gate are delayed (Figure 7-37, Figure 7-38). The calculations of the amplification factors show bigger differences in case of a deformable gate. The highest amplification factors of all configurations occur in case of a massless deformable gate by using acoustic elements for the reservoir (Figure 7-51, Figure 7-52).

Comparison regarding the stiffness of the radial gate:
The comparison of the eigenfrequency regarding the stiffness of the gate show higher frequencies in case of a rigid gate compared to the deformable gate cases (Figure 7-39, Figure 7-40). Furthermore these differences are bigger for Westergaard's added mass technique. In the acceleration time histories no trend is visible for both reservoir modelling techniques thereby the amplitudes for rigid gate models are slightly higher (Figure 7-41, Figure 7-42). Additionally the response spectra show higher accelerations of the models with rigid gate compared to the models with deformable gate (Figure 7-45, Figure 7-46). The acceleration amplification factors at 4.5 Hz are for both reservoir modelling techniques higher for the rigid gate case (Figure 7-51). This trend is also visible at the maximum acceleration amplification factor (Figure 7-52).

Comparison of Westergaard's added mass technique and acoustic elements:
The comparison of the results of the models with different reservoir modelling technique shows slightly higher maximum and minimum accelerations and displacements of the model with Westergaard's added masses, however the acceleration and displacement amplitudes of the Westergaard case are distinctly higher (Figure 7-48, Figure 7-49, Figure 7-50).

The calculation of the dynamic force in the abutment of the radial gate shows different results for the different calculation methods whereby the simulation with acoustic elements leads to the highest forces of 25.85 MN. The pseudostatic method yields 20.20 MN and the simulation with acoustic elements results in the lowest bearing force of 18.76 MN.

7.9 Conclusion and outlook

The dynamic simulation results in high accelerations in the abutment especially in negative x-direction (upstream). The comparison of the calculation method shows that the system is often underdamped in case of using the direct time integration compared to the modal analysis, dependent on the chosen Rayleigh damping factors. It is safe to assume that the full reservoir case results in higher accelerations and displacements in the radial gate in contrast to the empty reservoir case. The slight influence of the gate mass especially in case of a rigid gate was figured out. The worst combination, which leads to the highest accelerations is a full reservoir combined with a massless, deformable gate by using the direct time integration. The simulated accelerations in the abutment of this configuration go up to 0.63 g.

With the developed response spectra the maximum peaks of the stimulating acceleration time history and the resulting acceleration time history in the abutment can be compared. The comparison of the maximum acceleration peaks of the stimulating and resulting response spectra yields an amplification factor of 10 for the deformable gate without mass.

The elaboration of the dynamic forces in the abutment shows a maximum increase to 18.76 MN (acoustic elements), 20.20 MN (Pseudostatic) or 25.85 MN (Westergaard's added masses), which is about the three- to fourfold of the static loads.

Finally it can be concluded that the most accurate way of modeling (acoustic elements, deformable gate, mass of 100 t) doesn't yield the highest loads at the gate. This means that dependent on the model the results can be much too conservative, which may lead to overbuilt structures.

Due to the issue that the maximum peaks in the response spectrum of the stimulating accelerations occur in the same frequency range as the maximum peaks of nearly all resulting acceleration response spectra further investigations can be dynamic simulations with different acceleration time histories to examine the influence of the stimulating time history on the acceleration amplification factors.

Bibliography

Bandi, A. et al. (2006). *Energy Technologies. Subvolume C: Renewable Energy.* Berlin Heidelberg: Springer-Verlag.

Bathe, K. J. (2002.). *Finite-Elemente-Methoden.* Berlin Heidelberg: Springer-Verlag.

Chopra, A. K. (2011). *Dynamic of Structures. Theory and Applications to Earthquake Engineering.* New Jersey: Prentice Hall.

Clough, R. W. (1993). *Dynamic of Structures*. New York: McGraw-Hill.

Dassault Systemes (2013). *Abaqus 6.13. Abaqus/CAE User's Guide.*

DIN Deutsches Institut für Normung e.V. (2004): *(DIN 19700-11) -Stauanlagen - Teil 11: Talsperren*.

Erbisti, P. C. (2004). *Design of hydraulic gates.* Lisse: Swets & Zeitlinger B.V.

escoaet - European school of computer aided engineering technology, 2015. *Rayleigh Dämpfung.* Available at: http://www.esocaet.com/wikiplus/index.php/Rayleigh-Dämpfung [Accessed 05 01 2015].

Flesch, R.(1993). *Baudynamik praxisgerecht.Band I Berechnungsgrundlagen.* Wiesbaden Berlin: Bauverlag GmbH.

Freymann, R. (2011). *Strukturdynamik. Ein anwendungsorientiertes Lehrbuch.* Heidelberg: Springer-Verlag.

Geiger, H. (2012). *Talsperrenüberwachung einer Gewölbemauer am Beispiel der Hierzmannsperre.* Masterarbeit. Technische Universität Graz

Giesecke, J. & Mosonyi, E. (2009). *Wasserkraftanlagen. Planung, Bau und Betrieb.* Berlin Heidelberg: Springer-Verlag.

Goldgruber, M. (2011). *Numerische Untersuchung der Felskeilstabilität im Widerlager der Luzzone Staumauer bei Erdbebenbelastung.* Diplomarbeit. Technische Universität Graz.

Gross, D., Hauger, W., Schröder, J. & Wall, W. A. (2012). *Technische Mechanik 3. Kinetik.* Berlin Heidelberg: Springer-Verlag.

Gross, D., Hauger, W. & Wriggers, P. (2009). *Technische Mechanik 4. Hydromechanik, Elemente der Höheren Mechanik, Numerische Methoden.* Berlin, Heidelberg. Springer-Verlag.

Institut für Wasserbau und Wasserwirtschaft (2012). *Konstruktiver Wasserbau Grundlagen. Lernbehelf.* Graz. Technische Universität Graz.

Institut für Wasserbau und Wasserwirtschaft (2013). *VU Numerik im Wasserbau: Einführung Fluid-Structure-Interaction Modelling in Hydraulic Engineering.* Technische Universität Graz.

Lewin, J. (2001). *Hydraulic Gates and Valves in Free Surface Flow and Submerged Outlets*. London: Thomas Telford Ltd.

Meskouris, K., Hinzen, K.-G., Butenweg, C. & Mistler, M. (2011). *Bauwerke und Erdbeben: Grundlagen - Anwendung - Beispiele.* Wiesbaden: Vieweg + Teubner Verlag.

Österreichische Staubeckenkomission, 2001. *Erdbebenberechnung von Talsperren - Part 1-6.* Available at: http://www.bmlfuw.gv.at/wasser/nutzung-wasser/Richtlinien.html [Accessed 05 01 2015].

Pagger, S. (2014). *Seismic acceleration amplification over the height of a gravity dam,* Masterprojekt. Technische Universität Graz.

Strobl, T. & Zunic, F. (2006). *Wasserbau - Aktuelle Grundlagen - Neue Entwicklungen.* Berlin Heidelberg: Springer-Verlag.

US Army Corps of Engineers (1995). *EM 1110-2-2200: Gravity Dam Design*. Washington DC.

US Army Corps of Engineers (2000). *EM 1110-2-2702: Engineering and Design. Design of Spillway Tainter Gates.* Washington DC.

Vöth, S. (2006). *Dynamik schwingungsfähiger Stysteme. Von der Modellbildung bis zur Betriebsfestigkeitsrechnung mit MATLAB/SIMULINK.* Wiesbaden: Friedr.Vieweg & Sohn Verlag.

Wieland, M. (1978). *Erdbebenbedingte dynamische Beanspruchung einer Gewichtsmauer mit Berücksichtigung der Interaktion des Stausees,* Dissertation. Eidgenössische Technische Hochschule Zürich.

A Appendix

A.1 Python script for the analytical calculation of the hydrostatic pressure on the gate

```
import numpy as np

#.....................................................
# Calculation of the hydrostatic pressure on the Gate
#.....................................................

# water density [kt / m^3]
d = float(0.001)

# Radius gate [m]
R = float(17.7)

# Width gate [m]
b = float(12.5)

# Elevation water level [m.a.s.l]
EL_WL= float(385)

# Elevation sill [m.a.s.l]
EL_S= float(371)

# Elevation bearing [m.a.s.l]
EL_B= float(377.6)

#-no other definitions required!

# heights
h = EL_WL - EL_S
h1 = EL_WL - EL_B
h2 = EL_B - EL_S

alpha1 = np.arcsin(h1/R)

alpha2 = np.arcsin(h2/R)

# -- Horizontal component --
Wh = h * h/2 * b * d

# -- Vertical component --

# Total area circle
Atot = R**2*np.pi

palpha1 = alpha1/(360*np.pi/180)
palpha2 = alpha2/(360*np.pi/180)

A1 = h1 * (R*np.cos(alpha1))/2
A2 = h2 * (R*np.cos(alpha2))/2

A3 = Atot * palpha1 - A1
A4 = Atot * palpha2 - A2
```

```
A5 = (R - h1 / np.tan(alpha1))*h1 - A3

bcircle = R * (alpha2*2)
scircle = 2*h2
hcircle = (R - h2 / np.tan(alpha2))

Acircle = R * bcircle / 2 - (scircle*(R - hcircle ))/2

A6 = Acircle /2 + hcircle*h1

Wv = (A6 - A5) * b *



# Resulting waterpressure

W = round(np.sqrt(Wh**2 + Wv**2),3)

# Force angle

beta = round(np.arctan(Wv/W) * 180/np.pi,3)

A = round(W/2,3)

print '----RADIAL GATE: ', b, 'x', h,'m, R=', R,'m ----'
print 'The resulting static waterload   W = ', W, 'kt', '=', W*10, 'MN'
print 'The resulting bearing force      Av = ', Wv/2, 'kt', '=', A*10, 'MN'
print 'The resulting bearing force      A = ', A, 'kt', '=', A*10, 'MN'
print 'The waterload-angle              beta = ', beta, 'degree'
```